

Mathilde Meling

# A Combined Upcycling Route for Silicon Powder Waste and a Silicon Alloy

Masteroppgave i Materialteknologi

Veileder: Gabriella Tranell

Medveileder: Maria Wallin

Juni 2023



Mathilde Meling

# **A Combined Upcycling Route for Silicon Powder Waste and a Silicon Alloy**

Masteroppgave i Materialteknologi  
Veileder: Gabriella Tranell  
Medveileder: Maria Wallin  
Juni 2023

Norges teknisk-naturvitenskapelige universitet  
Fakultet for naturvitenskap  
Institutt for materialteknologi



Kunnskap for en bedre verden





## Preface

This thesis titled "A Combined Upcycling Route for Silicon Powder Waste and a Silicon Alloy" was written for the course TMT4905 and was conducted at the Department of Materials Science and Engineering at the Faculty for Natural Sciences at the Norwegian University of Science and Technology (NTNU), during the spring semester of 2023.

The project has received funding from the European Union's HORIZON Action Grant program under Grant Agreement N° 101058583.

First, I would like to give many thanks to my supervisor, Professor Gabriella Tranell, for all her guidance, insight, feedback, and discussions. I would also like to thank my co-supervisor Maria Wallin for her valuable insight and for answering all my questions along the way. Thank you both for letting me be a part of such an interesting and important project.

I am very grateful to have worked with Elif Emil Kaya and Nishan Simkhada, who deserve many thanks for all the valuable discussions, feedback, help in the lab, and for being excellent company.

Many thanks should also go to Dmitry Slizovskiy for helping me in the lab, both with training, and experimental setup, through the execution of the experiments, and for always being available to answer questions. I am also grateful for the help from Ivar Andre Ødegård during the vacuum experiments and for the guidance from Arman Hoseinpur Kermani. Morten Peder Raanes also deserves thanks for conducting the EPMA.

I would also like to thank Ingvild Runningen, Pål Skaret, Ruben Åge Hansen, Marit Elinda Olaisen Odden, and Berit Vinje Kramer for training, helping with equipment, solving my problems, and answering my questions.

Lastly, I want to thank Veronika Djupvik and the rest of the team at Elkem for everything from letting me be a part of very exciting experiments, interesting discussions, and sharing their insights and experience, to giving great restaurant recommendations.



## Abstract

Silicon is a vital element in products that surround us daily, like solar panels, electronics, and chemical applications. The need for a sustainable, circular silicon value chain is pressing. State-of-the-art silicon production is done through carbothermic reduction, a process that is inherently damaging to the climate, as it produces CO<sub>2</sub>. An alternative to this is silicon production through aluminothermic reduction of quartz in slag, which enables a carbon-free process, which can utilize materials unsuited for state-of-the-art silicon production. The metal produced through this process contains about 74% Si, 10% Al, and 16% Ca (SisAl metal). [1] During the production of solar cells, about half of the silicon becomes waste products. The silicon powder waste created during wafer sawing (kerf) is a major waste product. The kerf consists of almost pure silicon powder but holds some impurities from the cutting process and an inert oxide layer on the surface particles, which causes challenges in the recycling processes [2], [3].

This thesis has investigated a combined refining route for SisAl metal and kerf, starting with slag refining, followed by vacuum treatment and directional solidification. For slag refining, different mass ratios of the kerf, SisAl metal, 1,1/1 CaO/SiO<sub>2</sub>-slag, and quartz were melted in induction furnaces at 1550°C. The initial experiments found that 40 minutes of holding time were sufficient, and the ratio 1,5/1/2/0,9 of kerf, SisAl metal, slag, and quartz showed promising results regarding silicon yield and melt properties. The slag refining was done on a 200 g scale, 20 kg scale, and 100 kg scale. On the 20 kg scale, the metal reached purities between 96,2-98,9% silicon, and on the 100 kg scale, the product had 97,79 % silicon. Vacuum induction refining was done on a 400 g scale at 1550°C for 60, 90, and 100 minutes achieving 99,5%, 99,4%, and 99,5 % pure silicon, respectively. Directional solidification was discussed as a possible next step in the refining scheme with the help of theoretical calculations.

This work is a part of NTNU's contribution to the EU Horizon Resilex project, which aims to increase the circularity in the PV industry. The project has received funding from the European Union's HORIZON Action Grant program under Grant Agreement N° 101058583.

## Graphical Abstract

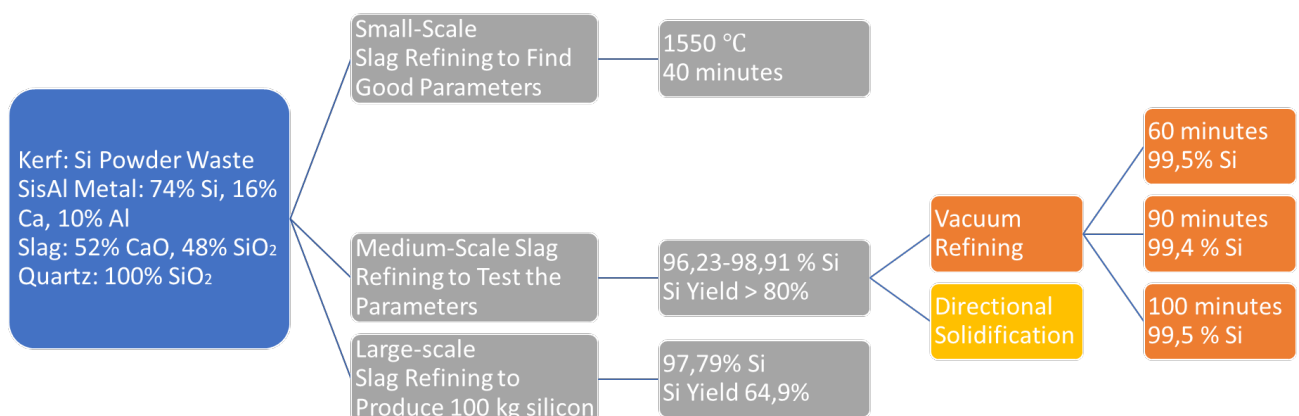


Figure 0.1: The flowchart illustrates the work conducted for this thesis and the main results where relevant.

## Sammendrag

Silisium er et avgjørende element i produkter som omgir oss hver dag, som solcellepaneler, elektronikk og i kjemiske produkter. Behovet for en bærekraftig og sirkulær verdikjede for silisium er presserende. Dagens produksjon av silisium utføres ved karbotermisk reduksjon, en prosess som er skadelig for klimaet siden den produserer CO<sub>2</sub>. Et alternativ til dette er produksjon av silisium gjennom aluminotermisk reduksjon av kvarts i slagg, som muliggjør en karbonfri prosess og kan utnytte materialer som ikke egner seg for dagens silisiumproduksjon. Metallet som produseres gjennom denne prosessen inneholder omtrent 74% Si, 10% Al og 16% Ca (SisAl-metall) [1]. Under produksjonen av solceller blir omtrent halvparten av silisiumet avfallsprodukter. Et betydelig avfallsprodukt er silisumpulveravfall(kerf) som oppstår under skjæring av wafers til solceller. Kerfen består av nesten rent silisumpulver, men inneholder noen urenheter fra skjæreplassen og et inert oksidlag på partiklens overflate, noe som skaper utfordringer i resirkuleringsprosessen [2], [3].

Denne avhandlingen har undersøkt en kombinert raffineringsskema for SisAl-metall og kerf, som starter med slagg-raffinering, etterfulgt av vakuumraffinering og retningsstyrt størkning. For slaggraffineringen ble forskjellige massekombinasjoner av kerf, SisAl-metall, 1,1/1 CaO/SiO<sub>2</sub>-slag og kvarts smeltet i induksjonsovner ved 1550°C. De første eksperimentene viste at 40 minutters holdetid var tilstrekkelig, og forholdet 1,5/1/2/0,9 av kerf, SisAl-metall, slagg og kvarts viste lovende resultater med hensyn til silisiumutbytte og smelteegenskaper. Slagg-raffineringen ble utført på 200 g-, 20 kg- og 100 kg-skala. På 20 kg-skalaen oppnådde metallet mellom 96,2% - 98,9% silisium, og på 100 kg-skalaen hadde metallproduktet 97,79% silisium. Vakuuminduksjonsraffinering ble gjort for 400 g metall ved 1550°C i 60, 90 og 100 minutter, og oppnådde henholdsvis 99,5%, 99,4% og 99,5% rent silisium. Retningsstyrt størkning ble diskutert som et mulig neste trinn i raffineringsskemaet.

Dette arbeidet er en del av NTNUs bidrag til EU Horizon Resilex-prosjektet, som har som mål å øke sirkulariteten i solenergibransjen. Prosjektet har mottatt finansiering fra Den europeiske unions HORIZON Action Grant-program under avtalennummer 101058583.

# Table of Content

Preface .....	i
Abstract .....	iii
Graphical Abstract .....	iii
Sammendrag.....	iv
1 Introduction .....	1
1.1 Background and Motivation.....	1
1.2 Objective.....	2
2 Theory and Literature Study.....	3
2.1 The Role of Silicon in Our Society.....	3
2.1.1 Silicon as a Critical Raw Material .....	3
2.1.2 Worldwide Silicon Production.....	3
2.1.3 Silicon Production in Norway .....	4
2.1.4 Future Projections .....	5
2.2 Silicon Production .....	6
2.2.1 Carbothermic Reduction in Submerged Arc Furnace (SAF).....	6
2.2.2 The SisAl Process.....	8
2.3 Silicon Refining.....	10
2.3.1 Slag Refining .....	11
2.3.2 Vacuum Refining.....	19
2.3.3 Directional Solidification .....	23
2.4 Silicon for the Solar Industry .....	25
2.4.1 The Siemens Process.....	25
2.4.2 Material Losses in the Solar Industry .....	25
2.5 Kerf Recycling.....	26
2.5.1 Slag Treatment of Kerf .....	28
2.5.2 Vacuum Refining for Kerf Recycling .....	30
2.5.3 Directional Solidification of Kerf .....	30
2.5.4 Other Strategies for Kerf Recycling .....	31
3 Methodology.....	33
3.1 Materials.....	34
3.1.1 SisAl Metal .....	34
3.1.2 Kerf .....	34

3.1.3	Slag and Quartz.....	34
3.2	Slag Refining.....	35
3.2.1	Small-Scale Experiments.....	36
3.2.2	Medium-Scale Trials.....	38
3.2.3	Large-Scale Trials .....	41
3.3	Vacuum Refining .....	42
3.3.1	Equipment .....	42
3.3.2	Experimental Matrix .....	43
3.3.3	The Course of the Experiment .....	43
3.3.4	Sampling during the Holding Time.....	43
3.4	Directional Solidification .....	44
3.5	Analysis .....	44
3.5.1	Preparation for analysis .....	44
3.5.2	Electron Probe MicroAnalysis (EPMA) .....	45
3.5.3	ICP Analysis.....	45
3.6	Theoretical calculations – FactSage .....	45
4	Results and Discussion .....	47
4.1	Slag Refining.....	47
4.1.1	Small-Scale Experiments.....	47
4.1.2	Medium-Scale Trials.....	57
4.1.3	Large-Scale Trial.....	67
4.1.4	Evaluation of the Suggested Slag Refining Process .....	75
4.2	Vacuum Refining .....	77
4.2.1	Experiment V1 .....	77
4.2.2	Experiments V2 and V3.....	78
4.3	Directional Solidification .....	81
4.4	Evaluation of the Combined Refining Route .....	83
4.4.1	The Purity of the Product.....	83
4.4.2	The Sustainability of the Process .....	83
5	Conclusions .....	85
6	Further work .....	87
7	Bibliography .....	89
8	Appendix .....	93

8.1	First set of Experiments .....	93
8.1.1	Method .....	93
8.1.2	Results .....	93
8.2	Small-Scale Trials (Second Set of Experiments).....	94
8.2.1	Element Mapping by EPMA .....	94
8.3	Medium-scale trials.....	98
8.3.1	Mass Balance .....	98
8.3.2	Material Losses and Silicon Yield .....	98
8.3.3	EPMA .....	99
8.3.4	Metal and Slag Analysis .....	102
8.4	Large-Scale Trials.....	105
8.4.1	Analysis of Metal and Slag .....	105
8.4.2	Theoretical Mass Balance .....	106

# 1 Introduction

## 1.1 Background and Motivation

Silicon is a vital element in products that surround us every day, and the need for a sustainable, circular silicon value chain is pressing. The European Union has characterized silicon as both a critical raw material and a strategic raw material. Silicon is economically important due to its presence in products for power production, electronics, in the chemical industry, and as an alloying element. The supply risk is also substantial, as the EU is dependent on China for 63% of its silicon supply. Silicon recycling rates are low, as the silicon used in the chemical industry and for alloying does not have functional recycling schemes. Solar panels and silicon used in electronics can however be recycled, and it is therefore important to develop robust, circular value chains for these products. [4]

State-of-the-art silicon production is based on the carbothermic reaction where  $\text{SiO}_2$  is reduced to silicon while carbon is oxidized to  $\text{CO}_2$ . As long as carbon capture is not done, this process is inherently environmentally harmful due to the creation of  $\text{CO}_2$ . [5] Alternative routes to produce silicon are important to create a sustainable value chain. The SisAl Process is one alternative method, utilizing aluminothermic reduction. In this process, the  $\text{SiO}_2$  is reduced by aluminium to silicon, and the aluminium forms alumina with oxygen. This process does not produce any greenhouse gases, can utilize secondary raw materials, and both the metal product and the oxide product can be used by several industries. The silicon produced in the SisAl process contains about 75% silicon and has to be refined further if it is to be used in applications demanding high-purity silicon. [1]

The market for silicon-based solar panels is growing rapidly. The production of silicon for solar cells is still mainly linear, with about half of the silicon becoming waste products along the way. The silicon powder waste (kerf) created during wafer sawing is a major waste product. In 2017, the silicon loss during wafer sawing was nearly 160.000 tons, and as solar cell production grows, so does the amount of kerf waste generated[6]. This waste is not only a hazard to the environment if disposed of, due to the fine silicon particles, it is also a resource that should be utilized. Efficient recycling of this material is therefore a key part of making the silicon solar power value chain circular.

This kerf consists of almost pure silicon powder that has gone through several energy- and resource-consuming refining steps. The wafers are cut when the metal has reached solar-grade purity, which is 99,9999% pure silicon. Even though the kerf is made of this pure silicon, it contains some impurities from the cutting process and an inert oxide layer on the surface particles, which causes challenges in the recycling processes. [2], [3]

Kerf recycling has become a popular research topic, and several different methods are being investigated to utilize this challenging powder. The suggested recycling routes consist of several steps, and the products seldom meet the requirements for solar-grade silicon. The need to recycle waste products in the silicon solar panel production chain is pressing, as it, in combination with recycled end-of-life panels, can reduce the need for virgin silicon. [7]



This work is a part of NTNUs contribution to the EU Horizon Resilex project, which aims to increase the circularity in the PV industry. The project has received funding from the European Union's HORIZON Action Grant program under Grant Agreement N° 101058583.

## **1.2 Objective**

The overall objective of this thesis is to find a sustainable route to upcycle kerf and SisAl metal that is suitable for the industrial scale. The process investigated in this thesis consists of slag refining while diluting the kerf with SisAl metal followed by vacuum refining and/or directional solidification. Since the SisAl process utilizes secondary raw materials and the kerf is a waste product, the process will be resource efficient and have a high degree of circularity. The goal is to produce a metal of a purity that can be used to produce solar panels, through blending with metal from other sources.

This thesis aims to investigate how different raw material mixes, holding times, and temperatures affect the composition of the produced metal. The different parameters will be investigated at different scales for the slag refining process, from producing 200 g to 100 kg metal. The effects of the addition of different amounts of quartz in the raw materials mix will be investigated. Theoretical calculations will be done to investigate the possible outcomes of directional solidification of the metal produced through slag refining.

## **2 Theory and Literature Study**

### **2.1 The Role of Silicon in Our Society**

#### **2.1.1 Silicon as a Critical Raw Material**

Silicon is the second most abundant element on the earth, after oxygen, and it is mainly found bound as  $\text{SiO}_2$ . Still, several issues are related to the production and availability of silicon. Due to its high supply risk and economic importance, the European Union has characterized silicon as a critical raw material (CRM) since 2014. [8]

The high economic importance of silicon is due to its irreplaceable presence in numerous products invaluable to modern society. To characterize the economic importance of a material in the EU, the importance of the end-use products using the material is evaluated. Then, the possibilities for substitutions are investigated. Today, 54% of the silicon used in the EU is used in chemical applications, 38% is used for aluminum alloys, 6% is used for solar applications, and 2% is used for electrical applications. All these applications are deemed important. At this time, there is no feasible substitute for silicon in most of these applications. [8]

Silicon has a substantial risk of disruption in supply and is therefore characterized by having a high supply risk. The EU is highly dependent on the import of silicon, and China controls 66% of the global market. As much as 63% of the silicon used in the EU is imported. The possibility of recycling is also a key factor when assessing the supply risk of a material. For silicon in the EU, the end-of-life recycling is close to non-existing, and the end-of-life recycling input rate is evaluated to be 0%. [8]

The EU has set several goals to ensure access to a secure and sustainable supply chain. Among these goals is the goal that no more than 65% of the EU's annual consumption of each of the strategic raw materials at any relevant stage of processing should come from a single third country. This goal is relevant to the silicon supply chain, as silicon is considered a strategic material and the EU is so strongly dependent on China. Another target is that at least 40% of the EU's annual processing of strategic materials should be done domestically by 2030. [4]

#### **2.1.2 Worldwide Silicon Production**

Silicon has played a vital role in our society for a long time. The sum of the production of metallurgical-grade silicon and ferrosilicon has remained relatively stable over the past 10 years, with values varying between 7000 and 8500 thousand metric tons of Si content per year. [9] What has changed, is the use of silicon. More silicon is being used for electronic and solar power purposes. The production of silicon is shifting towards more production of Si rather than ferrosilicon, as illustrated in *Figure 2.1*[10].

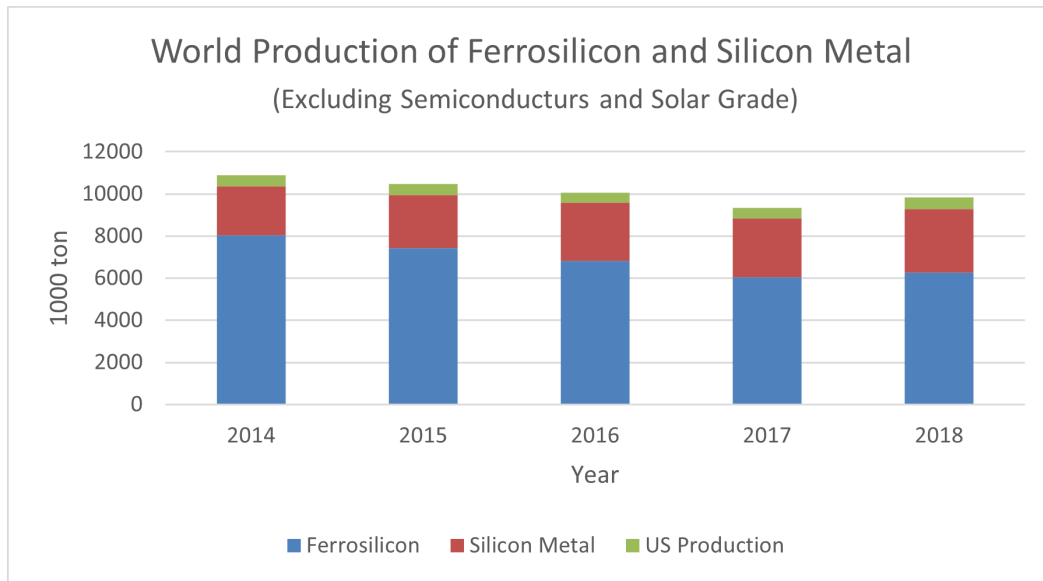


Figure 2.1: World Production of Silicon. US production is added separately as the data for ferrosilicon and silicon metal were not available.[10]

The production of solar-grade silicon (SoG-Si) has increased dramatically. Figure 2.2 shows a tenfold increase from 2007 to 2016.

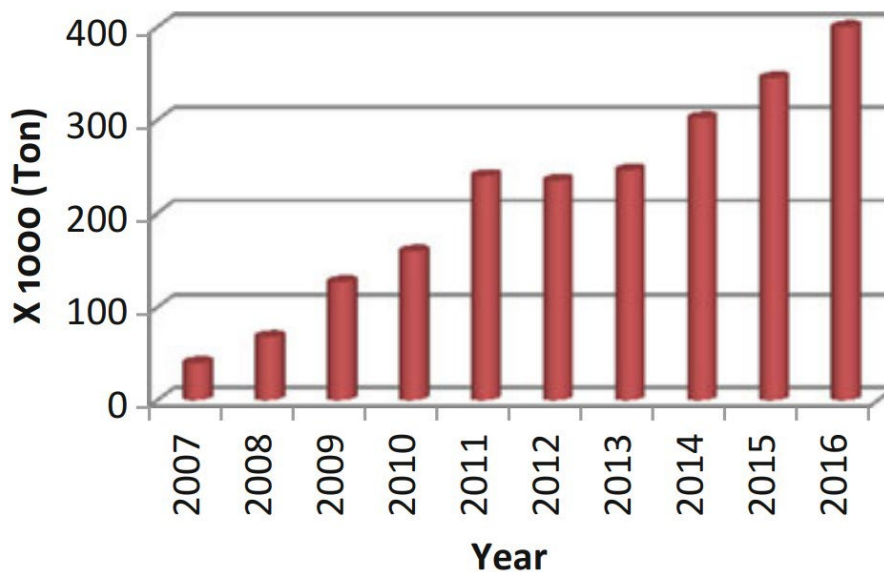


Figure 2.2: Polycrystalline Si production in the world from 2007 to 2016 [11]

### 2.1.3 Silicon Production in Norway

Norway has had a stable annual silicon production at around 150 000 metric tons of silicon metal, and 250 000 metric tons of ferrosilicon for the past ten years [10]. This sums up to a total Si content of 350 000 metrics ton per year, as illustrated by the graph in Figure 2.3. With this number, Norway holds 6% of the global market supply and is the 4<sup>th</sup> largest supplier of Si. [8]

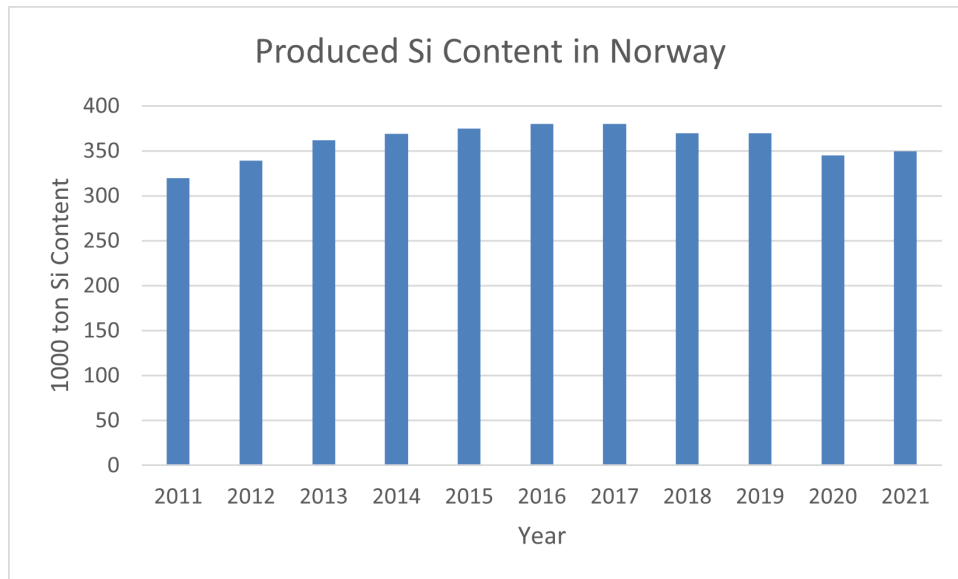


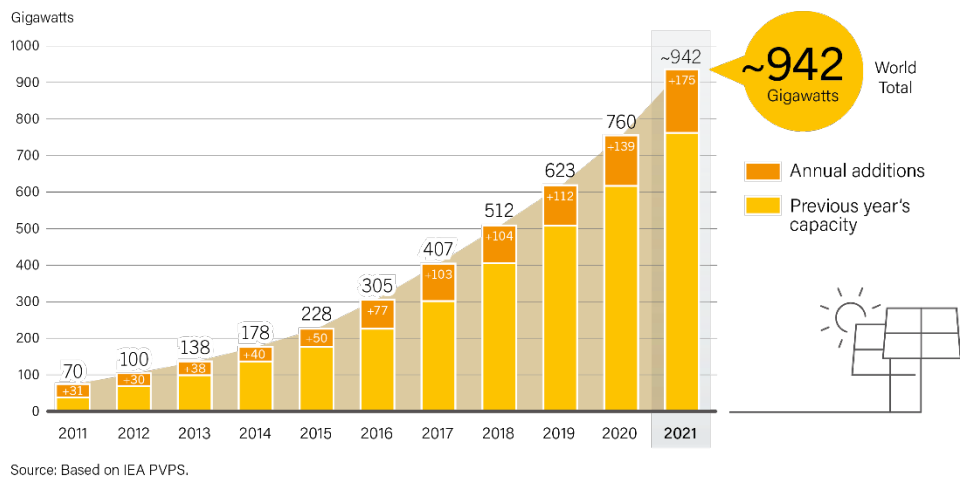
Figure 2.3: Produced Si content in Norway in the last 10 years. [9]

### 2.1.4 Future Projections

Like the rest of society, the process industry is working towards sustainability. The goal set by “Process 21” is that the process reaches zero production emissions by 2050. This goal has a high impact on the priorities of the silicon industry going forward, and circularity through the value chain is an important part of the solution. The use of secondary raw materials and increased recycling rates are both important factors to achieve this goal, along with sustainable power production. [12]

The changes are already highly noticeable, and the global solar PV capacity has increased tenfold over the last decade. This rapid increase is only expected to intensify, and the demand for solar-grade silicon increases with it. [13] The cost of PV energy has seen a significant decrease over time. The price reduction has played a significant role in the global increase in deployment. The REPowerEU Plan will further increase the demand for Si-based solar modules. The world solar PV capacity is expected to 8 fold by 2050. [14]

## Solar PV Global Capacity and Annual Additions, 2011-2021



REN21 RENEWABLES 2022 GLOBAL STATUS REPORT

Figure 2.4: Global capacity of solar PV, and annual additions. From 2011 to 2021. [13]

## 2.2 Silicon Production

### 2.2.1 Carbothermic Reduction in Submerged Arc Furnace (SAF)

Today, the most used method for the production of metallurgical-grade silicon is through carbothermic reduction of quartz lumps in a submerged arc furnace (SAF). The process is illustrated in Figure 2.5. To the left in the picture, the feed of carbon and quartz is illustrated. Following the tubes from the charging chambers, the raw materials are fed into the electric arc furnace, where the reduction of quartz to form silicon takes place. Then, the off-gas is treated, and the liquid metal is often refined through ladle refining before it is solidified. [5]

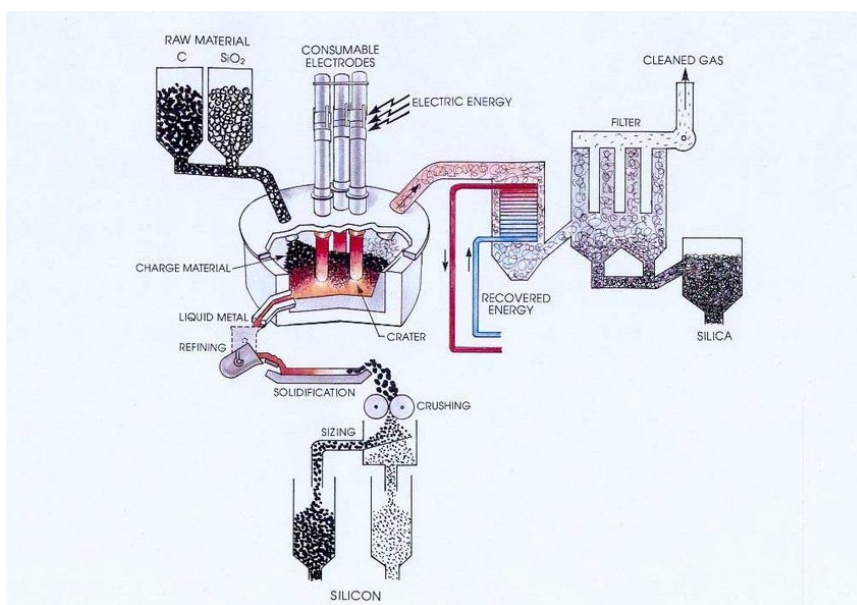
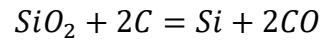
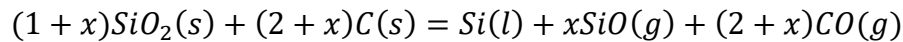


Figure 2.5: Illustration of the production of silicon through a submerged arc furnace. [5]

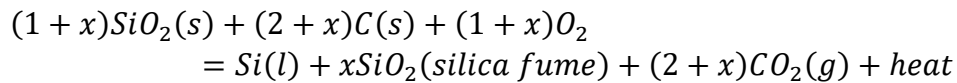
The carbothermic reduction happening in the furnace can be simplified as written in Equation 2.1. This reaction does not take any losses into account, and a more correct description of what happens inside the furnace is described by Equation 2.2. The formation of SiO gas is the main cause of silicon loss in the furnace. Equation 2.3 includes the reactions that take place after the furnace, which is the oxidation of SiO and CO as the gasses react with oxygen in the air. [5]



Equation 2.1



Equation 2.2



Equation 2.3

The physical properties of the raw materials are important. The quartz, which is the SiO<sub>2</sub> source, has to be lumps larger than 10 mm. Materials finer than this cannot be used in the submerged arc furnace (SAF), as a gas flow between materials is essential to the process. The carbon materials that can be used in the process are coal, reactive coke, charcoal, and woodchips. The reactivity of the carbon materials is important and poses limitations on the carbon materials suited for the process. The size of the carbon materials is also important, and they are usually in the range between 1 mm and 30 mm. Purity requirements are placed on both the carbon and the quartz, as the impurities from these materials will affect the composition of the final product. If elements of higher nobility than silicon is introduced, these demand for chemical refining schemes to be removed. [5]

The typical product from these processes is metallurgical-grade silicon (MG-Si). MG-Si is generally defined as alloys containing more than 96 wt.% Si, but more commonly refers to alloys with 98,5 to 99,5 wt.% Si. At this stage, the alloys contain impurities, and the types and concentration of impurities determine that for which the alloy is suited. Further treatments are often required to meet customer requirements, for example for use in solar PV or electronics. [15]

As shown in Equation 2.1, the production of silicon through a carbothermic reduction in a submerged arc furnace is a process producing the greenhouse gas CO<sub>2</sub>. These direct emissions are the largest source of greenhouse gas emissions in the process in some places in the world, but the high energy demand of the process also means that if energy from fossil sources is being used, this also contributes largely to the emissions. Saevarsdottir et al. have studied the greenhouse gas emissions from the production of metallurgical-grade silicon caused by the direct emissions of the process and from the power used in the process in different regions. As shown in Figure 2.6, the direct emissions from the process are assumed equal everywhere, but the emissions from the power production vary widely between Africa at 11 kg CO<sub>2</sub>e/kg Si and EEA at 1 kg CO<sub>2</sub>e/kg Si in 2019. The figure also shows that the emissions from the power production for the combined world production have increased over the past 25 years. [16]

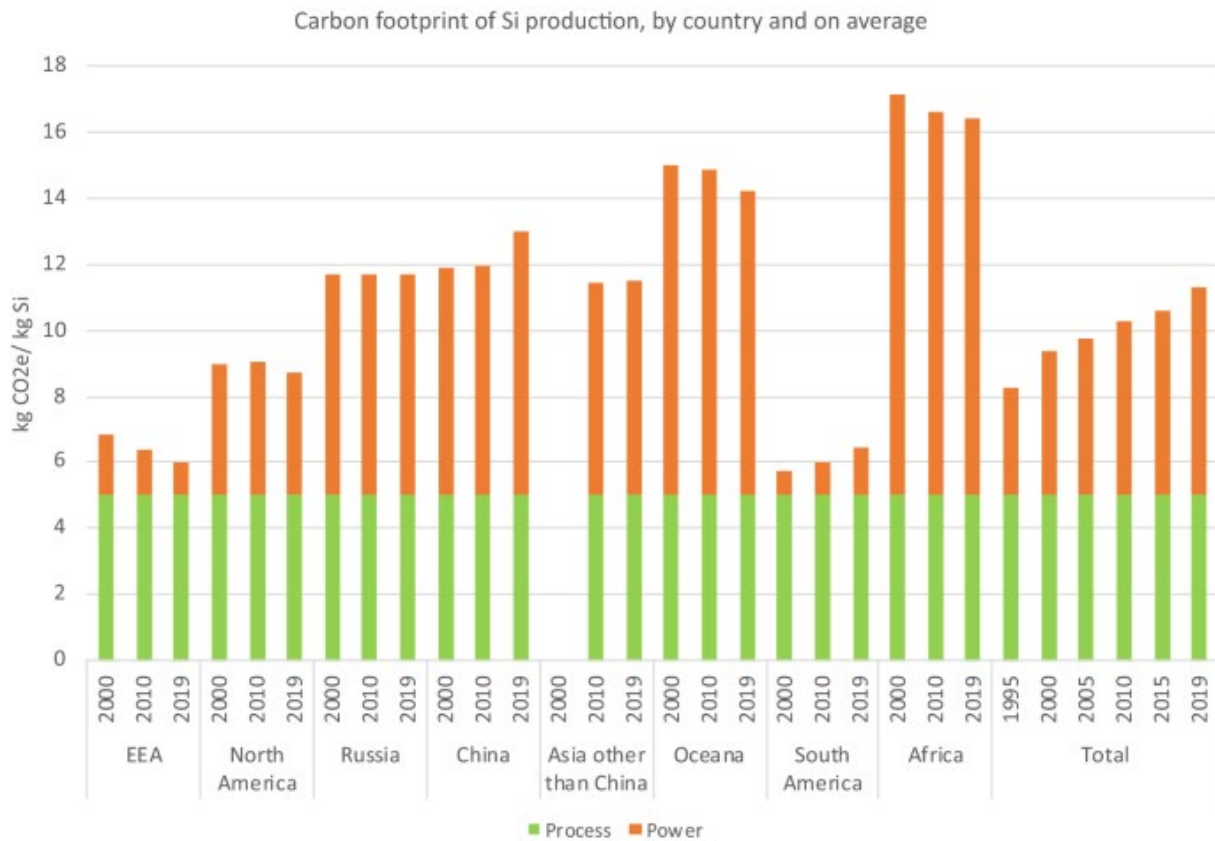


Figure 2.6: The figure shows the total emissions of greenhouse gasses from the production of metallurgical-grade silicon in different regions. The direct emissions from the process are equal for all places, but the emissions from power production differ. [16]

## 2.2.2 The SisAl Process

The SisAl Process is an alternative silicon production process that utilizes secondary raw materials and a sustainable carbon-free production process. The main concept of the SisAl process is the aluminothermic reduction of  $\text{SiO}_2$  in slag. Here, secondary aluminium replaces carbon materials as a reductant, and the result is the production of  $\text{Al}_2\text{O}_3$  rather than  $\text{CO}_2$ . [1]

### 2.2.2.1 Raw materials

Instead of primary raw materials, the SisAl process utilizes materials not suitable for state-of-the-art silicon production. The process uses Al scrap and aluminum dross as reductants, as replacements for the carbon materials used in the SAF-based metallurgical-grade silicon production. [1]

The  $\text{SiO}_2$  needed for the process can also come from secondary sources. Silica fines, which are too fine for traditional silicon production, are suitable for the SisAl process. The process is suited to a range of physical properties of the raw materials, because the reactions occur in a liquid-liquid state, as opposed to the gas-solid reactions in the carbothermic processes. Reactions in the liquid-liquid state mean there are no requirements for the raw materials' particle size or mechanical strength. [1] [17]

### 2.2.2.2 The SisAl Concept

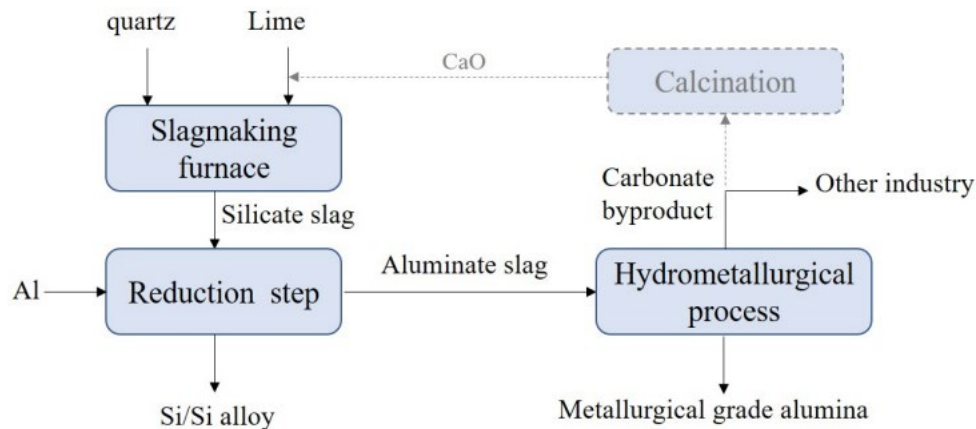
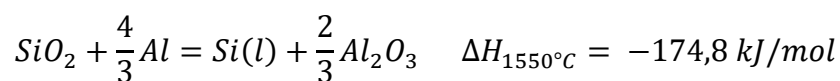


Figure 2.7: Schematic representation of the SisAl process [1].

The first step of the SisAl process is the production of a slag consisting of  $\text{SiO}_2$  and  $\text{CaO}$ . The slag production takes place in a vessel at a sufficiently high temperature to make the molten slag. Then, the aluminium is introduced to reduce the  $\text{SiO}_2$  in the slag and form Si and a calcium aluminate slag. The main reaction is described in Equation 2.4.



Equation 2.4

This reaction is exothermic and produces molten Si at 1550-1600 °C, which means that it has a limited energy demand, as the heat of the reaction can help melt the Al added.

After the molten silicon is produced, the calcium aluminate slag can be separated into  $\text{CaO}$  and  $\text{Al}_2\text{O}_3$ . The  $\text{CaO}$  can be recycled back into the process, and the  $\text{Al}_2\text{O}_3$  can be purified into high-purity alumina or used for a variety of applications in other industries, including primary aluminium production. [1]

### 2.2.2.3 The Products

The SisAl process can produce different Si alloys, depending on the raw material mix, the purity of the raw materials, and the operating choices. MG-Si can be produced, as well as Al-Si alloys of varying composition. The alumina is also a valuable product of the process. [1]

### 2.2.2.4 Benefits

The use of secondary raw materials with low life-cycle  $\text{CO}_2$  footprints gives the process a lower environmental footprint than processes with strict raw material demands. The low energy demand of the process further lowers these emissions compared to state-of-the-art methods for the production of MG-Si. The process is also versatile concerning both raw materials and



products. The process can also valorize byproducts from other processes, such as Si sculls from SAF, which create synergy with the SAF process. [1]

The SisAl process offers a circular approach to metal production, by using other processes' waste and byproducts as raw material and producing high-quality products, suited as input in other industries. The material flow is illustrated in Figure 2.8. [17]

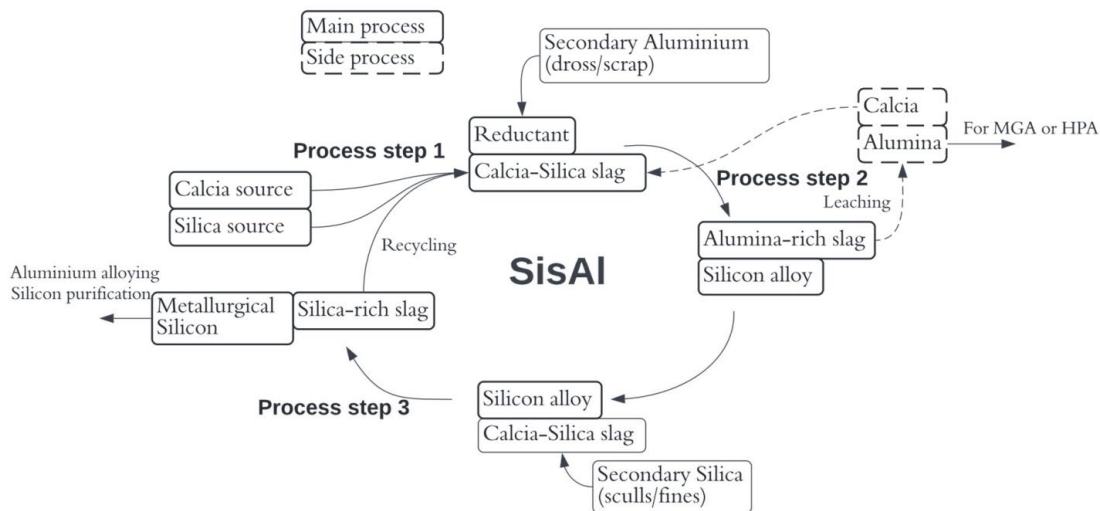
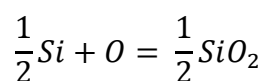


Figure 2.8: Illustration showing the circularity of the SisAl process, through the flow of materials. [17]

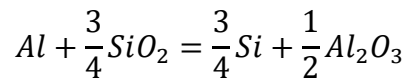
### 2.3 Silicon Refining

Silicon produced through the metallurgical route contains impurities, which limits the possible applications of the material. Refining processes can remove impurities and make silicon suitable for products with strict purity requirements, such as electronics and solar panels. The main impurities relevant for removal from metallurgical-grade silicon are Fe, Ca, Al, Ti, P, and B. The two latter do not occur in great quantities, but their properties make their removal important, and their removal is challenging. The first refining step after silicon production is usually ladle refining, followed by one or more other steps to reach the desired purity. Slag refining, vacuum refining, and directional solidification are all common refining steps and will be elaborated on. [18]

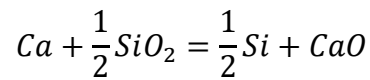
Ladle refining takes place directly after the silicon production when the molten silicon is tapped into a ladle. In the ladle, a mixture of oxygen and air is bubbled through the melt, and the oxygen reacts with silicon through Equation 2.5. Then, the air bubble will transport the SiO<sub>2</sub> upwards in the melt, and it can react with Al and Ca on its way up through Equation 2.6 and Equation 2.7, respectively. Oxidative ladle refining is suitable for removing elements less noble than silicon.



Equation 2.5



Equation 2.6



Equation 2.7

To avoid the oxides from forming inclusions in the melt, slag makers, such as a mix of CaO and SiO<sub>2</sub> can be added to the ladle. With more oxides present, all oxides can be absorbed into one oxide phase, which can be separated from the metal. [19]

### 2.3.1 Slag Refining

Slag refining is widely used for all high-temperature metallurgical processes, including the refining of silicon. The purpose of slag refining is to remove impurities, and in short, this is done by oxidizing the impurities and transferring them to a separate melt, immiscible with the molten metal. This separate melt is a mix of oxides and is called slag. The oxidation of impurities is based on the chemical equilibrium of redox reactions, where SiO<sub>2</sub> is reduced, and the impurity is oxidized. The oxidized impurities are then absorbed into the slag. [20] [21]

Slag refining can remove elements that have a higher affinity for oxygen than Si. The elements Al, Mg, Ba, and Ca are all good candidates for removal through slag refining. The most widely used binary slag system in research regarding metallurgical-grade Si is CaO- SiO<sub>2</sub>. Although this system is well suited for refining metallurgical-grade Si, other binary systems and multi-component systems have become popular research topics, as they can offer different properties, such as lower viscosities and melting points.[22] [23]

#### 2.3.1.1 General Slag Properties

Several criteria have to be met to enable good slag refining. Firstly, the slag and the molten metal phase have to be immiscible. Secondly, the slag should not introduce any new impurities to the melt. Therefore, the slag must be of high purity. Thirdly, the reactivity of the slag is important. Lastly, the physical properties of the slag are crucial. This concerns both viscosity and density. [20]

The purity of the product from slag refining can only be as good as the purity of the slag itself. If the slag removes some impurities from the melt, but at the same time introduces others, the outcome might even be worse than the initial metal if the introduced impurities are difficult to remove. Therefore, it is important to have good knowledge of the slag composition before using it for refining.

The reactivity of the slag can be described in different ways, but slag basicity is a widely used indicator. The slag's basicity is determined by the basicity and acidity of the oxides that make up the slag. The basicity or acidity of an oxide is determined by its structural properties. While

acidic slags promote the slag network polymerization, the basic slags depolymerize the slag. [20]

Basic oxides, such as CaO, BaO, or N<sub>2</sub>O, provide oxide ions necessary for the absorption of impurities into the slag. The ion is provided through the dissociation of the oxide into a metal cation and an oxygen anion. [24] Basic oxides have a high affinity for SiO<sub>2</sub>, and excessive amounts of these can hence lower the removal efficiency of impurities by decreasing the oxygen potential. A good balance is therefore important, as an increase in slag basicity is expected to improve impurity removal, but if the oxygen potential is decreased too much, it can have a negative effect. [23]

To be able to compare the basicity of different slags, the optical basicity for a molten slag can be calculated using Equation 2.8.  $\Lambda_i$  is the theoretical optical basicity of pure oxide  $i$ ,  $x_i$  is mole fraction and  $n_i$  is the number of oxygen atoms in each oxide component.

$$\Lambda = \frac{\sum x_i n_i \Lambda_i}{\sum x_i n_i}$$

Equation 2.8

The basicity of the slag also determines which oxides they are prone to react with. Acidic oxides prefer to react with basic oxides to be stabilized. An example is the acidic boron oxides, which prefer to react with basic oxides to become borate. [20]

The structural changes caused by polymerization or depolymerization affect the thermodynamic properties of slag. The activity coefficient  $\gamma$  of SiO<sub>2</sub> is strongly dependent on the slag composition.  $\gamma_{SiO_2}$  decrease with increasing SiO<sub>2</sub> content (with some exceptions) and increase with increasing cation field strength (Mg>Ca>Sr>Ba>Li>Na>K). [20]

The physical properties of the slag are also determined by the slag composition. The density of the slag depends on the oxides chosen for the slag, and their mixing ratios. The density is important only related to the density of the metal, as a difference in density makes it easier to separate slag and metal. The viscosity of slag is also determined by slag composition, but temperature also has a mentionable impact. [20]

### 2.3.1.2 Properties of CaO-SiO<sub>2</sub>-Al<sub>2</sub>O<sub>3</sub>-slag

The slag system used in the experiments presented in this thesis is the CaO-SiO<sub>2</sub>-Al<sub>2</sub>O<sub>3</sub>-slag system. The ternary phase diagram of the system is presented in Figure 2.9, with the initial slag composition marked with a blue X. The initial slag used was a 1,1/1 CaO-SiO<sub>2</sub>-slag. During the experiments, the slag composition changes, both due to the addition of more SiO<sub>2</sub> in some of the experiments and due to the oxidation of impurities in the metal.

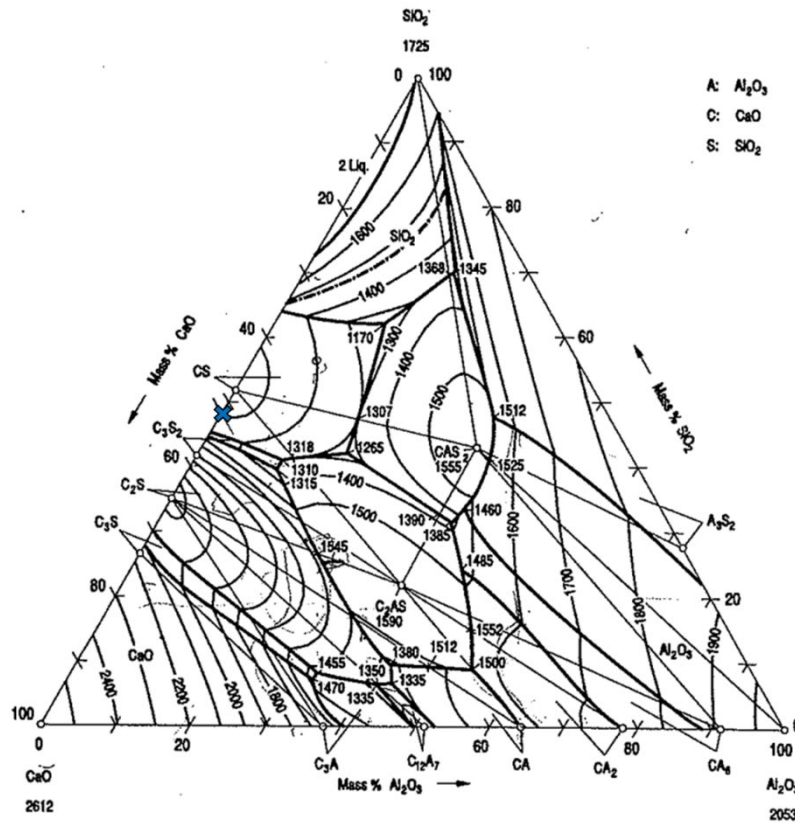


Figure 2.9: Ternary phase diagram of the slag system, blue x shows the initial composition of the slag that will be used in the experiments in this thesis.

The density of the slag is presented in Figure 2.10. In general, higher CaO content increases the density of the slag. As mentioned, the density of the slag is only interesting related to the density of the metal. The density of pure silicon can be calculated through Equation 2.9.[5] The relevant temperature for the experiments described in this paper is 1550 °C, and the corresponding density of pure silicon is 2,49 g/cm<sup>3</sup>. This is slightly lower than the densities for the relevant slag compositions.

$$\rho(Si)_{liq} = 2533 - 0,45(T - T_m)[kg/m^3]$$

Equation 2.9 [5]

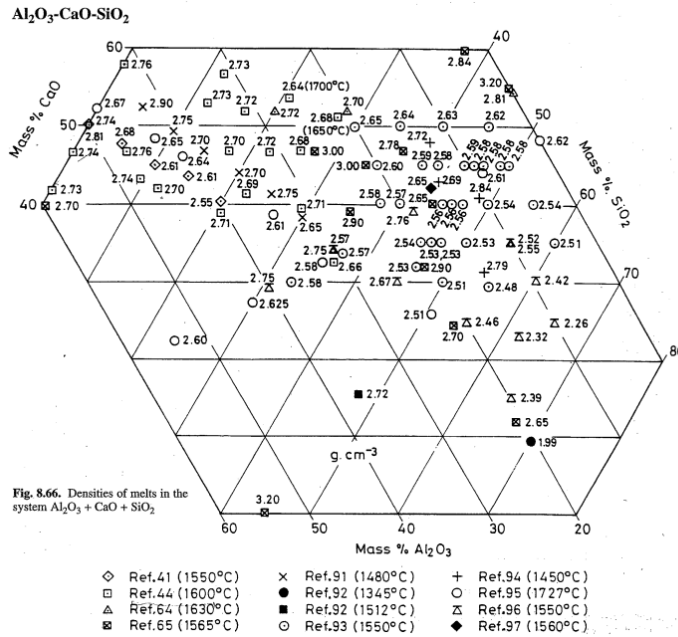


Figure 2.10: The density of the ternary  $\text{CaO-SiO}_2\text{-Al}_2\text{O}_3$ -slag at different compositions and temperatures is shown. The different sources referred to in the figure refer to the sources in the Slag Atlas [25].

The viscosity diagram for the same slag system is shown in Figure 2.11. The lines in the diagram show constant viscosities through varying concentrations. All numbers are given for 1550 °C. A general trend that can be seen in the diagram is the increase in viscosity with the increase of  $\text{SiO}_2$  and a decrease of  $\text{CaO}$ . This is due to the network-forming properties of the slag, and the increased acidity of the slag. The viscosity of the silicon at the same temperature can be found by using the equation presented by Sato et al.[26] given in Equation 2.10. At 1550 °C, this gives a viscosity of 0,53 mPa s for molten silicon, which is much lower than for the slag.

$$\log \eta / \text{mPa s} = -727 + 819/T$$

Equation 2.10[26]

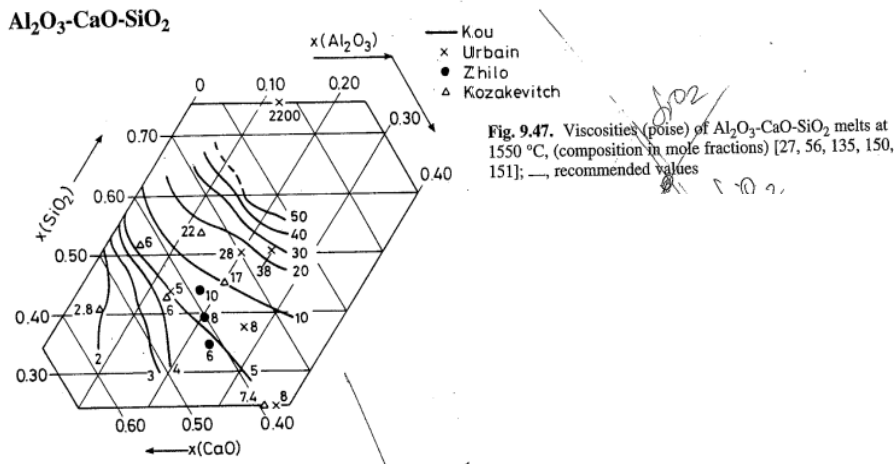
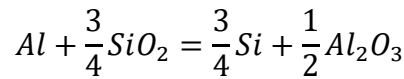


Figure 2.11: The figures show the viscosity of the  $\text{CaO-SiO}_2\text{-Al}_2\text{O}_3$ -slag at 1550 °C at different compositions and from various sources. The different sources referred to in the figure refer to the sources in the Slag Atlas [25].

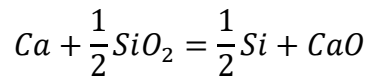
### 2.3.1.3 Slag Refining for Removal of Ca and Al

Slag refining can be used for the removal of several elements, but in this thesis, the removal of Ca and Al will be elaborated on. These are the main impurities in the raw materials used in slag refining process that is investigated. The system consists of a CaO-SiO<sub>2</sub>-slag, a silicon alloy with about 10% Al and 16% Ca, and silicon sawing dust (kerf).

The goal of the refining is to oxidize the Al and Ca in the molten metal and transfer it to the slag. This is done through redox reactions with SiO<sub>2</sub> in the slag, as shown in Equation 2.11 and Equation 2.12. These reactions assume a local equilibrium between the reduction of SiO<sub>2</sub> and the oxidation of impurities.[5] These reactions depend on the oxygen potential at the slag-metal interface, which again is dependent on the activity of SiO<sub>2</sub>.



Equation 2.11



Equation 2.12

The minimal concentration possible of an impurity in the molten metal is dependent on the ratio of the oxide activity of the oxide of the impurity, and the oxide of the metal. The concentration is also related to the activity coefficient of the impurity, and, through  $k$ , the activity of the metal. Equation 2.13 and Equation 2.14 demonstrate the limiting concentrations for Al and Ca in Si, respectively. [5]

$$[\%Al]_{Si} = k_{Al,Si} \cdot \frac{1}{\gamma_{Al}} \cdot \frac{(a_{Al_2O_3})^{\frac{1}{2}}}{(a_{SiO_2})^{\frac{3}{4}}}, \quad \text{with } k_{Al,Si} = \frac{(a_{Si})^{\frac{3}{4}}}{K_{Al,Si}} \cdot \frac{100}{M_{Si}} M_{Al}$$

Equation 2.13

$$[\%Ca]_{Si} = k_{Ca,Si} \cdot \frac{1}{\gamma_{Ca}} \cdot \frac{a_{CaO}}{(a_{SiO_2})^{\frac{1}{2}}}, \quad \text{with } k_{Ca,Si} = \frac{(a_{Si})^{\frac{1}{2}}}{K_{Ca,Si}} \cdot \frac{100}{M_{Si}} M_{Ca}$$

Equation 2.14

The equilibrium constant is calculated from the expression  $K = \exp\left(-\frac{\Delta G_T^0}{RT}\right)$ , where  $\Delta G_T^0$  is the change in standard Gibbs energy for the reactions presented in Equation 2.11 and Equation 2.12.,  $\gamma_{Ca}$  is the activity coefficient for Ca and  $a_{CaO}$  is the activity of CaO. [5]

The amount of slag needed to refine an alloy of a given composition, with a given target composition, can be calculated through Equation 2.15. This can be done for both Ca and Al, and the highest value gives the minimal amount of slag needed in the refining.[5]

$$W_R = \frac{\Delta[\%Al] \cdot \frac{M_{Al_2O_3}}{2M_{Al}}}{(\%Al_2O_3)_R} \cdot 1000 \frac{kg}{tonne \text{ alloy}}$$

Equation 2.15

$\Delta[\%Al]$  is the difference between initial and target concentration of Al in the metal, the M values are molar masses, and  $(\%Al_2O_3)_R$  is the amount of  $Al_2O_3$  in the refining slag. [5]

As the impurities are transferred from the metal to the slag, the composition of both change. If equilibrium conditions apply; the final composition of metal and slag are related as described in the solution diagram shown in Figure 2.12. The diagram shows the equilibrium concentrations of Al and Ca in a melt in equilibrium with different compositions of the  $SiO_2$ -CaO- $Al_2O_3$  slag at 1873 K. The target slag composition is hence important, as it is determining the limiting concentrations of Al and Ca in the melt. [15]

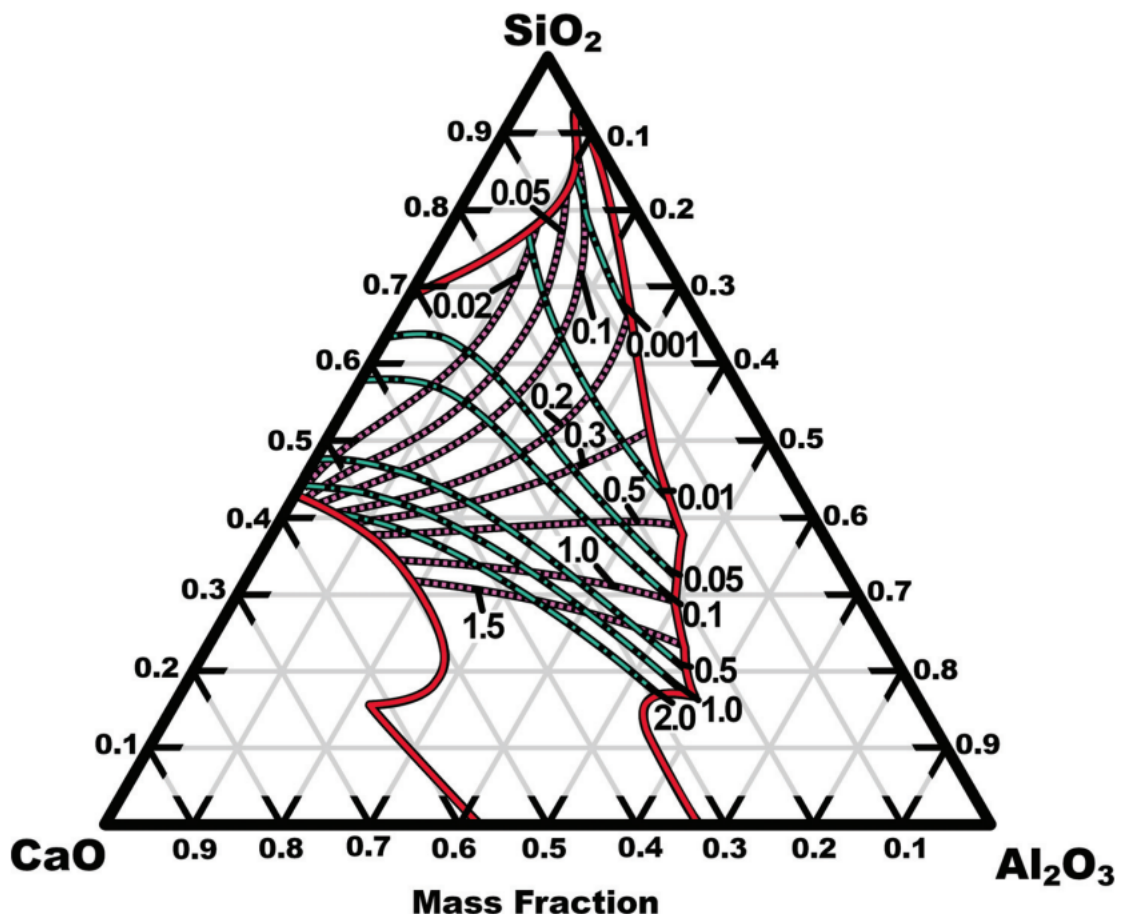


Figure 2.12: Solution diagram for Ca and Al dissolved in Si (l) where the silicon alloy is in equilibrium with a  $SiO_2$ -CaO- $Al_2O_3$  slag, at 1873 K. The dissolved concentrations of Ca (blue line with dot) and Al (pink stippled lines) are in wt.%. From Bjørnstad et al.[15]



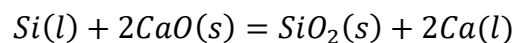
The diagram was created by Bjørnstad et. al. using FactSage7.3, supplemented by a new database of the activity coefficient of Ca in an infinitely dilute solution. The new database was based on a study by Jacobsen and Tangstad. [15], [27]

Slag refining of MG-Si has been widely investigated as an approach to remove B and P. [23], [24], [28] Some studies are however also investigating slag refining for removing other impurities, such as Huang et. al. [29] Following, some relevant studies on slag refining are presented.

A study by Huang et. al [29] investigated slag refining of metallurgical-grade silicon with CaO-SiO<sub>2</sub>-CaCl<sub>2</sub> (45%, 45%, 10%) slag and CaO-SiO<sub>2</sub>-CaF<sub>2</sub> (37,5%, 37,5%, 25%) slag, with a 1:1 metal-to-slag ratio. The study found that both slags were suited for removing B and Al, but for P, Fe, Ti, Mn, and Ca, the treatment either had no effect or introduced more impurities. The study also found that the metallic impurities tended to form intermetallic compounds in the precipitate phase after the slag refining.

Golam and Kahajavi [30] studied slag refining of Si-20wt.% Fe with a quaternary CaO-Al<sub>2</sub>O<sub>3</sub>-SiO<sub>2</sub>-Na<sub>2</sub>O slag. The main focus of the study was B and P removal from the alloy, and the highest B removal was found for slag with CaO/SiO<sub>2</sub> equal to 1,5, SiO<sub>2</sub>/Al<sub>2</sub>O<sub>3</sub> up to 2 and 10 wt.% Na<sub>2</sub>O. This slag had high basicity, which enabled B removal from the melt but also had sufficiently high oxygen potential from the SiO<sub>2</sub> to achieve a good oxygen potential at the slag-metal interface.

Jakobsson and Tangstad [27] investigated the activities and distribution of Ca and Mn between Si and CaO-MgO-SiO<sub>2</sub> slags at 1873 K. They found that the higher the CaO concentration in the initial slag, the higher concentration of Ca in the metal. This is due to the increased activity of CaO and decreased activity of SiO<sub>2</sub>, and the equilibrium in Equation 2.16 is shifted to the right. As part of their study, they did an experiment where calcium was added to the silicon before the slag refining took place, and they found that this experiment, with five wt.% Ca in the metal, gave results in line with the other results.



Equation 2.16

A recent study by Shan et al. investigated the slag system SiO<sub>2</sub>-CaO-Al<sub>2</sub>O<sub>3</sub> for the removal of Fe, Al, Ca, and Ti. Different CaO/SiO<sub>2</sub> ratios were investigated, and at 1550°C CaO/SiO<sub>2</sub>=0,38 was found to have the highest removal ratio for metallic inclusions. The removal ratios of Fe, Al, Ca, and Ti were 27,1%, 68,7%, 25,1%, and 99,1%, respectively. [31]

#### 2.3.1.4 Kinetics – Holding Time and Temperature

The refining temperature directly affects slag chemistry and is, thus, an important parameter in slag refining[32]. The viscosity of the slag is also influenced by temperature. Higher temperatures reduce the slag viscosity and hence facilitate mass transfer. [33]

The kinetics of the mass transfer of Ca and Al are important for the determination of the operating parameters in slag refining. It is crucial to have a high enough temperature and a sufficiently long holding time to reach the desired compositions.



Bjørnstad [15] found that the mass transfer behavior of Ca and Al showed similarities, indicating that the individual mass transfer of each is dependent on the other. The studied system was the mass transfer of Ca and Al from a liquid synthetic  $\text{SiO}_2\text{-CaO-Al}_2\text{O}_3$  slag to 99,999% pure Si at 1873K. Different holding times were investigated, and the study suggests mass transfer coefficients  $k_{t,Ca} \approx 3 \cdot 10^{-6} \text{m/s}$  and  $k_{t,Al} \approx 1 \cdot 10^{-5} \text{m/s}$  for Ca and Al respectively. The mass transfer coefficients are not necessarily the same from alloy to slag as they are from slag to alloy, but the trend is believed to be similar.

### 2.3.1.5 Stirring

Stirring during slag refining can increase the mass transfer rate and hence reduce the holding time. Stirring can both be done mechanically and by the use of gas.

#### Mechanical Stirring

Mechanical stirring has been investigated in several studies for a variety of systems and it has been found to improve mass transfer rate profoundly, as well as improved removal of certain impurities.

White and Sichen investigated how mechanical stirring influenced the rate of mass transfer in the slag refining of silicon. In the study, it was found that transient interfacial phenomena occurred related to the mass transfer of Ca. Further, the author suggests that the reduction of CaO at the interface leads to a rapid, temporary drop in apparent interfacial tension. This, in combination with stirring, facilitated emulsion formation, which increased the interfacial area by at least one order of magnitude. This increase in the interfacial area promotes the transfer of B, making mechanical stirring an effective way to increase the reaction rate of B extraction. When the slag and metal have reached equilibrium, the surface tension increases, and the emulsion collapses. [34]

Another paper studied the kinetics of the removal of Al from Si melt to slag with mechanical stirring. This paper found that slag and metal reached equilibrium after 300 seconds when stirring was done, and that under these conditions the reaction rate was controlled by the chemical reaction, not the amount of slag present or the slag composition. [35]

Tanaka et al. [36] studied the flow characteristics related to liquid/liquid mixing patterns in an impeller-stirred vessel through a two-dimensional experiment and a CFD (computational fluid dynamics) analysis and a system consisting of liquid paraffin and water. They found that the vertical upward flow near the wall gave one or two circulation flow zones, one near the oil/water interface and the other below it. The downward flow formed only one circulation flow zone near the bottom. The study also found that a higher rotation rate resulted in increased cross-sectional mean water velocity and turbulence energy near the oil/water interface.

#### Gas Stirring

Gas stirring has also been investigated broadly, but mainly for steelmaking.

Valentin et al. investigated stirring with Ar gas through a porous plug through both CFD and experimental work in a 170-t ladle. In the case of a gas flow rate of 27 STP  $\text{m}^3/\text{h}$ , the gas started by moving directly upwards from the inlet. Further up in the ladle, the momentum from the

circulating steel affected the path of the bubbles. Lastly, the bubbles reached a breakthrough zone at the surface, and experiments revealed typical open eyes. This high gas flow rate resulted in more widely spread bubbles at the surface, due to large circulation loops in the steel. Emulsification of the top slag can theoretically become an issue when the gas flow rate is above 15 STP m<sup>3</sup>/h, according to their calculations. [37]

Another study of gas stirring in steel production was performed by Shivaram et.al. [38] The paper compared the bottom porous plug and ported lances lowered into the melt. Through both computational fluid dynamics and plant observations, the study found that the use of bottom plugs was the most effective. The article also included schematics of how the gas lance was shaped, with the hole at a 45-degree angle, blowing the gas down in the melt.

### **2.3.2 Vacuum Refining**

Vacuum refining utilizes the difference in vapor pressure of elements to evaporate impurities from the molten metal. This technique is suitable for the removal of several of the typical impurities in metallurgical-grade silicon, such as P, Ca, Mg, Mn, and Al. Several factors participate in the determination of whether an element can be removed from a silicon melt or not.

The difference in vapor pressure between different liquid metal components at elevated temperatures is the first parameter crucial for determining if an impurity can be removed through vacuum refining. If an element has higher vapor pressure than silicon at a given temperature, that element can be removed through vacuum refining. Figure 2.13 show the vapor pressures of some pure substances as a function of temperature. All elements above silicon in this figure can be removed through vacuum refining, as they will evaporate from the molten silicon before the silicon itself will evaporate. [18]

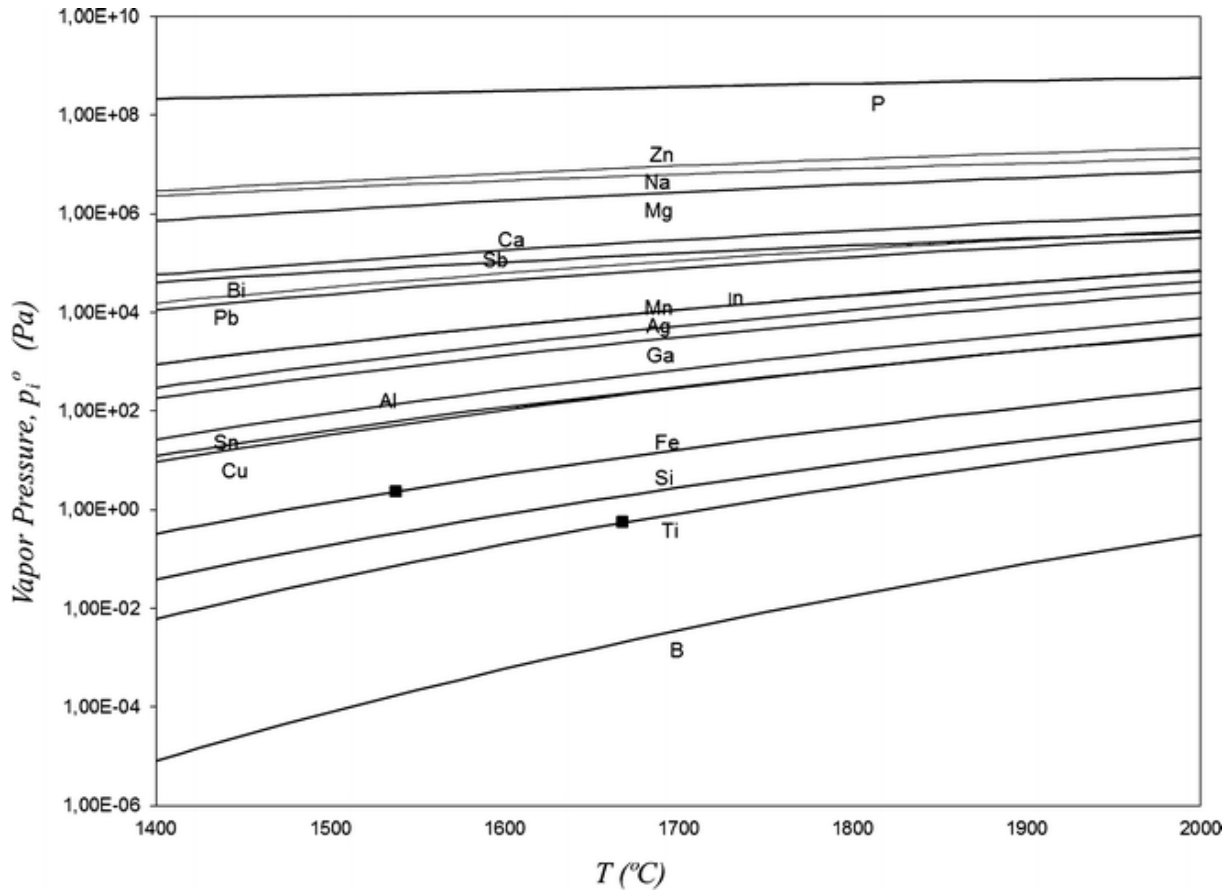


Figure 2.13: The changes in standard vapor pressure of pure substances with temperature. Symbol ■: melting point.[18]

This figure, however, only shows the vapor pressure of pure substances. When a substance goes into solution, the vapor pressure changes from the initial  $p_i^0$  to  $p_i^e$ . Assuming that the vapor above the melt has ideal, equilibrium behavior, the activity of the element  $i$  can be written as

$$a_i = \frac{p_i^e}{p_i^0} = \gamma_i X_i$$

Equation 2.17

When dividing the equilibrium partial pressure of impurity by the equilibrium partial pressure silicon, the following ratio is obtained:

$$\frac{p_i^e}{p_{Si}^e} = \beta_i \frac{X_i}{X_{Si}}$$

Equation 2.18

where  $\beta_i$  is the separation coefficient of impurity  $i$ , and can be written as:

$$\beta_i = \frac{p_i^0 \gamma_i}{p_{Si}^0 \gamma_{Si}}$$

Equation 2.19

The separation coefficient of an impurity is important when determining if an element will be evaporated from silicon. The separation coefficient describes the relationship between the concentration of an impurity in the melt and the gas. If the separation coefficient is smaller than unity, the equilibrium concentration of the element in silicon is more than that in the gas phase, which means that the impurity cannot be separated. If the separation coefficient is unity, the concentrations in the silicon and the gas phase are equal. When the separation coefficient is larger than unity, the equilibrium concentration of the element in the gas phase is more than in silicon, meaning that the element can be evaporated from the silicon melt. Figure 2.14 show the distribution coefficients of some elements dissolved in silicon. Most elements shown here have positive values, indicating that they can be removed through vacuum refining. Fe, B, and Ti are the exceptions, with negative separation coefficients. [18]

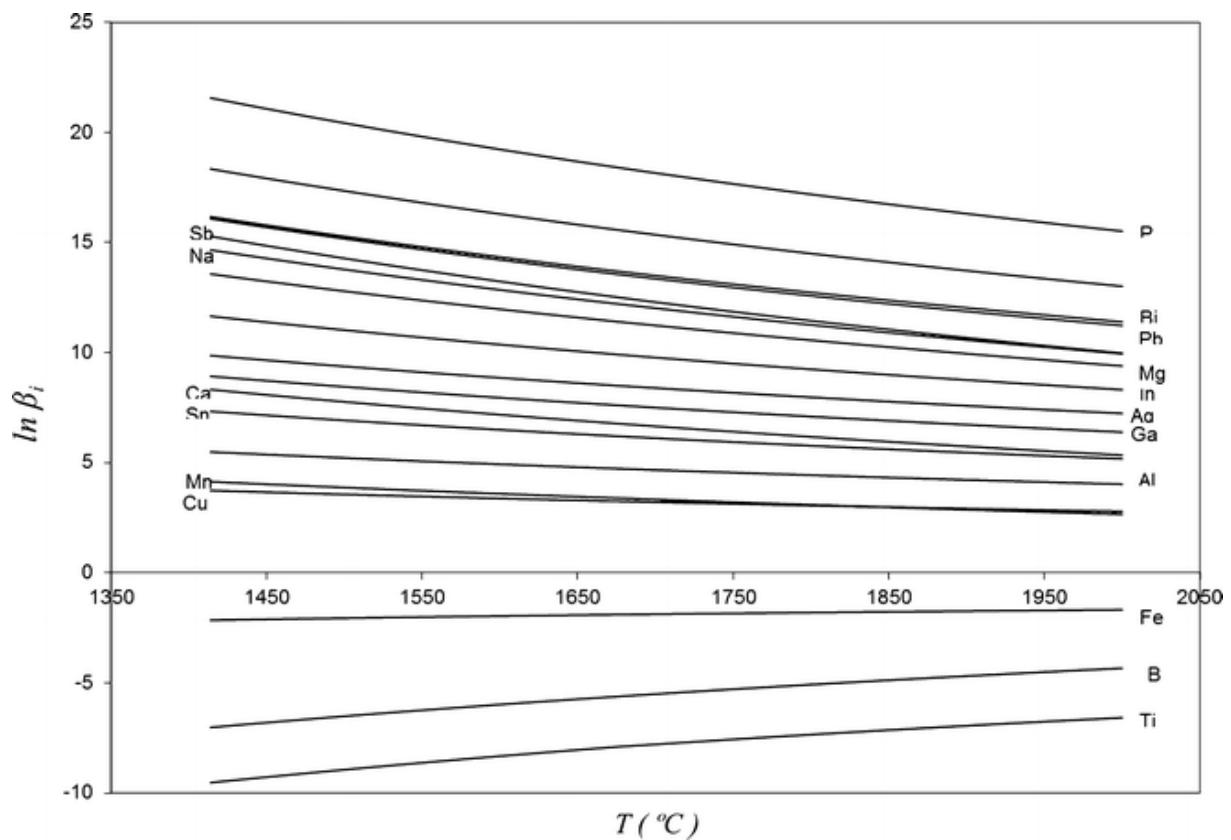


Figure 2.14: The graphs show the separation coefficients as a function of temperature for the dissolved elements in molten silicon.[18]

The theoretical parameters explained so far are valid under equilibrium conditions, but vacuum refining is a process under nonequilibrium conditions. Pressures less than the vapor pressure of the melt are maintained by using a vacuum pump. The ratio of the vacuum evaporation rates of impurity  $i$  and silicon can be written as[18]:

$$\frac{\dot{n}_i}{\dot{n}_{Si}} = \alpha_i \frac{(m_i^0 - m_i)}{(m_{Si}^0 - m_{Si})}$$

Equation 2.20

Where  $\alpha_{i-Si}$  is the volatility coefficient for element  $i$  in Si, and can be expressed as[18]:

$$\alpha_{i-si} = \frac{\gamma_i p_i^0}{\gamma_{Si} p_{Si}^0} \left( \frac{M_{Si}}{M_i} \right)^{1/2}$$

Equation 2.21

where  $\gamma_i$  is the activity coefficient of i,  $p_i^0$  is the standard vapor pressure of i, and  $M_i$  is the molar mass of i.

The volatility coefficient is dependent on the separation coefficient and the atomic weight of the impurity. This shows that the atomic weight also influences the volatility of an impurity. Figure 2.15 show the volatility coefficients of the same elements as the previously presented separation coefficients. When the volatility coefficient is larger than zero, the evaporation of the impurity dominates the evaporation of silicon. When the volatility coefficient is unity, the same amounts of impurity and silicon are expected to evaporate from the melt. When the volatility coefficient is smaller than zero, the evaporation of silicon dominates the evaporation of the impurity, meaning the impurity cannot be removed through vacuum refining. The most significant difference between this graph and the graph showing the separation coefficients is that Fe has a volatility coefficient above zero. This means that Fe can be evaporated from silicon through vacuum evaporation, although the process is slow. A high silicon loss is also expected when eliminating small amounts of Fe. [32] [18]

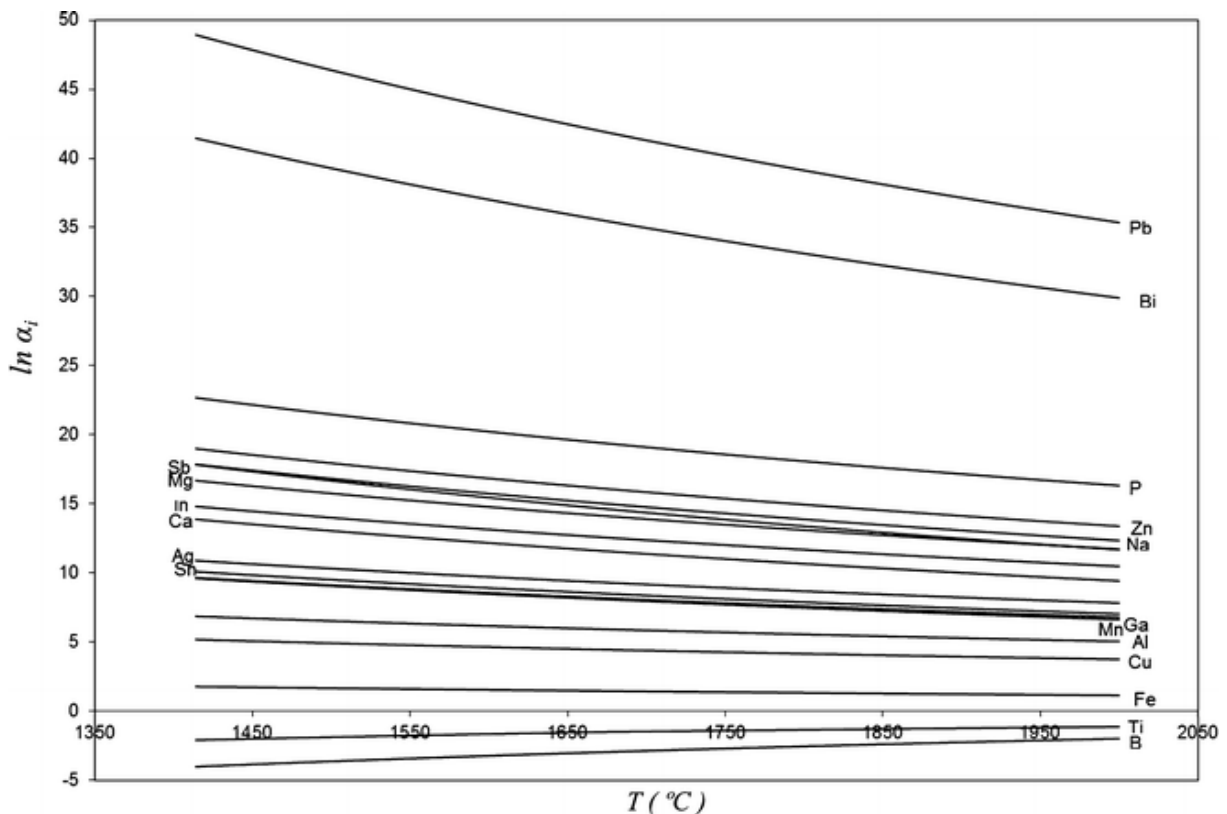


Figure 2.15: The graphs show the volatility coefficient as a function of temperature for a group of elements typically present in metallurgical-grade silicon. [18]

Temperature and vacuum conditions are key factors in vacuum refining. As all the presented graphs show, all variables discussed are dependent on temperature. Higher temperatures

increase the vapor pressure of an element, but the separation coefficients both tend to move towards unity when the temperature increases. [18]

A study by Hoseinpur and Safarian investigated P removal from silicon through vacuum refining at ultra-high temperatures (up to 1900°C). The study found that P could be removed completely from silicon melts with 92,71 ppmw P. The study also investigated silicon evaporation during refining. The silicon loss was increased with increasing temperatures up to about 1800 °C, where the silicon loss had a rapid decrease before starting to increase again. The power consumption of the process was increasing evenly with increasing refining temperatures up to 1800 °C, where the power requirement had a rapid decrease before leveling out. The study also concluded that the use of ultra-high temperatures in vacuum induction refining processes reduced the overall power consumption needed to produce solar-grade silicon.[39]

Vacuum refining has also been investigated to remove Ca, Al, and P from crude metallurgical-grade silicon. Deng et al. investigated the use of vacuum refining after smelting and after oxidative ladle refining and found it beneficial in both cases. When vacuum refining was conducted after smelting with 3 – 5 mPa at 1723 K for 2,5 hours, the removal ratio of Ca, Al, and P reached 82.56%, 52.91%, and 79.17%, respectively. When the same vacuum process was applied after oxidation refining, the cumulative removal efficiencies were 98,08% for Ca, 83,85% for Al, and 79,17% for P. The study concluded that vacuum refining can complement or replace oxidation refining to purify crude metallurgical-grade silicon. [40]

### 2.3.3 Directional Solidification

Directional solidification is a refining process based on the distribution of impurities between solid and liquid metal. Most metallic impurities collect in the liquid phase and will move with the liquid phase during solidification. P, B, and O are the most important elements that cannot be removed through directional solidification. As the metal solidifies, the impurities gather in the melt, so the last part of the melt to solidify will thus hold the highest impurity content. Directional solidification is a much-used process for refining metallurgical-grade silicon, as many of the impurities present can be removed through this process. [19] [20] [33]

The distribution of impurity  $i$  between liquid and solid silicon can be described through the distribution coefficient:

$$k_i^0 = \frac{x_i^S}{x_i^L},$$

Equation 2.22

where  $x_i^S$  is the mole fraction of element  $i$  in the solid phase, and  $x_i^L$  is the mole fraction in the liquid phase. The solubility in silicon can be difficult to measure, both because it is very low for many impurities, and because some impurities segregate to the grain boundaries and hence lower the measured concentration in the crystalline material. [33]

Most metallic impurities found in metallurgical-grade silicon have low distribution coefficients and are suitable for removal through directional solidification [21]. One study found the distribution coefficients for metallic impurities in silicon to range from  $8 \cdot 10^{-2}$  for Al to  $1,7 \cdot 10^{-8}$  for W [41]. Some crucial elements in silicon refining for the solar industry are B and P. These elements are not suited for removal through directional solidification as their distribution coefficients are 0,8 and 0,35, respectively. [18]

The mold velocity out of the hot zone of the furnace highly contributes to the impurity distribution in the final ingot, and the micro and macro structures. A study by Martorano et al. investigated velocities between 5 and 110  $\mu\text{m/s}$ . They found that at the slowest velocity, the macrostructure consisted of columnar grains that were oriented approximately parallel to the ingot axis. With higher velocities, the grains became thinner and more inclined in the radial direction. The main impurities were found in the form of participated particles containing Si, Fe, Al, and Ti. These particles were found in the top of all ingots, and also in the middle and bottom of the ingots with higher mold velocities, with increasing frequency at higher velocities. For velocities of 5 and 10  $\mu\text{m/s}$ , directional solidification reduced the impurity concentration of metallurgical-grade silicon to the maximum limit for the feedstock for solar-grade silicon for all elements except Al. [42]

The theoretical impurity removal through directional solidification can be calculated through the Gulliver-Scheil equation:

$$C_s = k_0 C_0 (1 - f_s)^{k_0 - 1}$$

Where  $C_s$  is the content of the element in the solid silicon,  $k_0$  is the segregation coefficient,  $C_0$  is the initial concentration of the impurity, and  $f_s$  is the fraction solidified. [19]

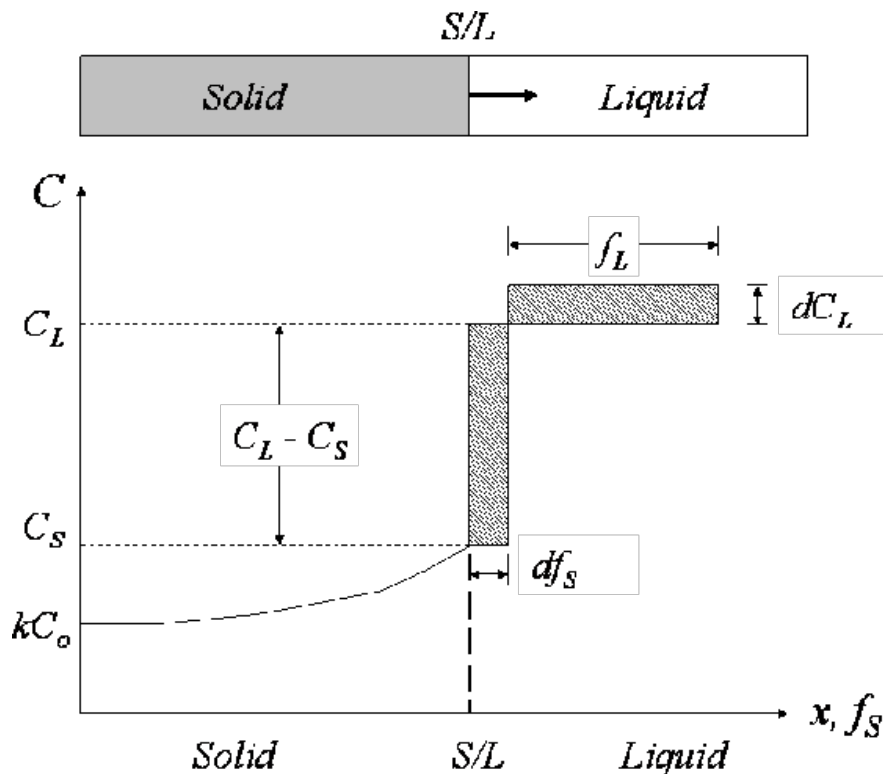


Figure 2.16: The figure illustrates the Gulliver-Scheil equation by showing the graph after half of the metal is solidified. [43]

The equation and variables are illustrated in Figure 2.16. As the metal solidifies, the concentration of the impurity rises, so the metal purified first will be the purest. The last metal to solidify will contain large amounts of impurities, as this is in equilibrium with the final melt, where large amounts of impurities have gathered.

## 2.4 Silicon for the Solar Industry

### 2.4.1 The Siemens Process

Most solar-grade silicon is produced through the Siemens process, which holds 90% of the market share. In the Siemens process, metallurgical-grade silicon reacts with HCl in a hydrochlorination synthesis reactor. The product is a gas stream made of a mixture of chlorosilanes, including  $\text{SiHCl}_3$ , which is most important as it will be used as a precursor in the production of polysilicon. The chlorosilanes are then purified by running the gas through distillation columns, to produce ultrapure  $\text{SiHCl}_3$ . Finally, the Siemens reactor is used to disintegrate the  $\text{SiHCl}_3$  and solar-grade silicon is deposited.[44]

The main advantage of the Siemens process is the ability to produce silicon of very high purity. While metallurgical routes introduce several metallic impurities that can be difficult to remove, the Siemens process eliminates impurities early on, and the deposited silicon is essentially impurity-free. The Siemens process poses some issues both regarding cost and the environment. The Siemens process requires hundreds of kWh/kg, alongside a large investment cost. The process causes environmental problems from halogenated silicon compounds that hydrolyze in the air and are highly flammable. In addition there are substantial material losses. [45]

### 2.4.2 Material Losses in the Solar Industry

Si used in solar panels has a purity of 99,9999%, called Solar-Grade Silicon (SoG-Si). To reach this purity, silicon produced through the metallurgical route has to go through several refining steps. A combination of different refining steps, each targeting its own set of impurities, can reduce the concentration of impurities to an acceptable level.

Throughout the lengthy process of solar PV production, several material losses occur. Already in the first step of the silicon production process, mechanical and size requirements for the raw materials exclude large quantities of undersized quartz from the process. Further, losses are occurring in the furnace while producing metallurgical-grade silicon, due to the formation of  $\text{SiO}$  gas.[5]

In the refining steps that are needed to convert metallurgical-grade silicon to solar-grade silicon, several material losses occur. If the Siemens process is used, the silicon yield is limited to about 30% [46]. In slag refining, some silicon is oxidized and becomes part of the slag, and in vacuum refining, some silicon is evaporated. During directional solidification, the top of the ingot is cut off. Then, when the wafers are cut, more than 35% of the ingot ends up as silicon kerf, which is a fine sawing dust. When these numbers are summed up, only a fraction of the silicon produced at metallurgical grade is made into solar PV. [7]



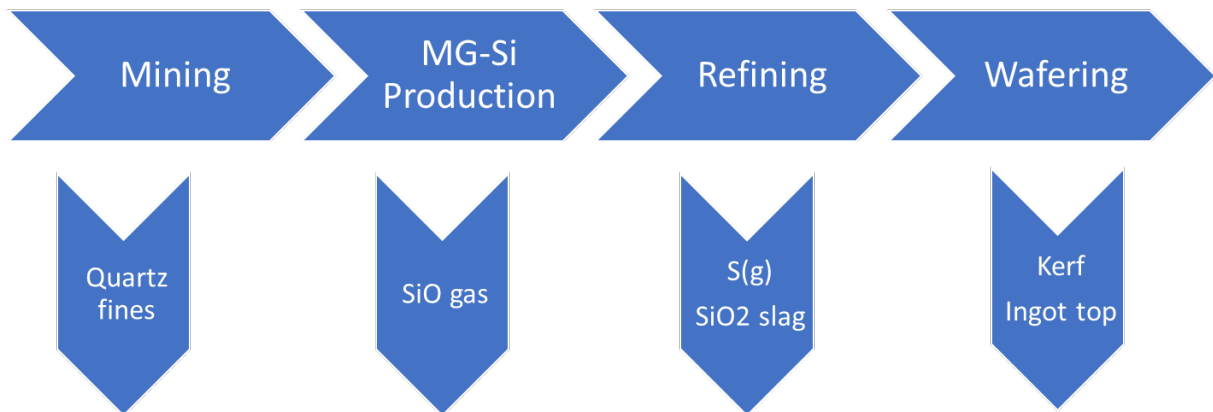


Figure 2.17: Illustration of the wastes and by-products produced in the solar cell value chain from mining to wafering, assuming a metallurgical route.

The most significant loss of material occurs in wafer sawing. The ingot is sawed with a diamond wire, to make the thin silicon wafers that are used in solar PV. Since the wafers are so thin, the amount of material lost in the sawing process is almost as much as the material left in the wafers. More than 35% of the material is turned into sawing dust, kerf, in this process.[3]

State-of-the-art solar PV production is an energy, material, and carbon-intensive process. It is a linear approach with several material losses along the way. With a goal of zero emissions in the process industry by 2050, the need for change is apparent. A shift towards circularity is necessary to create a sustainable industry.

## 2.5 Kerf Recycling

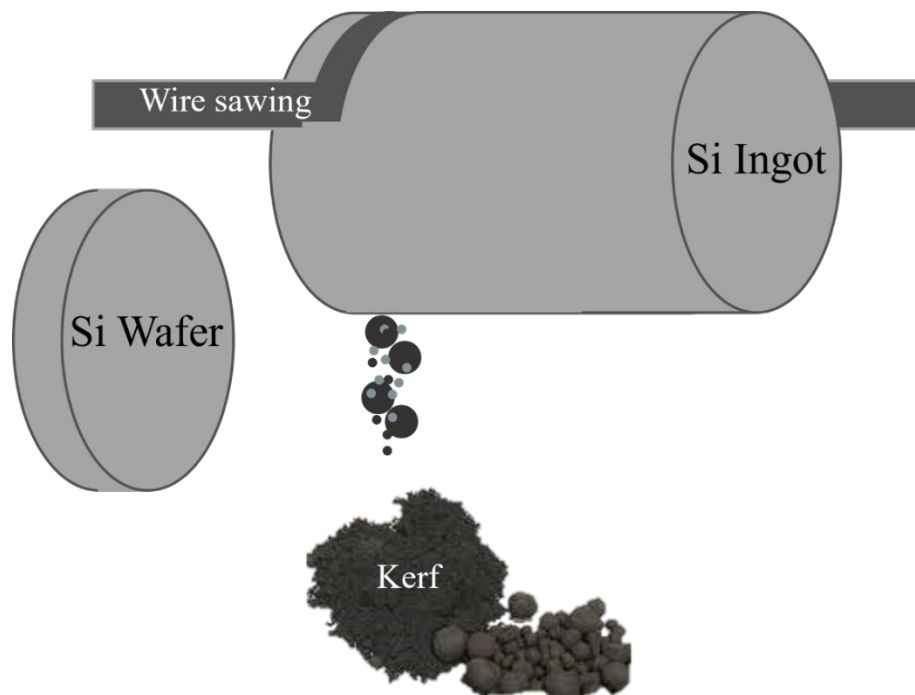


Figure 2.18: Illustration of wire sawing of Si ingot to create Si wafers, with fine Si sawing dust being made (kerf).

Kerf is fine silicon sawing dust, made when a silicon ingot is sawed into wafers, as illustrated in Figure 2.18. The wire can be made of different materials, and SiC or diamond-covered wires are the most common, with diamond wires being the preferred type as it introduces the least amount of impurities. When the wafers are made, more than 35 % of the silicon ingot is transferred into the kerf. The kerf is dispersed into a water-based cutting fluid. Depending on the producer, the kerf slurry is usually separated into solid kerf filter cakes and a liquid phase through a filter press. [3]

Through this process, impurities are introduced to the kerf. The silicon ingot is solar-grade, which means that it contains 99,9999% Si. The kerf originates from this material and therefore has the same purity at the beginning of the process. The wire used to cut the wafers is the first source of contamination. From a wire made of steel, with electroplated nickel and diamonds, Fe, N, and C may present themselves as impurities in the kerf. The wire spools are made of Al, and this may therefore also be an impurity. The cutting fluid contains organic compounds, surfactants, and water, and all these components will contaminate the kerf. Lastly, the filtration aid usually contains silica, alumina, and iron oxide, and this can also contaminate the kerf. What started as very pure silicon, has now changed to a mass with several different impurities, whose concentrations depend on the production process. [3]

The ICARUS project is investigating waste materials from the PV value chain. The chemical composition and particle sizes of kerf have been investigated. The B content in a Norwegian kerf investigated was around 0,35 to 0,4 ppm, whereas in an Asian kerf, it was slightly higher, up to 0,6 ppm. The Ga content varied between different sources of the kerf, from 0,05 to 0,65 ppm. The concentration of P also varied, from 4 ppm to 15 ppm. The study found that the kerf from Asian sources that were analyzed had higher levels of P than the Norwegian kerf. For the metal impurities, the Asian sources had lower Al concentrations, with less than 11000 ppm while the Norwegian source had 0,72 wt. %. For Fe and Ni, the concentrations varied between the different sources. Fe varied between less than 100 and 1000 ppm and Ni between 100 and 200 ppm. The composition is hence different between different suppliers.[2], [3]

The particle size of the kerf was investigated by SEM images and laser diffraction analysis. The ICARUS study found that kerf consists of “ribbon-like, irregularly shaped angular particles, agglomerates, and nano-sized particles,” with the ribbons being up to 4 $\mu$ m long. Most particles were found in the range between 0,5 and 4  $\mu$ m. [2]

The recycling of kerf has become a popular research topic, as the rapid growth in the global PV industry brings a rapid growth in waste products. In 2017, the silicon loss during wafer sawing was nearly 160.000 tons[6]. Several different recycling strategies have been investigated. Directional solidification, different filtration techniques, sedimentation, metallurgical alloying, slag refining, and vacuum refining are some of the more common components in the suggested recycling routes. [7]

There are several challenges concerning the recycling of kerf. When the goal is to produce high-purity silicon, impurity removal is crucial. The physical properties of the kerf also pose issues, as kerf consists of small particles of about 1  $\mu$ m in diameter.[47] SiC particles are also common in the kerf, especially when SiC has been used to saw the wafers, and it is difficult to

separate SiC particles from Si particles of similar size.[7] Due to differences in methods for sawing wafers, the kerf from different suppliers may have differences in composition. This makes it difficult to create one streamlined process suitable for recycling all kerf. [3]

A review study done by Li et al. in 2022 found that current purification processes reached a bottleneck of <5 N, below the required 6N purity for solar-grade silicon. The purification processes also reduced the recovery ratio and consumed large amounts of acids and other materials or required energy-intensive processes. It was therefore suggested that other applications of recycled kerf than the production of solar-grade silicon should be investigated. This could among others be alloying or functional ceramic materials, with both being in huge demand. A simpler recycling process that can easily be implemented on an industrial scale is therefore an interesting research topic to complement the more complex recycling routes. [48]

This thesis will investigate slag refining, vacuum refining, and directional solidification of kerf, and following are some examples of the research done in those areas.

### 2.5.1 Slag Treatment of Kerf

Kerf made through diamond wire sawing has an inert SiO<sub>2</sub> layer on the surface of the particles. Slag treatment can remove this impurity layer, and the waste slag after SiO<sub>2</sub> removal seems to be recyclable. [22] Several different slag systems with their own set of properties have been investigated.

One study with promising results regarding the removal of SiO<sub>2</sub> and B was conducted by Zhang et al. The recycling route presented started with pressure-less sintering of the kerf at 1400°C. This process step reduced the oxygen content from 14,83 to 7,24%. Thereafter, the kerf was melted, and CaO-SiO<sub>2</sub>-slag was added. Different mass ratios were investigated to find the optimal ratio for boron removal, which was found to be CaO/SiO<sub>2</sub> equal to 1,2 and with an optical basicity of 0,68. With a 1:1 mass relationship between kerf and slag and 40 minutes of holding time, 86,91% of the boron was removed. The study also included experiments with the addition of CaF<sub>2</sub>, but found that this did not increase the boron removal rate, and was therefore excluded, despite its positive physical properties with a reduced melting temperature of the slag, and reduced viscosity. [49]

Another slag system was investigated by Yang et al. They used Na<sub>2</sub>CO<sub>3</sub>-CaO slag with NaCl and Na<sub>3</sub>AlF<sub>6</sub> additives to treat dried kerf filter cakes. In the experiments, the filter cakes and the slag were mixed homogeneously and compressed in the crucible. The experiments were conducted in a closed induction furnace in an argon atmosphere, for two hours at 1823 K. The results from the study showed that the additives had a positive effect, by stabilizing the impurities in the slag and reducing slag viscosity. Feed mass ratios of Na<sub>2</sub>CO<sub>3</sub>:CaO:NaCl = 12,8:1,7:8,6 and Na<sub>2</sub>CO<sub>3</sub>:CaO: Na<sub>3</sub>AlF<sub>6</sub> = 12,8:1,7:8,6 gave Si recovery ratios of respectively 76,39% and 79,25%, and purities of respectively 99,985% and 99,986%. NaCl and Na<sub>3</sub>AlF<sub>6</sub> are also economically feasible additives for large-scale applications.[50]

The combination of electromagnetic separation and slag treatment has been considered for the recycling of kerf. In a study by Li et al., this method was investigated, and 99,47% pure Si was produced. The electromagnetic stirring on its own had an obvious effect on the silicon separation, as it separates the metallic melt and the non-metallic inclusions. CaO-SiO<sub>2</sub> and CaO-SiO<sub>2</sub>-Na<sub>3</sub>AlF<sub>6</sub> slags were investigated, and both further improved the separation rate of silicon. The use of slag was especially efficient for the removal of Al and B. Regarding Ca and Fe, the slag introduced more impurities than what was found in the analysis of the kerf. This process was conducted by first pelletizing the kerf with the slag, followed by melting in a graphite crucible before electromagnetic stirring was used for the silicon product from the first melting. [51]

Combinations of slag treatment and acid leaching are also considered a feasible processes to purify kerf. Huang et al. found that Na<sub>2</sub>-SiO<sub>2</sub> slag refining can enhance the silicon yield and had a 63,2% Si yield from the kerf. The recycling process had a removal efficiency for the total concentration of Fe, Al Ni, B, and P of 99,2%, from 6998 to 58 ppm. The study suggests that both the oxidation from the slag treatment and the segregation of impurities to intermetallic precipitate phases facilitated the impurity removal. The intermetallic precipitates were removed by acid leaching. The slag treatment was also necessary to remove the surface oxide layer. [52]

A common aspect of most kerf recycling routes is the removal of the inert oxide layer on the surface of the kerf particles. This layer can also be removed using cryolite, as investigated by Chen et al. In their experiments, the kerf was mixed with 10,5wt% cryolite and sintered at 1400 °C to a dense structure. During the sintering, the surface oxide layer was digested into a liquid phase. The next step of the recycling process was slag treatment with CaO/SiO<sub>2</sub> with a mass ratio of 2, at 1600°C. The Na from the cryolite formed Na<sub>2</sub>O, which can enhance the oxygen ion activity and hence the boron absorbing capacity of the slag. The boron removal efficiency reached 86,56%. [53]

To recover Si from the kerf, a good separation between Si and SiC is important. Li et al. therefore studied the contact angle between a CaO-SiO<sub>2</sub>-MgO-slag and SiC and found that the angle was larger for SiC, which confirmed the feasibility of slag treatment for the removal of SiC particles. Prolonged slag refining gave the SiC particles time to transfer across the slag/metal interface and dissolve in the slag. [54]

Testing on an industrial scale is important to investigate the applicability of the suggested refining routes. Wei et al. studied the refining of kerf containing 13-16 wt.% SiO<sub>2</sub> by adding CaO in different amounts with a range of refining times. In the refining process, CaO reacted with the SiO<sub>2</sub>-layer on the surface of the kerf particles and formed compounds with low melting points and viscosities. The silicon cores were then able to melt into liquid silicon. The lab-scale study found 8 % CaO and a 50-minute holding time to be the optimal parameters, giving a 55,59% recovery ratio and 99,56% pure silicon. This was then tested on an industrial scale with successful results and a kerf recovery ratio of up to 60%. An economic evaluation was also done, and the benefits were found to be substantial. [55]

### 2.5.2 Vacuum Refining for Kerf Recycling

Vacuum refining has been investigated as part of the recycling process for kerf. Kong. et.al. suggested a two-stage process consisting of pelletizing the kerf, followed by vacuum refining. This approach was found to be efficient for the removal of some impurities, with removal ratios of 29,86% for P, 82,73% for Al, and 92,93% for Ca with a refining time of 90 minutes at 1973 K. The silicon produced in this project reached a purity of 99,65%. The recovery rate of the silicon powder was 68,65% for vacuum refining. When the same experiment was repeated in the atmosphere, the recovery rate was only 56,5%. The study also found that the removal rates of Al, Ca, P, and Fe increased with increasing refining times. The removal rate for Al went from 70% at 60 minutes to about 80% after 110 minutes. 90 minutes was found to be the optimal time as the removal rates of impurities improved very slowly after this, and the recovery rate of Si started trending downwards. [47]

Other pretreatments of the kerf can also be used to prepare it for vacuum refining. Lu et al. investigated a method starting with laser granulating technology, followed by vacuum refining. During the laser melting, 74,2% of the C was removed, along with most of the metal impurities. No impurities are introduced in this process. The proposed process achieved a silicon yield of 94,7%. The product needs further treatment to reach solar grade, and vacuum directional solidification is proposed. [56]

### 2.5.3 Directional Solidification of Kerf

Directional solidification is a much-used refining strategy for silicon and is often a step in the recycling of kerf. A study by Zhu et al. [57] investigated induction smelting of kerf from diamond wire sawing, followed by directional solidification, without the use of additives. A longer smelting time was related to higher purity, and the lowest impurity concentrations were found after 4 hours of smelting. A disadvantage to the approach was the loss of Si through the formation of volatiles, and the silicon recovery rate was 79% after 4 hours of smelting. By limiting the smelting time to 1 hour the silicon recovery rate was increased to 97,68, and the product was within the MG-Si range. After the directional solidification, the remaining Ca, Al, Fe, B, and P concentrations were reduced by 99,7%, 99,2%, 98,68%, 95,21%, and 76,15%, respectively, and the final composition of the ingot exceeded 99,99% Si. [57]

One study by Hu et al. investigated direct current-assisted directional solidification. The direct current was used to enhance the impurity separation process. The local temperature in front of the solid-liquid interface in the directional solidification and the behavior of the impurities in front of the interface was improved. The result of the experiments was a silicon metal with a purity of nearly 5.5N. [58]

Another strategy for directional solidification of the kerf is radial directional solidification. This technique was investigated by Imose et al. [59], and compared to other directional solidification practices. Radial directional solidification is a technique where the silicon is solidified towards the radial center. The article suggests two rounds of radial directional solidification to reach SOG-Si. [59]

#### 2.5.4 Other Strategies for Kerf Recycling

All techniques used for refining metallurgical-grade silicon to make solar-grade silicon can also be utilized to refine kerf. The physical properties have to be taken into consideration, and a pelletizing step is, therefore, recommended for some procedures. A review article by Lei et al. suggests a recycling route starting with a slag treatment, followed by a combination of solvent refining and directional solidification under a vacuum. [22]

Acid treatments are also considered relevant for kerf recycling, and Yang et al. investigated 5wt% of HF, HCl, H<sub>2</sub>SO<sub>4</sub>, HNO<sub>3</sub>, and combinations of those. The procedure studied was acid leaching, followed by calcination and deoxidation. HF was found to be an effective acid, especially for Ni removal. The organic compounds were burned off at 500°C for 3h, and after this, only 0,4 wt.% C remained. With the mixed acids used, more than 94% of the metallic impurities were removed. B and P had removal rates of about 70% and were at sub-ppm levels. The deoxidation took place in a vacuum at high temperatures for 2h, and oxygen was reduced to 4,6wt%. [6]

Kerf recycling through a chemical approach using a hydrobromination reaction has been investigated by Tomono et al. First, the kerf slurry cake consisting of kerf, cutting lubricant, and metallic impurities were treated with acetone, and for some of the samples HNO<sub>3</sub> and HCl. The study showed that although the acetone removed some of the lubricants, the following heat treatment was necessary for complete removal. Then, the dry sample was exposed to HBr gas at 400°C in a flow reactor, where the reactivity was evaluated based on the conversion of HBr. The acid treatment was efficient for the removal of lubricant and metallic impurities, but the disadvantages caused by the decrease in reactivity with HBr due to the oxidation of silicon outweighed the advantages. The bromination was much more efficient in impurity removal than the acid treatment. The conclusion was made that HBr enables the purification of kerf without acid treatment. [60]

Another option for kerf recycling is through Al-Si alloying. This approach was studied by Wei et al. In this process, compressed kerf, cryolite, and aluminium reacted in a smelter. The cryolite additives dissolve the SiO<sub>2</sub>-layer on the surface of the kerf particles, transferring the exposed silicon to the molten Al. The effect of smelting temperature, holding time, and cryolite/kerf ratio on the Si content of the alloy and the kerf recovery ratio were investigated. The study found that a smelting temperature of 1150 °C, a holding time of 30 min, and a cryolite/kerf ratio of 6.3 were optimal. These conditions produced an alloy containing 12,02 % Si and the recovery ratio of kerf was 64,25%. The produced alloy had a uniform distribution of Si. The generated slag can be recycled and used as an additive for the next batch of experiments. This is hence a circular approach, that also holds cost benefits as it reduces the production cost of Al-Si alloys. [61]



### 3 Methodology

The experimental work in this thesis comprises slag refining in three different scales, vacuum refining, and theoretical evaluation of directional solidification. The effect of different raw material mixes, holding times, and temperatures on the composition of the produced metal was investigated.

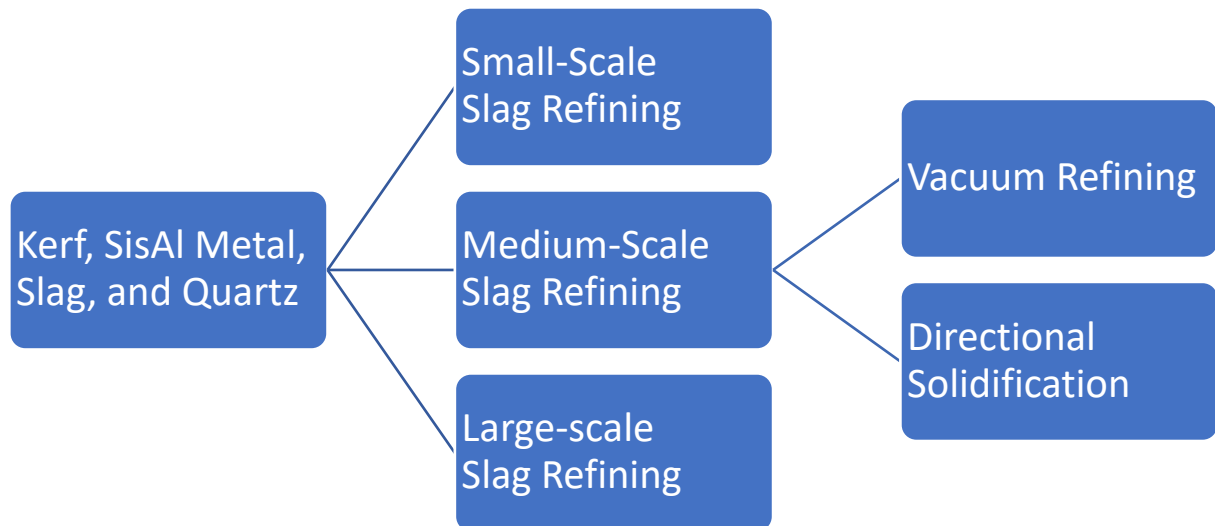


Figure 3.1: A diagram illustrating the different experiments conducted in this thesis.

Prior to the work presented in this thesis, small-scale(200g) slag refining experiments were conducted to investigate different mass ratios of the raw materials. The small-scale slag refining experiments done for this thesis investigated varying holding times, casting temperatures, and the addition of quartz. These experiments were conducted to find good parameters for the medium-scale (20kg) slag refining experiments. The results from the medium-scale experiments led to the choice of parameters for the large-scale (100 kg) slag refining experiment.

Silicon produced in the medium-scale experiments was refined further through vacuum refining. Three experiments were conducted, with total holding times of 60, 90, and 100 minutes. Directional solidification was investigated through theoretical calculations.



## 3.1 Materials

### 3.1.1 SisAl Metal

The silicon alloy used in the experiments was produced through the SisAl process and will hence be referred to as SisAl metal. SisAl metal can be produced from a variety of raw materials. The aluminium used in the process can come from secondary sources such as scrap aluminium, aluminium shavings, or dross. Dross is a waste product from the metal production industry and is a mass of solid impurities floating on top of molten metal. The impurities are made by oxidation of the top layer of the metal.

T15 was used in the small-scale experiments, T09 and T10 were used in the medium-scale experiments, and T06, T09, and T18 were used in the large-scale experiment. The composition of the metal is given in Table 3.1.

Table 3.1: The SisAl metal used in the trials, analyzed by XRF. The metal was produced in experiments conducted by Elkem in the EU-funded project SisAl Pilot: GA No 869268.

SisAl Metal	Si [%]	Al [%]	Ca [%]	Fe [%]	Mg [%]	Mn [%]	Ni [%]
T06	72,6	11,5	14,6	0,5	0,2	0,06	0,05
T09	71,9	10,8	15,6	0,4	0,6	0,21	<0,05
T10	69,4	12,1	16,6	0,5	0,6	0,23	<0,05
T15	74,7	8,0	16,0	0,4	0,2	0,06	<0,05
T18	73,5	9,1	16,2	0,4	0,2	0,06	<0,05

### 3.1.2 Kerf

The kerf used in the small-scale experiments was in the shape of a fine, dried powder. The kerf used for the medium-scale experiments came from filter cakes and contained 49% water. The kerf was therefore dried at Elkem before the experiments. The kerf used in the large-scale experiment was pelletized. The composition of all three kerfs is given in Table 3.2.

Table 3.2: The compositions of the different kerf materials used in the experiments are given in the table.

Form	Si [%]	Al [%]	Ca [%]	Fe [%]	Ni [%]	Mg [%]	C [%]	O [%]	S [%]	Na [%]
Powder	99,5	0,035	0,016	0,023	0,030		0,048	0,26		
Filter cake	94,3	0,022	0,10	0,017	0,004		0,79	4,66		
Pellets	95,0	0,90	0,142	0,012	0,010	0,033	0,089	3,63	0,049	0,072

### 3.1.3 Slag and Quartz

The slag used in the slag refining experiments was a prefused 1,1/1 CaO/SiO<sub>2</sub> slag. The composition of the slag is given in Table 3.3. The quartz used in the experiments was quartz fines, assumed to be almost 100% SiO<sub>2</sub>.

Table 3.3: The slag used in the slag refining, analyzed by XRF.

Element	Amount [wt.%]
MgO	0,28
Al <sub>2</sub> O <sub>3</sub>	0,19
SiO <sub>2</sub>	47,7
CaO	50,6
Fe <sub>2</sub> O <sub>3</sub>	0,11

### 3.2 Slag Refining

Slag refining is the first step of the refining process investigated in this master thesis. The raw materials used in the experiments are quartz, slag, SiAl metal, and kerf. These are heated in a crucible in an induction furnace and held at around 1550°C while the slag refining takes place. The product is a new Si alloy and a slag. The process is illustrated in Figure 3.2.

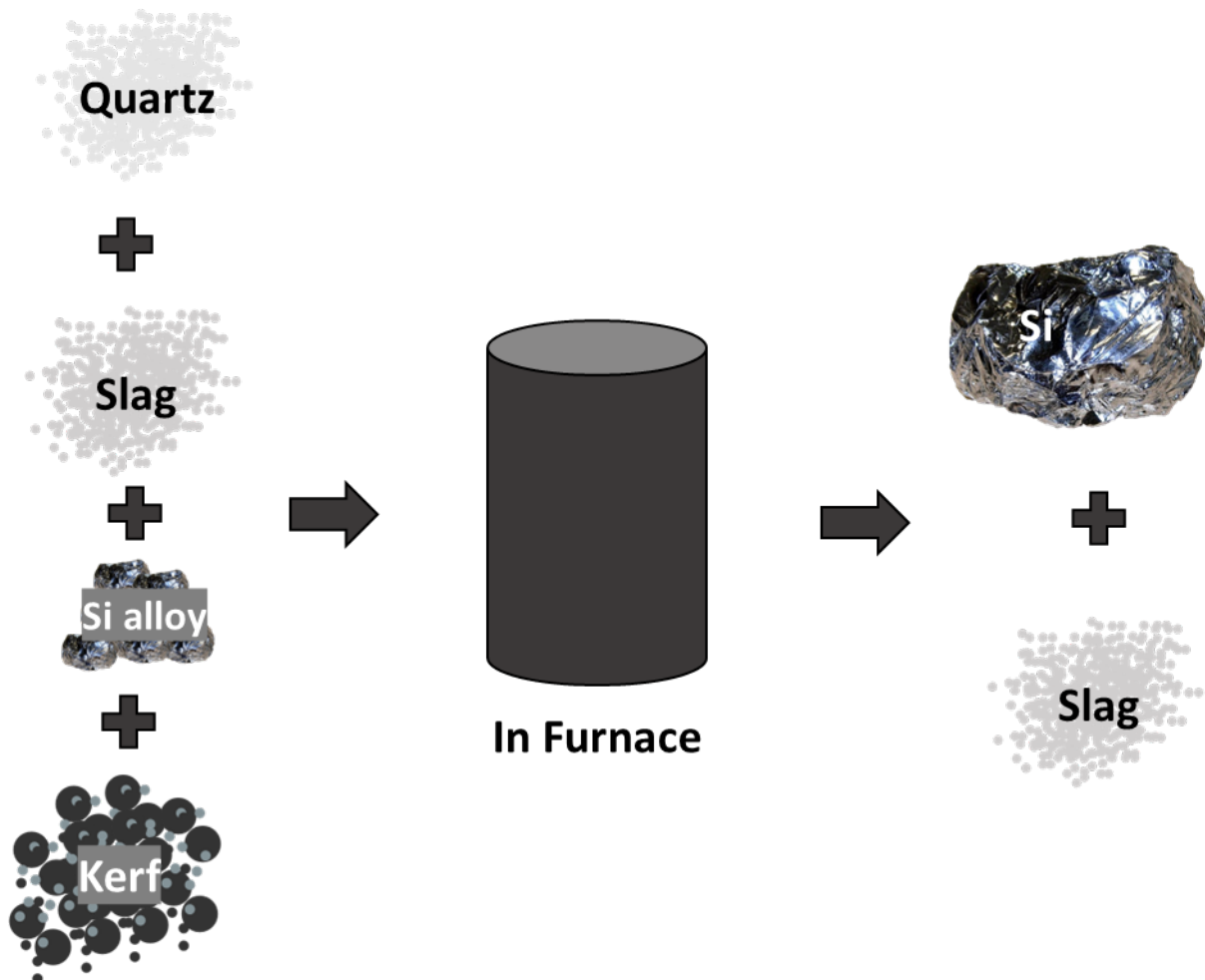


Figure 3.2: Overall illustration of the slag refining. Kerf, SiAl metal, slag, and in some cases, quartz, are placed inside a crucible in a furnace to produce a Si alloy with higher purity than the SiAl metal, and slag.

### 3.2.1 Small-Scale Experiments

Small-scale experiments producing about 200 g of metal each were conducted at NTNU. The goal of these experiments was to prepare for the medium-scale trials by testing different holding times, casting temperatures, gas stirring, and the addition of quartz.

#### 3.2.1.1 The Furnace and Experimental Setup

The furnace used for these experiments was a 75-kW open induction furnace, shown in Figure 3.3.

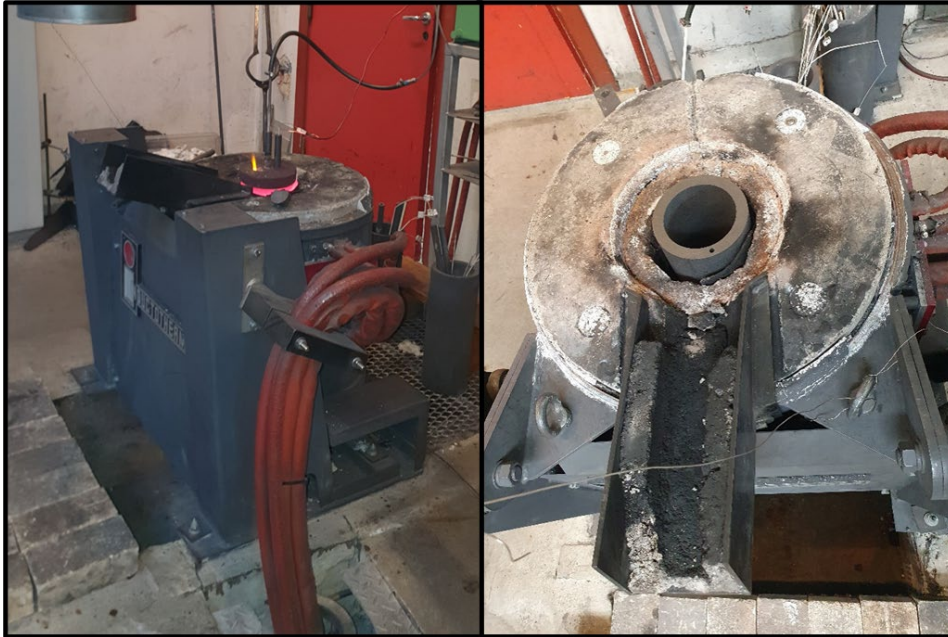


Figure 3.3: The picture shows the 75-kW induction furnace used in the small-scale experiments from the side (left) and above (right).

The raw materials were filled into a graphite crucible that was placed inside the furnace. The graphite crucible is 40 cm high and has an outer diameter of 15 cm and an inner diameter of 11,5 cm. To avoid air in the system, a graphite lid was used on top of the crucible. The lid had three holes, one for a thermocouple, one as an inlet for Ar gas, and one to relieve pressure buildup and use for the addition of quartz. The setup is shown in Figure 3.4. Before the pressure built up, the last hole was covered by a graphite knob to avoid introducing air to the system. In some of the experiments, quartz was added during the holding time. This was done through a steel funnel, as shown in Figure 3.4.

The gas lance was made from a graphite thermocouple cover, which is a closed-end graphite tube, and an open-end alumina tube that fit tightly inside the graphite tube. The graphite tube was 50 cm long and had an outer diameter of 2 cm and an inner diameter of 8 mm. Close to the bottom of the side of the graphite tube, three holes with 3 mm diameter were drilled and evenly distributed. The drill was angled so that the holes had a 45-degree angle upwards into the rod, steering the gas flow downwards. The alumina tube was placed inside the graphite tube, to make sure the gas went through the holes at the bottom, and not through the porous graphite higher up.



Figure 3.4: To the left: Picture of the lid used in the experiments. In the middle: picture of the setup in the crucible, with lid, graphite tube to protect the thermocouple, and gas lance. The last hole is covered with a knob during heating, and a funnel is inserted when quartz is added. To the right: the stacking of raw materials in the furnace.

At the end of the experiment, the molten product was attempted cast. The casting was done by first removing the lid, thermocouple, and gas lance. Then, the crucible was lifted manually, using tongs. Another tong, specially designed for casting, was then wrapped around the crucible, and used for carrying the crucible away from the furnace, and eventually tilting over a graphite mold. The equipment is shown in Figure 3.5.

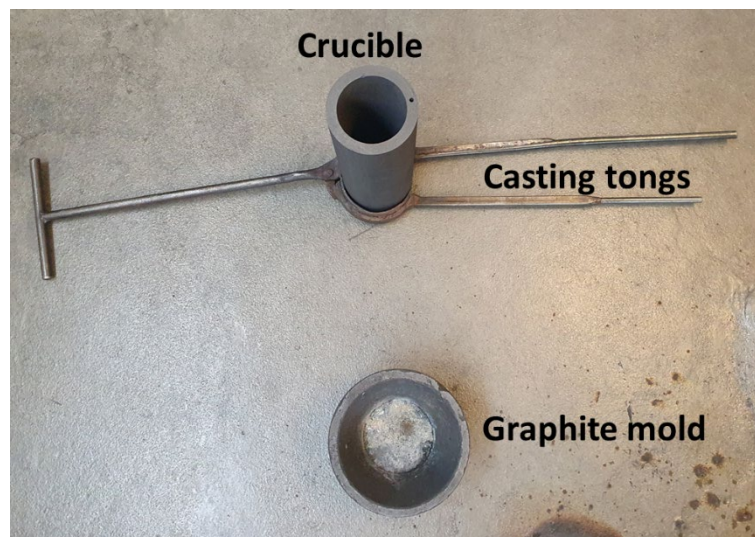


Figure 3.5: The picture shows the casting tongs placed around the crucible, and the mold the material was cast into. The crucible was held by the tongs and tilted above the mold to allow the material to flow into the mold.

### 3.2.1.2 Experiments

For the small-scale experiments, the goal was to prepare for the medium-scale trials (20 kg scale). In these trials, casting, holding times and temperatures, and the addition of quartz were investigated, while the ratio 2:1:2 between kerf, SisAl metal, and slag was used for all experiments.

Table 3.4: The table shows the experimental matrix for the small-scale experiments.

Experiment	Kerf [g]	SisAl Metal [g]	Slag [g]	Quartz [g]	Holding T [°C]	Gas stirring [min]	Total holding time [min]	Casting T [°C]
2.1	250	125	250	0	1550	45	60	1600
2.2	250	125	250	40	1550	0	45	1600
2.3	250	125	250	40	1550	0	25	1550
2.4	250	125	250	40	1550	0	60	1550
2.5	250	125	250	0	1550	50	60	1550
2.6	250	125	250	40	1550	20	60	1600
2.7	250	125	250	40	1550	30	40	1600
2.8	250	125	250	40	1550	10	20	1600



Figure 3.6: The illustration shows the timeline of the experiment.

First, the melt was heated to the holding temperature with a heating rate of about 50°C per minute, resulting in 30 minutes needed to reach 1550°C. When this temperature was reached, the pressure had built up, and the bolt covering the hole in the lid was removed. Quartz was added to the melt after 20 minutes for experiments 2.2, 2.3, and 2.4, after 40 minutes for experiment 2.6, and 10 minutes for experiments 2.7 and 2.8. For the experiments that used gas stirring, the gas supply at the top of the crucible was replaced by a gas lance that emerged into the melt, stirring the material, after the quartz was added.

All experiments in the second set of experiments were attempted cast. Samples were taken both from the cast material and the material left in the crucible. To retrieve samples from the crucible, the crucible was broken using a hammer. Then, the metal and slag were separated, and samples were taken out.

### 3.2.2 Medium-Scale Trials

The medium-scale trials were conducted at Elkem Technology's research facility in Kristiansand. The experiments were conducted by the local research team, instructed by Veronika Djupvik, together with the author of this thesis and NTNU employee Nishan Simkhada. The experiments were done following the recipe constructed by the author of this thesis based on the result of the small-scale trials at NTNU. Six experiments were conducted in total, each producing approximately 20 kg of metal and 30 kg of slag.



### 3.2.2.1 The Furnace and Equipment

The experiments were conducted in an induction furnace with a capacity of 225 kW, in a 40 liters graphite crucible. A graphite lid was sawed in two, and a hole was drilled in one half to make room for the gas lance. The lid was pushed aside during charging and removed before casting. The furnace was tiltable, and the material was cast into graphite molds.

A thermoelement was placed outside the crucible, touching the crucible wall. The furnace was run by setting a target temperature for this thermoelement. A separate thermoelement was used to check the temperature in the melt. This element was dipped into the melt, and the temperature was noted manually.

A hollow graphite rod with three holes with a 3 mm diameter close to the bottom served as a gas lance. The gas flow was four liters per minute throughout the experiments.



Figure 3.7: Pictures of the furnace used for the medium-scale trials. The furnace was a 225-kW induction furnace, with a 40 liters crucible, and a tap chute. To the right, the leftovers from an experiment can be seen in the crucible and chute.

### 3.2.2.2 Experimental Procedures

Table 3.5: Mass of materials used in each experiment at Elkem and a short description of the course of experiments. SisAl metal from T10 was used in 3.1, 3.2, and 3.3, T09 was used in 3.4, 3.5, and 3.6, and Kerf 2 was used in all experiments.

Exp.	SisAl Metal [kg]	Kerf [kg]	Slag [kg]	Quartz [kg]	Course of Experiment
3.1	11,0	16,5	22,0	3,5	Crucible change, kerf and slag melted, SisAl metal added, 20 minutes, Quartz added, 20 minutes, casting
3.2	11,0	16,5	22,0	3,5	Kerf and slag melted, SisAl metal and quartz added, 40 minutes, casting
3.3	11,0	16,5	22,0	10,2	Kerf and slag melted, SisAl metal and part of the quartz were added, 40 minutes while more quartz was added, casting
3.4	11,0	22,0	22,0	10,2	Kerf and slag melted, SisAl metal and quartz added, 40 minutes, casting

<b>3.5</b>	11,0	16,5	22,0	9,0	Crucible change, kerf and slag melted, SisAl metal and quartz added, 40 minutes, casting
<b>3.6</b>	11,0	22,0	22,0	9,0	Kerf and slag melted, SisAl metal and quartz added, 40 minutes, casting

Six experiments were conducted in total. The overall goal of these experiments was to gain insights before planning the large-scale trial (100 kg scale). The parameters tested in these experiments were the time of quartz addition, amount of quartz added, and Kerf : SisAl Metal : Slag mass ratios. All experiments had the same target temperature of 1550 to 1580 °C in the melt and a holding time of 40 minutes.

In experiments 3.1 and 3.2, the goal was to decide if it would be best to add the quartz together with the SisAl metal, or 20 minutes later. In experiment 3.3, the goal was to investigate how much quartz that could be added to the melt without raising the temperature, while the slag was still castable. 3.4 used the result from 3.3 to determine the amount of quartz added, but in this experiment, all the quartz was added together with the SisAl metal. Experiments 3.1, 3.2, 3.3, and 3.5 were conducted using a 1,5:1:2 relationship of Kerf : SisAl Metal : Slag, whereas experiments 3.4 and 3.6 were conducted using a 2:1:2 relationship. In experiments 3.5 and 3.6, the amount of quartz was reduced to 9 kg, to make sure the slag would flow easily and that all the quartz would dissolve into the melt.

### **The Course of the Experiments**

Due to the moisture in the kerf, it had to be part of the first materials charged into the furnace, to avoid any metal-over-water accidents. Previous work has shown that kerf does not melt well without the presence of slag [22], [62]. Therefore, the kerf and the slag were co-charged at the beginning of the experiment. The kerf has a remarkably high volume-to-mass ratio before it is melted, and it was therefore necessary to add the material stepwise, as the material melted. During charging, the furnace had a flow of Ar directly under the lid. When the materials were melted, the gas lance was lowered into the melt and the gas was used to stir the materials.

When all the kerf and slag were melted, the SisAl metal was added. For all experiments except 3.1, the metal was co-charged with quartz through several smaller additions, to make sure everything melted properly. The amount of quartz added in this step was 3,5 kg for 3.2, 6 kg for 3.3, 10,2 kg for 3.4, and 9 kg for 3.5 and 3.6.

For 3.2, 3.4, 3.5, and 3.6, there were no more additions. For experiment 3.1, all the 3,5 kg of quartz that were used in this experiment were added 20 minutes after all the SisAl metal was added. In experiment 3.3, more quartz was added gradually through the 40 minutes of holding time. The total amount of quartz added up to 10,2 kg for experiment 3.3.

5 minutes before casting, the gas lance was removed to allow the melt to settle before casting. The melt was cast through the tilting of the furnace, and the material was cast into two graphite molds. The first mold was filled with metal, as the metal came first out of the crucible. When slag was observed, the furnace was tilted back, the molds were changed, and the slag

was cast in the second mold. The separation between metal and slag varied between the experiments, and there was metal trapped in the slag in all of the experiments, but to different degrees.

After every experiment, there were some materials left in the crucible and in the tapping chute. The metal in the chute weight about 0,9 kg after experiment 3.6, and the material left in the crucible was estimated to be up to 3 kg for all experiment. This material was left in the furnace and became part of the following experiment.



Figure 3.8: To the left: Casting of material. The furnace is tilted, and the mold is elevated. In the middle: The hot metal is left in the molds to cool down. To the right: The metal was cast in the first mold and the slag in the second. The products were removed from the molds and left on the floor for the remainder of the cooling period.

### 3.2.3 Large-Scale Trials

The large-scale trials were conducted at Elkem Technology's research facility in Kristiansand. The experiments were conducted by the local research team, instructed by Veronika Djupvik, together with NTNU's postdoctoral fellow Elif Emil Kaya and employee Nishan Simkhada. The experiment was done following the recipe constructed by the author of this thesis based on the result of the medium-scale trials. One experiment was conducted in their larger induction furnace, producing 109 kg of metal.

#### 3.2.3.1 The Furnace and Equipment

The experiment was conducted in an induction furnace. The furnace was lined with magnesite refractory as the inner lining and a graphite crucible of 234 liters as a susceptor. The furnace has a steel lid, where graphite lances were connected for temperature measurements and gas stirring. The lid was cooled with air between the steel shell and refractory underlining.



### 3.2.3.2 Experimental Procedure

Table 3.6: Raw materials used in the large-scale trial and the amounts of each. Kerf 3 was used, and the SisAl metal came from three different sources, 18 kg from T06, 28,5 kg from T09, and 28,5 kg from T18.

	Kerf [kg]	SisAl metal [kg]	Slag [kg]	Quartz [kg]
Large-scale trial	110	75	147	68

The raw materials used in the experiment are showed in Table 3.6. The relationship between the different raw materials is about 1,5:1:2 for kerf: SisAl metal: Slag, and 0,9 parts kerf.

First, the furnace was charged with 75 kg of prefused slag. This melted over a period of 7 hours. After this, the SisAl metal and the rest of the slag were charged every other time for the next two hours. In the following two hours, the kerf was added and melted. Lastly, the quartz was added and melted over a period of one hour.

When all the materials had melted, the holding time of 40 minutes started. During both the charging and the holding time the melt was stirred with gas with a flow of 10 l/min. When the holding time was up, the gas stirring, and the power of the furnace were decreased to settle the melt.

The metal was tapped by tilting the furnace and tapping the material into five graphite molds. The metal was tapped first, followed by the slag. Initially, the separation seemed good, but large metal droplets were seen when tapping the slag.

## 3.3 Vacuum Refining

A small-scale vacuum refining experiment was conducted to get an idea of how the metal would react to vacuum refining. Metal produced in the medium-scale experiments was used.

### 3.3.1 Equipment

The furnace used in the experiments was a closed induction furnace. The furnace can be filled with a gas of choice, or a vacuum can be applied. The furnace was operated at around 5kW. Pictures of the furnace are presented in Figure 3.9.

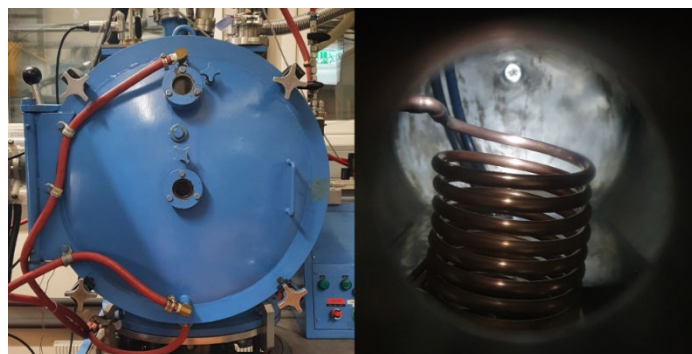


Figure 3.9: Pictures of the furnace used for vacuum refining. The furnace is a closed induction furnace, where the crucible is placed inside a coil.

The crucible used inside the furnace has a diameter of 80 mm and a height of 150 mm and was filled two-thirds full of metal. Graphite wool was used as insulation between the coil and the crucible. To measure the temperature in the material, a thermocouple was placed inside an alumina tube, in a graphite tube in the crucible.

### 3.3.2 Experimental Matrix

In the first experiment, samples were taken during the holding time, with a total holding time of 60 minutes. The second and third experiments had 90- and 100-minute holding times, respectively. These holding times were chosen based on the results of the study by Kong et al. [47].

Table 3.7: The table shows the experimental matrix for the vacuum experiments.

Experiment	Metal [g]	T [°C]	Samples taken	Total holding time [min]
V1	422,0	1550	5	60
V2	358,9	1550	1	90
V3	425,9	1550	1	100

### 3.3.3 The Course of the Experiment

First, the metal was placed in the graphite crucible and placed inside the furnace. Then, the furnace was closed, and the chamber was flushed with Ar two times. Ar flushing is the process where the furnace is first vacuumed, then filled with Ar, and then vacuumed again. This is done to make sure there is no air in the furnace during the experiments. Then, in Ar atmosphere, the power of the furnace is turned on, and the furnace is heated to 1550 °C. The heating process takes about 30 minutes. Then, the temperature was kept at 1550 °C and the vacuum was maintained for the desired holding time.

When the holding time was over, the power was turned off, and the metal was left to cool down in the vacuum inside the furnace. When it was sufficiently cool, the furnace was flushed with argon before air was let into the furnace chamber, and the product could be removed.

### 3.3.4 Sampling during the Holding Time

In the first experiment, samples were taken during the holding time. When the temperature reached 1550°C, the first sample was taken. Then, the furnace chamber was placed under vacuum, with a pressure between 0,5 and 0,01 mbar. The material was held at the said temperature and pressure for one hour. During the holding time, samples are taken out every 10 minutes for the first 40 minutes, resulting in five samples (at 0 min, 10 min, 20 min, 30 min, and 40 min).

The samples are taken using a quartz tube with a 6 mm outer diameter and 2 mm inner diameter, connected to a tube with a syringe at the end, as shown in Figure 3.10. Before the sample was taken, the part of the equipment with the quartz tube, below the gold-colored circular plate, was placed in a chamber connected to the furnace. This chamber was then flushed with Ar. Before the samples could be taken, the furnace had to be filled with Ar. Then,

a valve in the bottom of the chamber containing the sampling equipment was opened, and the quartz tube was lowered into the crucible. The syringe was used to extract a sample, and the tube was moved back into its chamber. The valve was then closed, and the sample could be removed, and the furnace could be put in vacuum. For every sample, a new quartz tube was added to the equipment.

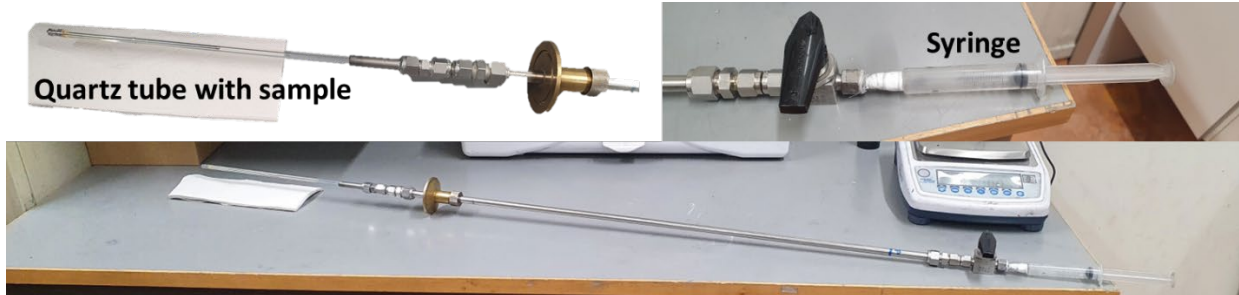


Figure 3.10: Picture of the equipment used to take samples during vacuum refining.

### 3.4 Directional Solidification

The theoretical impurity removals of Al, Ca, and Fe through directional solidification were calculated through the Gulliver-Scheil equation:

$$C_{sAl} = k_{Al}C_{0Al}(1 - f_S)^{k_{Al}-1}$$

$$C_{sCa} = k_{Ca}C_{0Ca}(1 - f_S)^{k_{Ca}-1}$$

$$C_{sFe} = k_{Fe}C_{0Fe}(1 - f_S)^{k_{Fe}-1}$$

Where  $C_s$  is the content of the element in the solid silicon,  $k_0$  is the segregation coefficient,  $C_0$  is the initial concentration of the impurity, and  $f_S$  is the fraction solidified. [19] The initial concentrations were taken from the metal produced in experiment 3.5.

Experimental work was planned, but due to circumstances outside the author's control, these will take place at a later date. Therefore, only theoretical results based on the calculations will be presented for the directional solidification.

### 3.5 Analysis

#### 3.5.1 Preparation for analysis

Samples were taken from both the cast material and the material left in the crucible. The pieces were cut into suitable samples for analysis using a diamond cutting blade in a Labotom 5 cutting machine. These samples were then molded in EpoFix epoxy in cylindrical molds with a 25 mm diameter. When the epoxy had hardened, the samples were polished according to the polishing program presented in Table 3.8. The samples were cleaned in an ultrasound bath between steps.

Table 3.8: A polishing program for the samples to prepare them for EPMA.

	Grinding paper		Lubricant	Time [min]	Force [N]	Rotation
1	SiC foil	#80	Water	2:00	240	300/150
2	SiC foil	#320	Water	2:00	240	300/150
3	SiC foil	#500	Water	2:00	240	300/150
4	MD-Largo	9 µm	DiaPro All/Lar.9	3:00	240	150/150
5	MD-Dac	3µm	DiaPro Dac3	3:00	180	150/150
6	MD-Chem	1 µm	OP-S NonDry	1:00	90	150/150

### 3.5.2 Electron Probe MicroAnalysis (EPMA)

Electron Probe MicroAnalysis (EPMA) was used to create images to show the different phases present in the sample, giving an idea of how much there was of each.

Secondary electron images were made to show the presence of different phases. X-ray elemental mapping images were made to show the presence of the selected elements. For this project, those elements are Si, Al, and Ca. In addition to the x-ray element mappings, the EPMA was also used to perform point analyses of some areas of the samples. The instrument was a JXA-8500F Field Emission Electron Probe Microanalyzer and was operated by Senior Engineer Morten Peder Raanes at NTNU.

### 3.5.3 ICP Analysis

Some material was sent for analysis to Degerfors Laboratories AB in Bruksparcken, Sweden. Different analysis techniques were used, among them the X-Ray Fluorescence (XRF) technique. Thermo Fischer Scientific's ARL 9900 Series XRF device was used to analyze the samples.

## 3.6 Theoretical calculations – FactSage

Theoretical results were calculated using the software FactSage 8.2 with databases FactPS, FACTsolid, FToxid, and FACTmishable.[63]

The input used in the calculations was the same as the raw materials used in the respective experiments. The inputs are given in Table 3.9.

Table 3.9: The table shows the input used for the FactSage calculations.

Experiment	Si [kg]	Al [kg]	Ca [kg]	SiO <sub>2</sub> [kg]	CaO [kg]
<b>Small-Scale Trial 2.2</b>	0,342	0,010	0,020	0,159	0,127
<b>Medium-Scale Trial 3.3</b>	21,6	1,4	2,1	20,7	11,5
<b>Large-Scale Trial</b>	164,3	7,8	11,7	138,0	77,0



## 4 Results and Discussion


In the following sections the results of the experiments will be presented and discussed.

### 4.1 Slag Refining

#### 4.1.1 Small-Scale Experiments

The main results from the small-scale experiments are presented in Table 4.1 alongside the method and the raw materials used for the experiments.

Table 4.1: The table shows the method, raw materials, and main results from the small-scale slag refining experiments.

Ex.	Method			Raw materials [g]				Result		
	Slag refining in 75 kW induction furnace	Gas Stirring [min]	Holding time [min]	Kerf	SisAl Metal	Slag	Quartz	Si purity	Cast [g]	Losses [g]
2.1		45	60	250	125	250	0	-	-	-
2.2		0	45	250	125	250	40	96,4%	39	80
2.3		0	25	250	125	250	40	mid	246	106
2.4		0	60	250	125	250	40	high	130	160
2.5		50	60	250	125	250	0	low	176	87
2.6		20	60	250	125	250	40	high	391	161
2.7		30	40	250	125	250	40	high	315	120
2.8		10	20	250	125	250	40	low	197	114

##### 4.1.1.1 Method

###### The Choice of Parameters

The parameters used in the small-scale experiments were chosen based on the results of previously performed experiments. These experiments investigated a similar procedure as described for the small-scale trials, but investigated three different mass ratios, 1 part kerf to 1 part SisAl metal and 2 parts slag (1:1:2), 1,5 parts kerf to 1 part SisAl metal and 2 parts slag (1,5:1:2), and 2 parts kerf to 1 part SisAl metal and 2 parts slag (2:1:2). The experiments and their results are explained in the appendix. The result from these trials showed that all three mass ratios tested gave promising results. The ratio 2:1:2 was chosen for further study because it was of interest to investigate a high ratio of kerf, as recycling of kerf is one of the main objectives of this thesis.

###### Casting

In the small-scale experiments, the product was attempted cast, with varying results. Some examples are shown in Figure 4.1. In experiment 2.1, no material was castable. In experiment 2.2, 38 g metal was cast. In the rest of the experiments, a substantial amount of material was cast, due to increased casting temperature. Most of the cast material was metal, with some slag as the last material to be cast.

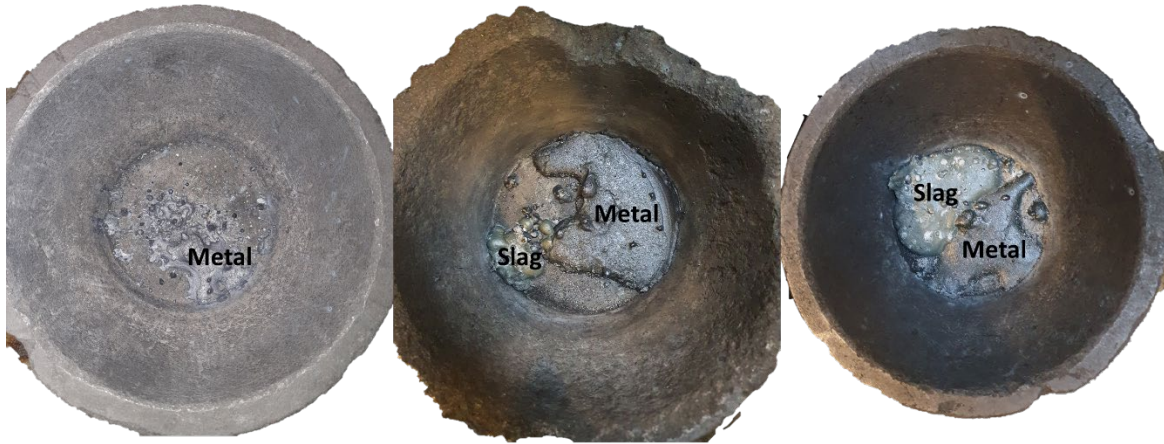


Figure 4.1: The casted material from experiments 2.2, 2.8, and 2.7 (left to right). The slag has a greenish color, and the metal is grey.

The casting issues were caused by the high viscosity of the material. A higher temperature gives lower viscosity, and for some of the experiments, the temperature was increased to 1600 °C before casting, which improved the castability significantly. During casting the crucible was lifted from the furnace, transported two meters and the product was cast. The temperature is believed to have fallen quite rapidly during this process, as the viscosity observed in the melt before casting did not correspond to the behavior of the metal and slag during casting. The temperature in the melt before casting does therefore not correspond to the temperature in the melt during casting. During casting, the metal came first, followed by the slag. In some cases, it was only possible to cast metal, as the slag was too viscous. The materials that remained in the crucible were hard to separate, but the metal mainly stayed on top of the slag.

#### 4.1.1.2 Composition of the Products

##### Metal Composition

For this set of experiments, the exact composition was only analyzed for experiment 2.2, due to time limitations in planning the medium-scale trials. Element mapping done by EPMA was prioritized for the rest of the experiments, as it gives a visual overview of the composition of the sample. The scale bars to the right of the mappings show the intensity of the given element. All EPMA images are given in the appendix.

Table 4.2: XRF analyses of the produced metal from experiment 2.2.

Experiment	Si	Ca	Al
2.2	96,40 %	1,99 %	0,40 %

Figure 4.2 shows samples of the cast metal and the metal in the crucible from experiment 2.3. Here, the metal from the crucible has large slag inclusions and slightly larger, more scattered impurities, whereas the casted metal has evenly distributed thinner sheets of impurities. The slag inclusions in the metal show that there was no good separation between metal and slag in the crucible. Figure 4.3 shows the element mapping of sample 2.6, which shows fine lines of impurities. This image is an example of experiments that produced the purest metal. Figure



4.4 shows a sample from experiment 2.8, that has significant impurities that both occur frequently and are larger than in the previously presented images. This is an example of the least pure metal.

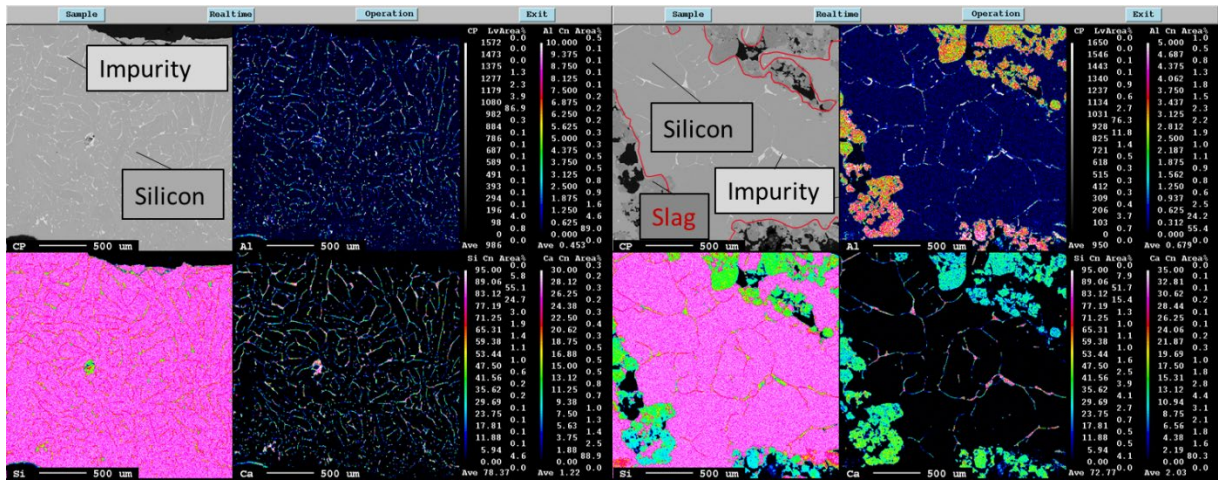


Figure 4.2: Element mapping of samples from experiment 2.3, an example of the metal characterized as medium pure. To the left: metal that was cast. To the right: metal and slag left in the crucible. The slag is enclosed by a red line.

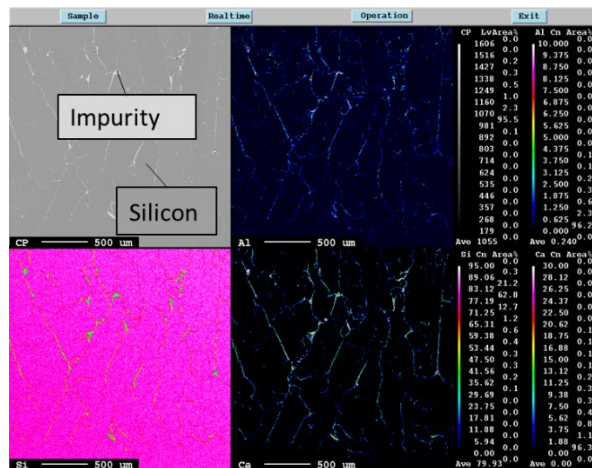


Figure 4.3: Element mapping of a sample from the cast material from experiment 2.6. An example of the metal characterized as the purer metal.

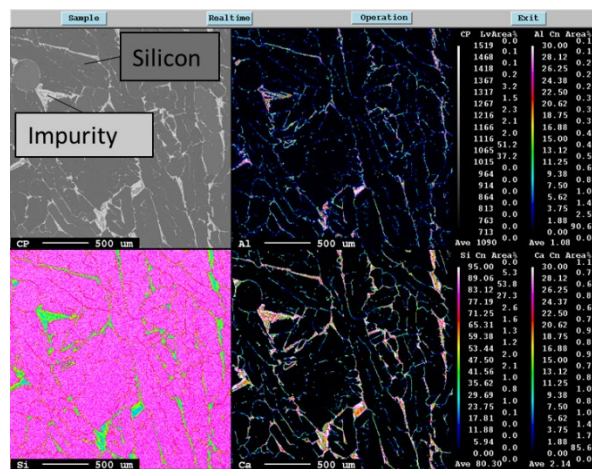


Figure 4.4: Element mapping of the cast metal from experiment 2.8. An example of a metal characterized as less pure.



The experiments have been divided into three categories based on the impurity content shown in the images, most pure (green), medium pure (yellow), and least pure results (red). The experimental matrix is repeated in Table 4.3 with these color codes to show the different parameters giving the different results.

Table 4.3: The table shows the experimental matrix for the small-scale experiments. The lines marked green (2.4, 2.6, 2.7) show the experiments that produced the purest metal, the yellow (2.3) show the intermediate, and the red (2.2, 2.5, 2.8) show the experiments with the poorest performance.

Experiment	Kerf [g]	SisAl Metal [g]	Slag [g]	Quartz [g]	Holding T [°C]	Holding time [min]	Gas stirring [min]	Casting T [°C]
2.1	250	125	250	0	1550	60	45	1600
2.2 (red)	250	125	250	40	1550	45	0	1600
2.3 (yellow)	250	125	250	40	1550	25	0	1550
2.4 (green)	250	125	250	40	1550	60	0	1550
2.5 (red)	250	125	250	0	1550	60	50	1550
2.6 (green)	250	125	250	40	1550	60	20	1600
2.7 (green)	250	125	250	40	1550	40	30	1600
2.8 (red)	250	125	250	40	1550	20	10	1600

The element mappings of samples from the cast metal from 2.4, 2.6, and 2.7 all show promising results with low impurity concentrations. They all included quartz additions and holding times of 60, 60, and 40 minutes, respectively. It seems that there is not much difference between a holding time of 40 and 60 minutes and that both give good results.

Experiment 2.4 did not include gas stirring; therefore, it seems that this was not crucial to obtain a good result when the holding time was 60 minutes. The effect of stirring on impurity removal has been investigated by other studies, and it has shown promise for the removal of Al from Si melt [35]. Stirring is believed to reduce the reaction time and is thus more important for shorter holding times. Experiment 2.2 had a holding time of 45 minutes and no gas stirring. The metal produced in this experiment appeared less pure than the one produced in the similar experiment 2.7 with 40 minutes of holding time and 30 minutes gas of stirring. Gas stirring appeared to have had a positive effect on the product for the experiments with holding times shorter than 60 minutes.

The element mappings of the cast metal from experiments 2.5 and 2.8 showed elevated levels of impurities. Experiment 2.5 had no quartz added and a holding time of 60 minutes with 50 minutes of gas stirring. Due to the poor result, it seems the addition of quartz had a positive effect on impurity removal. Experiment 2.8 included the addition of quartz, but only had 20 minutes of holding time, with 10 minutes gas of stirring. Although experiment 2.3 with a 25-minute holding time produced metal with slightly fewer impurities, the short holding times seem to be a disadvantage. Holding times of 25 minutes or shorter are therefore deemed insufficient.

This result is consistent with the theory, as the slag refining process is heavily dependent on the mass transfer of impurities. The high viscosity of this system causes slow kinetics, and

when experimenting with relatively low temperatures of 1550 to 1600 °C, longer holding times are needed to reach sufficiently low impurity concentrations. A holding time of 40 minutes with gas stirring was deemed the most suited. [33] [15]

**Impurities**

The impurities present in the metal were mainly made out of Al and Ca in addition to Si, as the SisAl metal contains about 16% Ca and 10% Al this is as expected. Table 4.4 and Figure 4.5 show different impurity phases that are present in the metal and their composition. The corresponding point analyses show that Fe is present in the impurities, along with Ti, V, Mn, and Cr. These impurity elements are believed to mainly originate from the kerf.

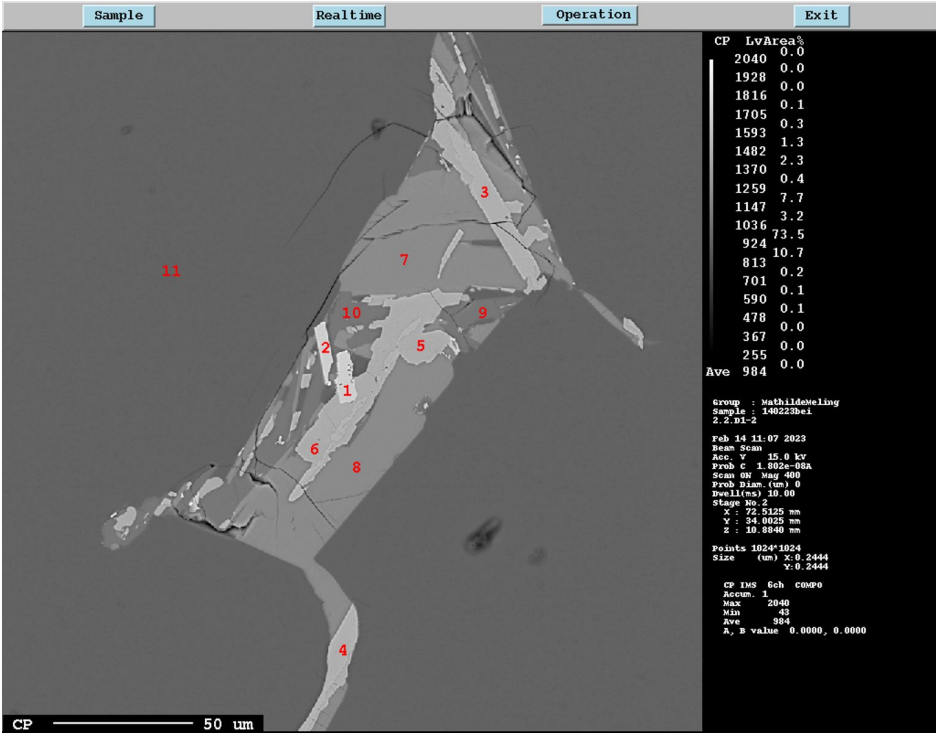


Figure 4.5: Enhanced image of the impurities present in the metal. The image shows impurities from experiment 2.2.

Table 4.4: The table shows the composition of the impurities. The numbers correspond to the points in Figure 4.5.

No.	Si	Al	Ca	V	Ti	Cr	Mn	Fe	Total
1	35.114	1.652	0.527	6.637	22.160	1.038	3.014	21.890	92.032
2	35.546	1.594	0.539	6.508	22.947	0.985	2.984	22.171	93.274
3	54.431	2.344	0.538	0.000	0.000	0.000	0.000	42.330	99.643
4	54.876	2.210	0.111	0.000	0.000	0.000	0.000	42.952	100.149
5	37.049	23.461	7.266	0.000	0.000	0.000	0.000	32.306	100.082
6	36.759	23.679	7.287	0.000	0.000	0.000	0.000	31.764	99.489
7	57.789	0.759	40.708	0.000	0.000	0.000	0.000	0.295	99.551
8	58.261	0.716	40.290	0.000	0.000	0.000	0.000	0.234	99.501
9	39.959	34.733	25.984	0.000	0.000	0.000	0.000	0.278	100.954
10	39.177	35.299	26.196	0.000	0.000	0.000	0.000	0.254	100.926
11	100.512	0.019	0.060	0.000	0.000	0.000	0.000	0.000	100.591

## Slag Composition

In Table 4.5, the concentration of the slag from experiment 2.2 is given. The composition was found by doing point analyses of three different points in the slag sample. All three points gave approximately the same value. Since all experiments used the same raw materials, it is assumed that they made similar slags.

Table 4.5: Composition of bulk slag from experiment 2.2

No.	SiO <sub>2</sub> [%]	Al <sub>2</sub> O <sub>3</sub> [%]	CaO [%]	Total [%]
1	50,756	8,610	43,190	102,556
2	51,546	7,847	43,674	103,067
3	50,977	8,032	43,879	102,888
<b>Average</b>	51,093	8,163	43,581	102,837

Since the slag was fairly inhomogeneous, as can be seen in the element mapping images in the appendix, this composition can only be considered an approximate composition of the slag. The point analysis technique is good for determining the composition of one point, but it cannot give the composition of the bulk of the material.

A FactSage calculation was also conducted for experiment 2.2, and the result was a slag composition of 42,3% SiO<sub>2</sub>, 51,3% CaO, and 6,3% Al<sub>2</sub>O<sub>3</sub>. The calculation shows which compounds exist at different temperatures given the raw materials used in the experiment. The calculation assumes equilibrium, and it is unlikely that the experiment reached equilibrium at any temperature, as the heating was done quite rapidly, and the holding time was limited. Figure 4.6 shows the calculation over the temperature interval of the experiment.

### FactSage Calculation for Experiment 2.2

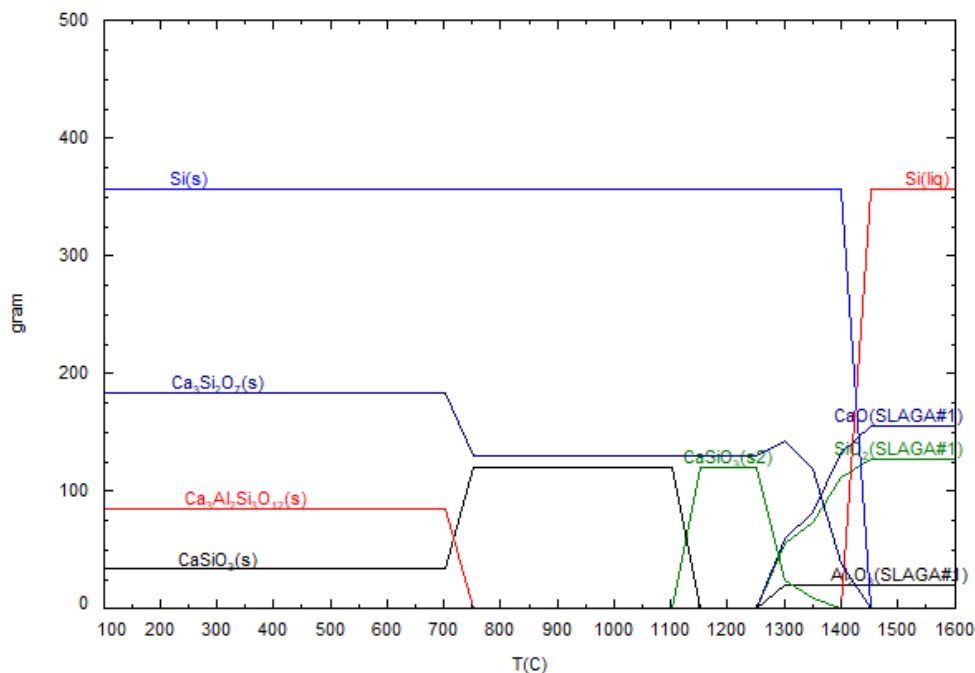


Figure 4.6: FactSage calculation for experiment 2.2. The figure illustrates the compounds that would be present at a given temperature if equilibrium was reached, and their quantities. The calculation is based on the raw materials used in experiment 2.2.

The theoretical slag composition calculated by FactSage differs from the point analysis composition as illustrated by Figure 4.7. In the FactSage calculation, it is assumed that all Al and Ca in the SisAl metal were oxidized by  $\text{SiO}_2$ . The metal composition from experiment 2.2 show that this did not happen, as there was still Ca and Al present in the metal. The elevated  $\text{SiO}_2$  content in the point analysis also shows that not all impurities were oxidized.

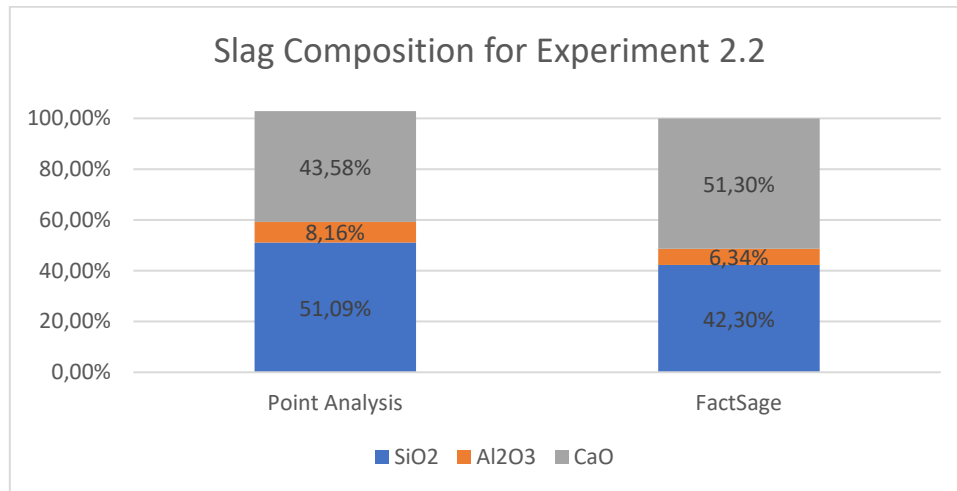


Figure 4.7: The figure shows the slag composition for experiment 2.2 from the average slag composition based on the point analyses and from the FactSage calculation.

Quartz was added in the experiments since some of the  $\text{SiO}_2$  in the slag is used to oxidize Ca and Al in the melt and transfer them to the slag, as discussed in section 2.3.1.3. The initial slag contained 47,7%  $\text{SiO}_2$ , and the additional quartz was added to ensure a high  $\text{SiO}_2$ -content in the slag throughout the experiment. This is important to achieve a pure silicon composition in the final product, as illustrated in the solution diagram for Ca and Al in Figure 2.12. Higher  $\text{SiO}_2$ -content in the slag enables lower concentrations of both Al and Ca in the final product.

When deciding how much quartz should be added, the positive effects on the final metal composition have to be weight against the changes to the slag properties. When the  $\text{SiO}_2$ -content increases, the viscosity follows. The density of the slag decrees with increasing amounts of  $\text{SiO}_2$ , bringing the density of the slag closer to the density of the molten metal. Neither of these changes is positive, as similar densities make the separation of slag and metal more difficult, and high viscosity slows down mass transfer and gas stirring become more difficult.

For the small-scale experiments, 40 g quartz was added. In these experiments, 250 g slag with 47%  $\text{SiO}_2$  was used. The final slag composition was found to have 51%  $\text{SiO}_2$ , as shown in Table 4.5. This show that the quartz added gave the final slag composition slightly higher  $\text{SiO}_2$ -content than the initial slag.

The theoretical amount of  $\text{SiO}_2$  needed to oxidize the Ca and Al impurities in the SisAl metal, assuming all impurities are desired oxidized, is for this case 32 g. In addition, the new oxides add to the total slag amount. This means that theoretically, more quartz additions are needed to reach a slag composition with higher  $\text{SiO}_2$ -content. According to the FactSage calculations, the final slag should have had significantly lower  $\text{SiO}_2$ -content than what was found. This,

combined with the EPMA element mapping images and the analysis of the metal from experiment 2.2, shows that not all of the impurities were oxidized.

#### 4.1.1.3 Mass Balance and Material Losses

Mass of metal and slag were not weighed for the small-scale experiment as it was not possible to separate slag and metal in the crucible. A mass balance was done using the relationship between metal and slag produced according to the FactSage calculations but incorporating the analyzed metal and slag composition of experiment 2.2, and the measured material losses. The mass balance is given by Figure 4.8.

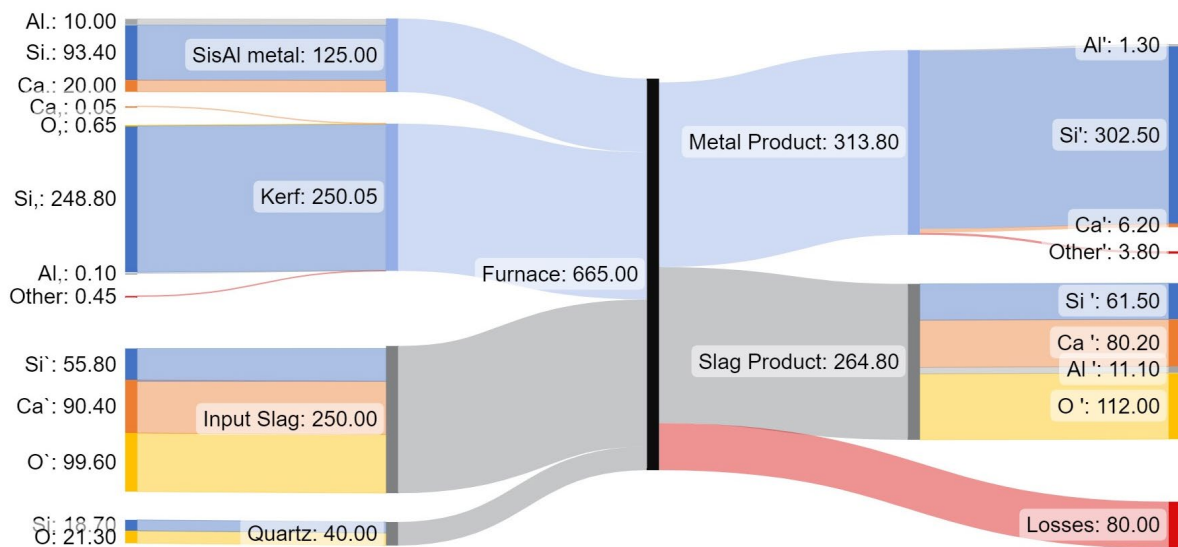


Figure 4.8: The figure shows a Sankey Diagram illustrating the mass balance of experiment 2.2 with slag composition according to the point analysis and metal composition according to the XRF analysis.

The mass balance show that the combined amount of Al in the products exceeds the amount of Al in the raw material, which shows that either the metal or, more likely, the slag composition was not valid.

The material losses varied widely between the different experiments, from 80 to 161 g. Most of the losses are linked to observable, physical losses that occurred during the experiments. One substantial source of these losses is the material that stuck to the graphite tubes that were used for stirring and to protect the thermocouple when they were removed from the melt. Some of the losses can also be assigned to the consumption of the graphite crucible. The losses are shown in Figure 4.8 along with the holding times. All experiments had the same total mass of raw materials, except experiment 2.5 which had 40 grams less as no quartz was added.

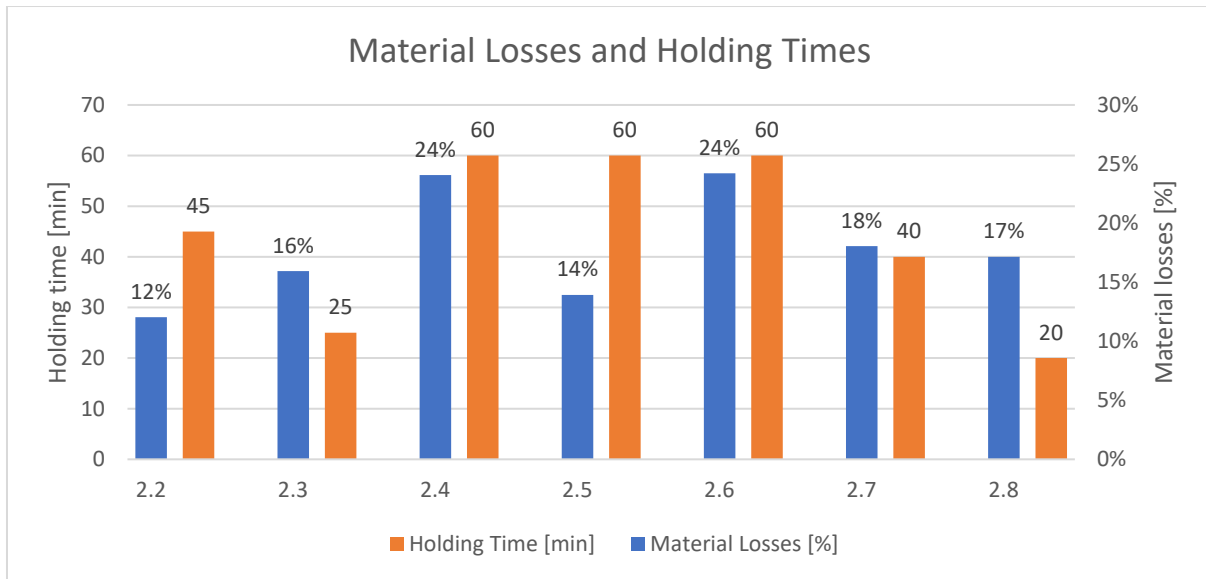


Figure 4.9: Material losses and holding times for the small-scale experiments.

A varying amount of material was lost during casting. In some cases, the casting mold most likely contained some moisture that evaporated when molten metal was poured on top of it. This caused metal droplets to be scattered around the lab during casting. The degree to which this occurred varied, and it was most substantial for experiment 2.4. All experiments experienced some losses during casting.

Little material is believed to have been lost through fuming, as little to no fuming was observed. During the addition of quartz powder, some of the fine particles were sucked up into the ventilation over the furnace, and some material was spilled during the addition.

Even though it is likely that most losses are linked to things that occurred during the experiments, the experiments with longer holding times tended to have higher losses, as illustrated in Figure 4.8. The experiments that experienced the highest losses both had holding times of 60 minutes, with experiments 2.4 and 2.6 losing 24% of their initial mass. Experiment 2.5 had the same holding time, but a loss of just 14%, which contradicts the idea that a longer holding time gave higher losses. Experiment 2.2 also contradicts the trend, with its low losses of 12% and relatively high holding time of 45 minutes. Gas stirring does not appear to have an effect, as experiment 2.2 had no gas stirring and experiment 2.5 had 50 minutes of gas stirring, and both had losses of about the same amount of material.

#### 4.1.1.4 Preliminary Conclusions and Choices Made for the Next Set of Experiments

The results from the small-scale experiments along with experiences from the lab and literature review were used to plan the medium-scale trials. The general preliminary conclusion from the small-scale experiments is that the experiments work and that it is likely that they are suited for upscaling.

The holding temperature was decided to be 1550°C moving forward. At this temperature, minimal fuming had been experienced in the small-scale trials, and by keeping the

temperature in this area, the material losses are believed to be small. Observations of the melt during the experiments revealed that the melt seemed to have a sufficiently low viscosity at this temperature, which allowed for good gas stirring. As the medium-scale experiments would be performed in a tiltable furnace that can cast the material directly, without removing the crucible from the furnace, it is expected that this temperature will also be sufficient for casting. Theoretically, the silicon should also have a slightly lower density than the slag at this temperature, which ensures that the silicon will separate from the slag and stay at the top of the furnace and be cast first.

The holding time was set to 40 minutes for the next set of experiments. The results from the small-scale trials did not give a definite result as to which holding time would produce the purest metal. No significant improvements were seen in the purity of the produced metal between the holding times of 40 and 60 minutes, suggesting that 40 minutes is sufficient. In addition, the high material losses for the experiments with longer holding times suggest that a shorter holding time would be beneficial considering silicon yield. Holding times of around 20 minutes also showed some promise but performed poorer concerning the purity of the product.


Both mass ratios 2:1:2 (kerf : SiAl metal : slag) and 1,5:1:2 were chosen for further investigation. This set of experiments had proven that 2:1:2 worked, but it was still interesting to test both mass ratios to find the best procedure.

The addition of quartz worked well experimentally and showed promising results regarding impurity removal as well. This will be investigated further in the next set of experiments, with the addition of quartz at various times in the process, and in different amounts.

## 4.1.2 Medium-Scale Trials

The main results from the medium-scale experiments are presented in Table 4.6 alongside the method and the raw materials used for the experiments.

Table 4.6: The table shows the method, raw materials, and results from the medium-scale slag refining experiments.

Ex.	Method		Raw materials [kg]				Result			Si Yield
			Kerf	SisAl Metal	Slag	Quartz	%Si	%Ca	%Al	
3.1		Holding time [min]	16,5	11,0	22,0	3,5	96,23%	1,94%	0,51%	89,24%
3.2			16,5	11,0	22,0	3,5	97,52%	1,05%	0,35%	92,25%
3.3			16,5	11,0	22,0	10,2	98,48%	0,23%	0,16%	84,94%
3.4			22,0	11,0	22,0	10,2	98,91%	0,20%	0,10%	83,88%
3.5			16,5	11,0	22,0	9,0	98,79%	0,37%	0,10%	89,88%
3.6			22,0	11,0	22,0	9,0	97,8%	0,99%	0,19%	75,01%

### 4.1.2.1 Method

Experiments 3.1 and 3.5 were conducted directly after a change of crucible. These experiments hence started from empty crucibles, while the other experiments were conducted in crucibles with leftover material from the previous experiment. This gave the experiments a disadvantage when calculating the material losses. The new crucible also meant that these experiments experienced less heat losses.

Experiments 3.1, 3.3, and 3.5 were conducted in the morning, starting from a cold furnace, whereas 3.2, 3.4, and 3.6 were conducted in the afternoon, directly after the casting of the previous experiment. This caused a difference in time before the kerf and slag were melted. It took about 3 hours to melt the materials in the experiments conducted in the morning. Even though experiments 3.4 and 3.6 included more materials, the experiments took about 20 minutes less time than 3.3 and 3.5, who were conducted in the afternoon.

The exact holding time and temperature for the different experiments varied. The temperature in the melt was not monitored continuously, and the wall temperature differed widely from the temperature in the melt. In experiment 3.1, which was the first experiment, it took some time to get the settings right, and this experiment used about one hour more to reach the desired temperature than the other experiments.

The amount of raw materials added also made a significant impact on the holding time. In experiment 3.2, where only 3,5 kg of quartz was added, the required time for the quartz to melt was much lower than for the following experiments with three times more quartz materials.



#### 4.1.2.2 Composition of Metal and Slag

The composition of the metal produced is presented in Figure 4.9. The first experiment performed significantly poorer than the rest of the experiments. This is partly due to the parameters used, but most likely also caused by issues finding good operation parameters, both regarding charging time and temperature settings. For the rest of the experiments, the variations are believed to be linked to the different raw material ratios.

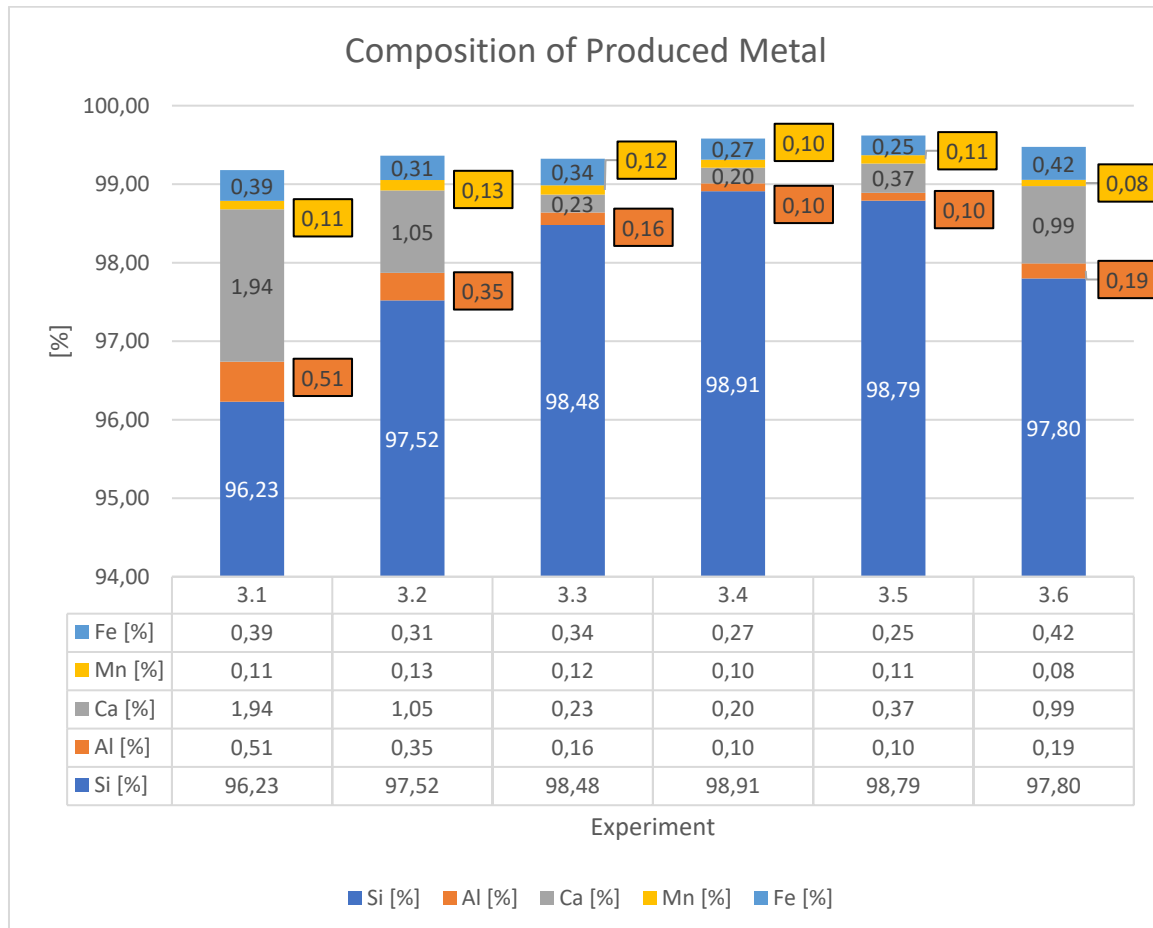


Figure 4.10: The table and graph show the composition of the metal produced at Elkem in the medium-scale trials. All elements were analyzed by XRF analysis. The most abundant elements are presented, but other elements are also present in smaller amounts, such as Ti, Ba, Mg, P, and B. For full analysis, see appendix.

The slag composition was measured by finding how much of each metal was present. The amount of silicon present as inclusions in the slag was analyzed for three of the experiments and is presented as “Free Si” in Table 4.7

Table 4.7: Analysis of elements in slag. Free Si is the silicon present as inclusions in the slag.

Element	Method	3.1 [%]	3.2 [%]	3.3 [%]	3.4 [%]	3.5 [%]	3.6 [%]
<b>Si (total)</b>	XRF	25,8	27,5	28,5	33,3	30,4	31,2
<b>Ca</b>	XRF	35,1	32,8	27,8	28,0	26,2	26,7
<b>Al</b>	XRF	4,6	4,4	4,1	4,1	4	4,6
<b>Free Si</b>	Titration		6,5	4,7	6,4		

The slag composition was found by converting these elements into oxides. The silicon inclusions were left out of these calculations, and the amount of silicon expected to be found in the form of  $\text{SiO}_2$  is then the total amount of silicon minus the amount of free silicon. For experiments 3.1, 3.5, and 3.6 the amount of free silicon was not measured, and their slag composition can therefore not be calculated. The slag composition is given in Figure 4.10.

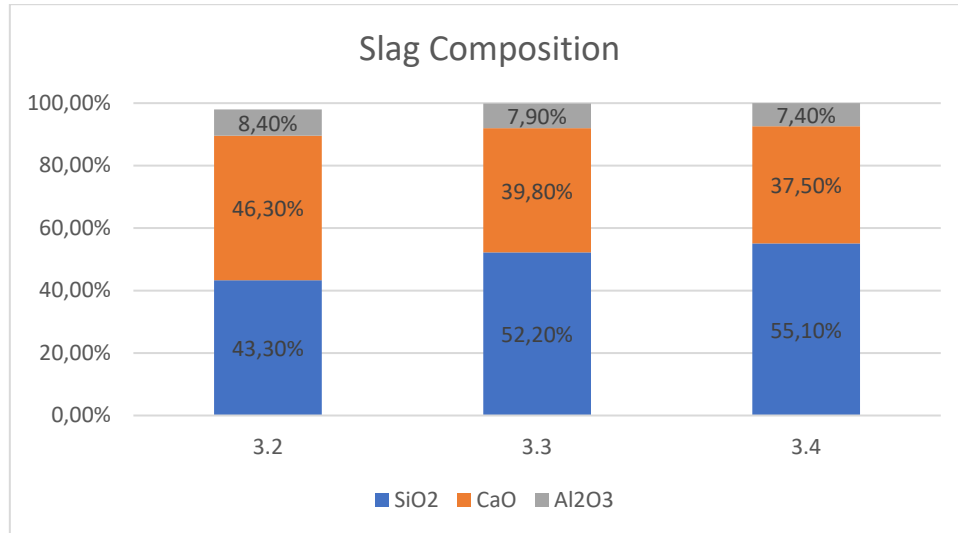


Figure 4.11: The composition of the slag, given for the three main components. Further details can be found in the appendix. Numbers are given in wt. %.

The slag composition and the metal composition are related, as described in section 2.3.1.3. As expected, based on the presented theory, the experiments that had the most  $\text{SiO}_2$  added had the lowest levels of Ca and Al in the produced metal. Experiments 3.3 and 3.4 both had 10,2 kg of quartz added to the experiment, whereas experiments 3.1 and 3.2 only had 3,4 kg and experiments 3.5 and 3.6 had 9 kg. The metal produced in experiments 3.1 and 3.2 had as much as 1,94% Ca and 0,51% Al, and 1,05% Ca and 0,35% Al, respectively. The poor results from experiment 3.1 are likely also caused by the short refining time with the additional  $\text{SiO}_2$  as the quartz was added halfway through the holding time. Experiments 3.3 and 3.4 had dramatically less of both Ca and Al, with 0,23 and <0,20 % Ca and 0,16 and <0,10 % Al, respectively. For experiments 3.5 and 3.6 the concentrations of Al stayed at around the same values, but the Ca concentrations rose to 0,37 and 0,99%, respectively. The concentrations of Al and Ca in the metal produced in the different experiments are illustrated in Figure 4.11.

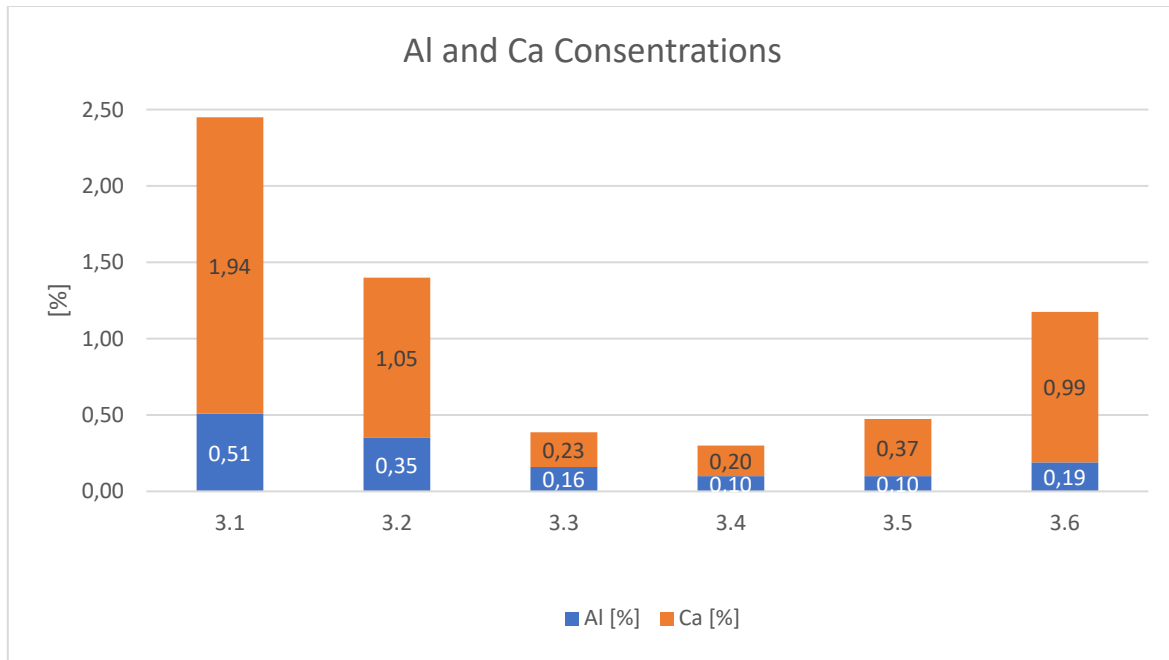


Figure 4.12: The concentration of Al and Ca in the metal produced in the different experiments. All numbers are given as wt.%.

Even though the concentrations of Ca and Al were small in experiments 3.3 and 3.4, further removal could be possible. A longer holding time could likely have further reduced the impurity concentrations, but due to kinetic limitations, it is not deemed probable to achieve significantly lower impurity concentrations within reasonable holding times.

The theoretical FactSage calculation in Figure 4.12 show that the expected slag composition was 49,78% SiO<sub>2</sub>, 42,63% CaO, and 7,59% Al<sub>2</sub>O<sub>3</sub> for experiment 3.3. The concentration of Al<sub>2</sub>O<sub>3</sub> is fairly similar to the analyzed result of the slag, but the rest of the slag is shifted towards less SiO<sub>2</sub> and more CaO. Still, the FactSage calculations correspond fairly well to the experimental results, as illustrated in Figure 4.13.

### FactSage Calculation for Experiment 3.3

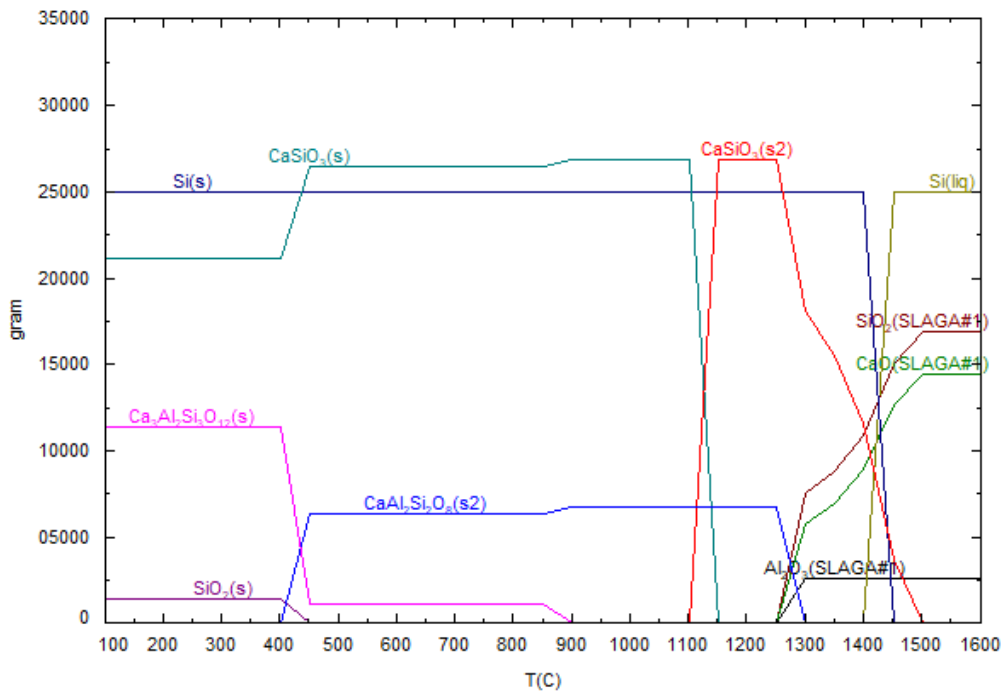


Figure 4.13: FactSage Calculations of experiment 3.3 showing the different phases that the theoretical calculation expects to be present at the different temperatures at equilibrium.

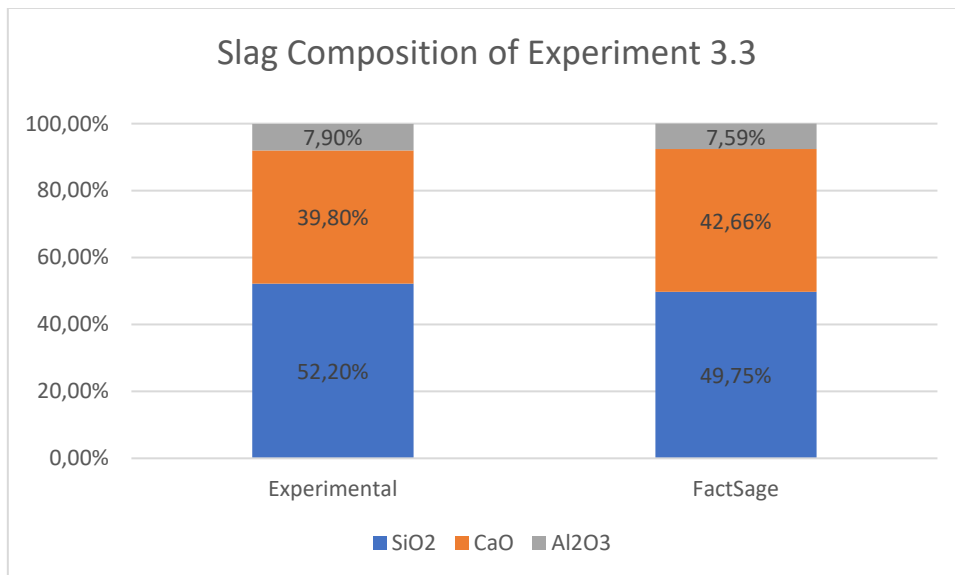


Figure 4.14: The figure shows a graph giving the experimental slag composition from experiment 3.3 and the corresponding FactSage calculation.

According to the FactSage calculations, 24,9 kg of silicon should have been produced in experiment 3.3, assuming equilibrium conditions. The practical experiment showed that only 18,6 kg of metal was produced. According to the FactSage calculations, the metal produced should have been pure silicon, which was not the case for the experimentally produced metal. The amount of silicon produced is also higher than the amount of silicon in the raw materials,

showing that FactSage calculations assume that SiO<sub>2</sub> is reduced when all the Al and Ca from the SisAl metal are oxidized.

The reduced SiO<sub>2</sub> content in the slag and the high amount of silicon produced correlate well, as it can be assumed that less SiO<sub>2</sub> was reduced in the experimental results since there were still impurities left in the metal. In addition to this, the experiment was not expected to reach equilibrium, which also explains the difference in slag and metal composition. Lastly, the silicon droplets left in the produced slag influenced the amount of metal produced and may also have influenced the slag composition.

#### 4.1.2.3 Element Mapping and Impurities by EPMA

The element mappings shown in the appendix show that all experiments produced silicon with low impurity concentrations. The impurity content is visibly reduced from the small-scale experiments. The impurities are also more spread out than for the cast material in the small-scale experiments. The molds used for these experiments were much larger and could fit 20 kg of metal. This meant that the metal cooled down slower, and the impurities had more time to gather.

Experiments 2.7 and 3.4 have many of the same parameters, such as the same kerf-SisAl metal-slag-ratio, the same holding time, and the about the same time with gas stirring. Still, the electron backscatter images show that the experiment performed in the medium-scale trial performed better with regard to impurity removal. This is shown in Figure 4.14. The largest difference between experiments 2.7 and 3.4 is the amount of quartz added, where 3.4 had 10,2 kg quartz to 22 kg slag, and 2.7 had 40 g quartz to 240 g slag. An image of metal from experiment 3.1, with 3,2 kg quartz to 22 kg slag, is therefore included to show that the medium-scale trials performed better, even with the same ratio of quartz added. Still, the figure shows that higher amounts of quartz improved the purity of the product.

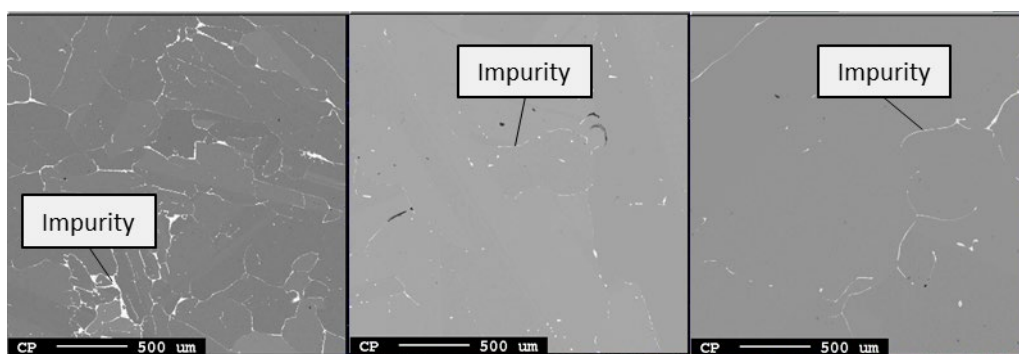


Figure 4.15: To the left: The metal from experiment 2.7, in the middle: metal from experiment 3.4, to the left: metal from experiment 3.1. All images are with impurities shown as white lines on a grey background.

The impurities are visible as lighter areas in the backscattered electron images. These impurities consist of several intermetallic phases. One impurity has been enlarged in Figure 4.15, and the compositions of the different phases are given in Table 4.8. As in the small-scale trial, the impurities mainly consist of Si, Ca, and Al, as these are the most abundant elements, but other elements such as Fe, Mn, and Ti are also present in noticeable amounts.

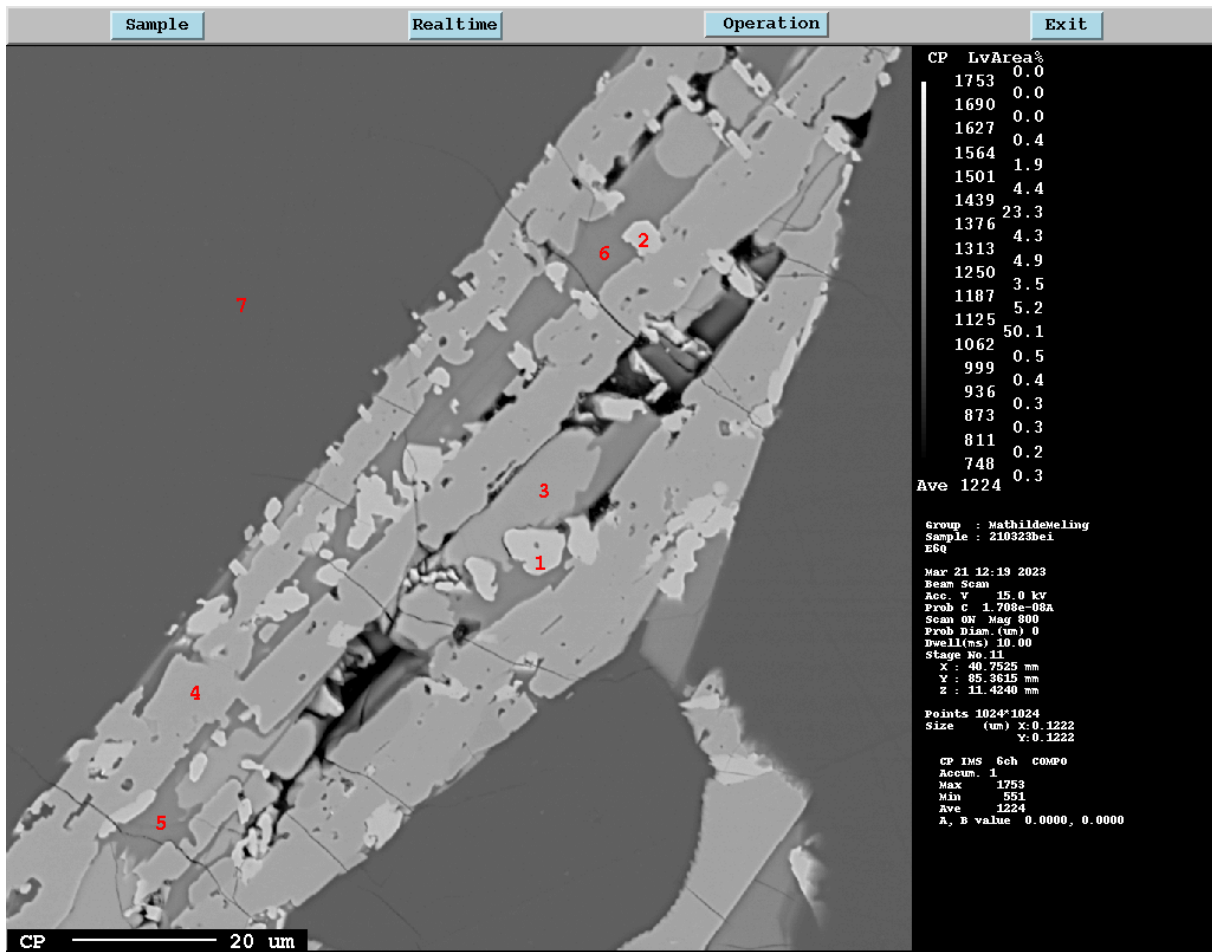


Figure 4.16: Enlargement of an impurity present in the sample from experiment 3.6 The numbers in the image correspond to the lines describing the composition of said phase.

Table 4.8: The table gives the compositions for the points marked in Figure 4.15. Composition is given in wt. %

Point	Si [%]	Al [%]	Ca [%]	V [%]	Ti [%]	Cr [%]	Mn [%]	Fe [%]	Ga [%]	Ni [%]	Cu [%]	Total [%]
1	35,254	0,416	0,637	3,167	26,072	0,209	11,979	19,715	0,000	0,000	0,000	97,449
2	35,715	0,393	0,567	1,332	26,979	0,224	12,730	20,538	0,000	0,000	0,000	98,478
3	41,442	3,429	37,388	0,062	0,144	0,011	0,363	0,991	3,402	2,032	9,566	98,830
4	50,042	3,543	0,426	0,111	0,229	0,089	12,450	30,802	0,079	0,255	0,079	98,105
5	54,815	0,653	39,026	0,071	0,071	0,000	0,344	0,807	1,598	0,115	0,338	97,838
6	55,279	0,645	39,660	0,068	0,131	0,062	0,300	0,784	1,452	0,040	0,172	98,593
7	97,353	0,018	0,063	0,021	0,036	0,003	0,068	0,260	0,016	0,000	0,039	97,877

#### 4.1.2.4 Mass of Slag and Metal

The total mass of slag and metal varied between the different experiments as the amount of quartz and kerf added varied, and the ratio between slag and metal produced varied from 1,5 to 2, as presented in Table 4.9. According to Equation 4.1, a slag/metal ratio of about 1 should be sufficient. [5] All experiments exceeded this criterion, and the amount of slag present is thus believed to be sufficient.

$$W_R = \frac{\Delta[\%Al] \cdot \frac{M_{Al_2O_3}}{2M_{Al}}}{(\%Al_2O_3)_R} \cdot 1000 \frac{kg \text{ slag}}{\text{tonne alloy}} = \frac{4,16 \cdot \frac{101,96}{2 \cdot 26,98}}{7,9} \cdot 1000 = 995 \frac{kg \text{ slag}}{\text{tonne alloy}}$$

Equation 4.1: Calculation based on Equation 2.15 [5]

Table 4.9: The mass of slag and metal produced is presented in this table, and the ratio between slag and metal is calculated.

Experiment	Slag [kg]	Metal [kg]	Slag/Metal
3.1	29,80	20,00	1,49
3.2	30,00	20,40	1,47
3.3	38,00	18,60	2,04
3.4	38,70	22,50	1,72
3.5	34,30	19,90	1,72
3.6	40,30	20,35	1,98

#### 4.1.2.5 Mass Balance

Experiment 3.3 will be investigated further with regard to mass balance.

The Sankey diagram in Figure 4.16 shows the distribution of Si, Ca, Al, and O in the different raw materials and products for experiment 3.3. The diagram illustrates where the different elements in the raw materials go, such as that the aluminium and calcium from the SisAl metal can be found in the slag output, along with the input slag and quartz.

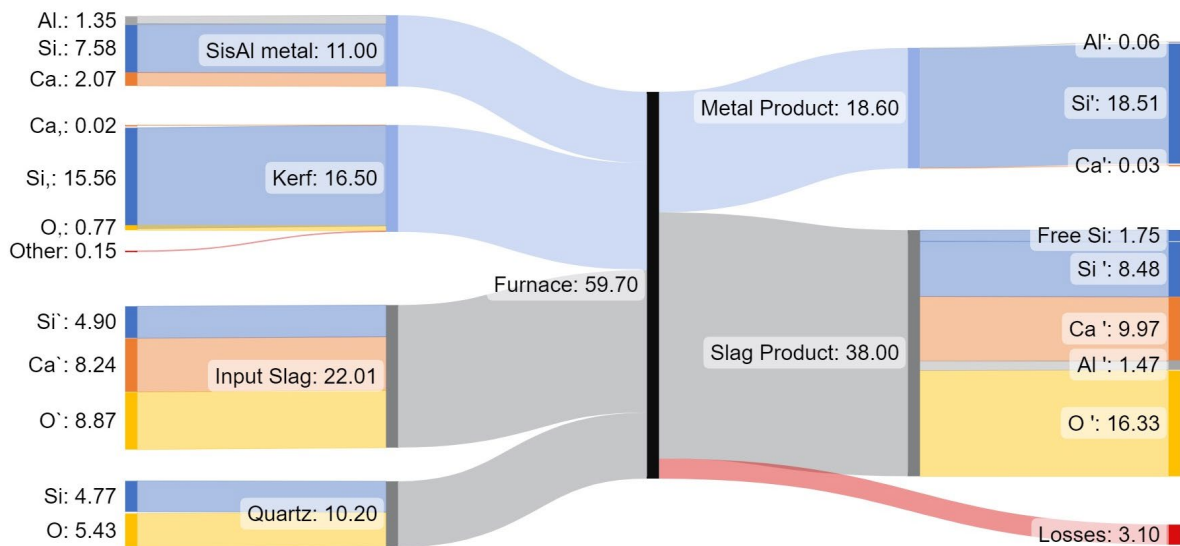


Figure 4.17: The figure shows a Sankey diagram showing the flow of Si, Al, Ca, and O through the system in experiment 3.3. The masses are given in kg.

The Sankey diagram shows that the slag refining was efficient for the removal of Al and Ca since there is much less of both in the final metal than in the silicon raw materials. More oxygen was found in the final slag than in the raw materials. This indicates that the melt was exposed to some oxygen during the experiment, or that either the amount of slag produced,

or the slag composition was incorrect. The slag composition may have varied throughout the melt, or there might have been more free Si in the slag than the analysis showed.

This figure also shows that there is more silicon in the final slag than in the initial slag and quartz combined. This is due to the silicon inclusions in the slag. The total amount of silicon entering the system is different from the silicon in the final products. This shows that some silicon losses have occurred throughout the experiment, which will be further discussed in the following section.

#### 4.1.2.6 Material Losses and Silicon Yield

In the medium-scale trials, the relative losses were smaller than for the small-scale experiments. Causes for material losses in the experiments include leftover materials in the crucible and the tap chute. The material losses in the different experiments are given in Figure 4.17. The mass of input materials, products, and losses are presented in the appendix.

The silicon yield of the different experiments is presented in Figure 4.17, and the basis for the calculation is given in the appendix. The yield was calculated from the silicon in the raw materials and the silicon in the produced material. The yield varies from 75% to 92%.

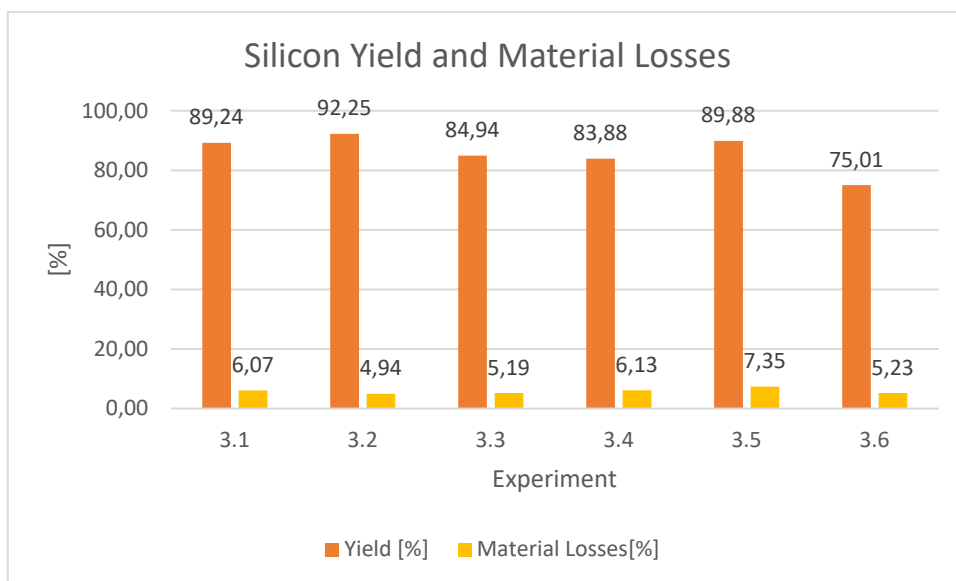


Figure 4.18: The silicon yield and material losses of the third set of experiments are presented. All values are given in wt.%.

The material losses are as expected, as there was some material left in the crucibles after casting. Experiments 3.1 and 3.5 had the highest material losses, which can be explained by the crucible change that took place directly before the experiments. These experiments included no leftover materials from previous experiments but did leave material in the crucible after casting, and the total material loss is therefore expected to be larger. Some of the material losses are also related to the evaporation of the remaining water content in the kerf.

There was little fuming observed during the experiments, and the material losses are believed to be mostly related to the physical losses in the crucible and during tapping. Fuming of silica



was attempted avoided by keeping a relatively low operating temperature of about 1550-1580 °C. Even though the amount of silicon lost through fuming is believed to be small, it is not believed to be zero.

There is no obvious connection between material losses and silicon yield, as illustrated in Figure 4.17, except that experiment 3.2 had both the lowest material loss and the highest yield. The silicon yield varied broadly between 75% and 92%. The metal inclusions in the slag are believed to be the main reason for the reduced silicon yield. During casting, there were also some larger amounts of metal cast with the slag due to poor separation at the metal-slag interface. The density of silicon at the casting temperature was calculated to be 2,49 g/cm<sup>3</sup>[5], and the density of the slag was found to be around 2,6 g/cm<sup>3</sup> in the diagram presented in Figure 2.10 [25]. This small density difference is believed to be a significant part of the reason for the poor separation between slag and metal. During casting, the furnace is tilted, and this process can stir the materials together. After cooling, it was attempted to find the larger chunks of metal in the slag and weigh them with the rest of the cast metal. This step left room for error, and some metal was left with the slag.

The last experiment, experiment 3.6, stood out with a silicon yield of only 75%, almost 10% less than the experiment with the second lowest silicon yield. In experiment 3.6, the amount of silicon produced was lower than expected and about 2 kg less than in experiment 3.4, which had the same amount of silicon in the raw materials. There are no obvious reasons for this, and it might just have been caused by poor separation between metal and slag.

#### **4.1.2.7 Preliminary Conclusions and Choices Made for the Next Set of Experiments**

Due to inconsistencies of the results from the experiments with 2 parts kerf, 1 part SisAl metal, and 2 parts slag, the raw material mix with 1,5 parts kerf, 1 part SisAl metal and 2 parts slag (1,5:1:2) has been chosen for the large-scale trials. Even though the purest metal was produced in experiment 3.4 with 2 parts kerf, the low silicon yield, and the large Ca concentration in experiment 3.6 poses an uncertainty concerning how well this raw material mix will perform in the next experiment.

The experiments with 1,5 parts kerf have performed consistently well, with high silicon yields and low levels of impurities for experiments 3.3 and 3.5. Therefore, an amount of quartz similar to the ratio used for these experiments will be used in the large-scale experiments.

Experiments 3.3 through 3.6 generally performed well, and their process parameters will therefore be used for the large-scale trials. The holding time used in the experiments appeared to have given the slag sufficient time to react with the metal. The same holding time will therefore be used in the large-scale trials. To avoid silicon losses through fuming, the temperature will be kept at around 1550 °C.

### 4.1.3 Large-Scale Trial

The large-scale trial consisted of one experiment producing 109 kg silicon. The raw materials used, and the most important results are given in Table 4.10.

Table 4.10: The table shows the raw materials used in the large-scale trial, the composition of the metal product, and the Si yield.

Method	Raw Materials				Results			
Large-scale slag refining	Kerf [kg]	SisAl metal [kg]	Slag [kg]	Quartz [kg]	Si	Ca	Al	Si Yield
	110	75	147	68	99,7%	0,26%	0,63%	64,9%

#### 4.1.3.1 Method

The initial batch of slag was hard to melt, most likely due to large quantities of fines in the solid slag. When a melt had been established, the melting rate improved drastically. SisAl metal and slag were then co-charged to maintain the high melting rate. When kerf was added to the melt, excessive amounts of smoke were observed, and fines were lost to the off-gas.

Quartz was the last raw material added, and after the addition of quartz the viscosity of the slag increased. The operator also experienced difficulties when trying to dissolve the quartz, and lumps of undissolved highly viscous quartz were observed. Both manual stirring with a graphite rod and increased gas stirring were attempted, but the lumps were not dissolved. The lumps are shown in the pictures in Figure 4.18.



Figure 4.19: Undissolved lumps visible in the slag tapping.

Before the metal was tapped, the gas flow and the power of the furnace were reduced to settle the melt. The metal was cast first and there was no slag cast together with the metal. When the slag was cast, substantial amounts of metal were seen in the slag. The metal formed both larger pearls, as shown to the left in Figure 4.19, and smaller inclusions in the slag. The larger pearls were sorted out and added to the cast metal as part of the metal product.



*Figure 4.20: Left: Slag tapping where metal pearls are visible on the top of casting as round pearls. Right: Solidified metal tapping.*

After tapping, roughly 40 kg of unreacted quartz and highly viscous slag was observed in the bottom of the crucible.

#### 4.1.3.2 Composition of Metal and Slag

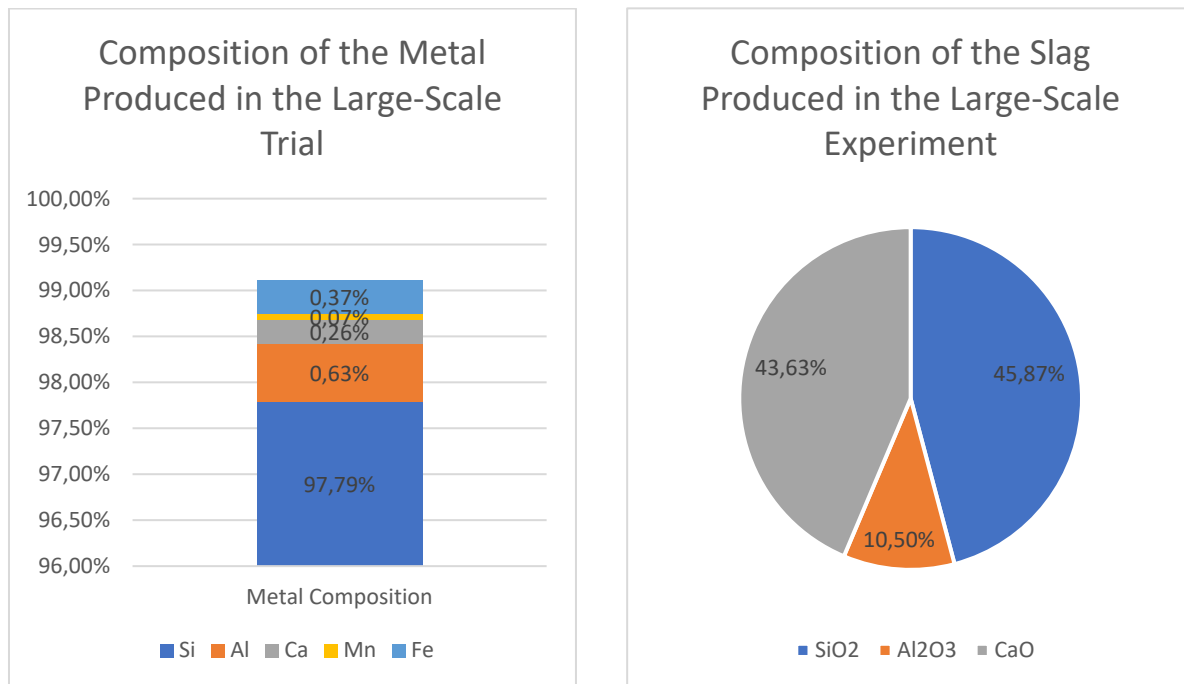


Figure 4.21: Metal composition after large-scale trial (left) and slag composition after large-scale trial (right).

The large-scale trials produced 109 kg of silicon that reached a purity of 97,79%, and the composition is shown in Figure 4.20. The slag composition is given to the right, with 45,87% SiO<sub>2</sub>, 43,63% CaO, and 10,50% Al<sub>2</sub>O<sub>3</sub>, calculated based on the content of elemental Si, Al, and Ca found in the slag analysis in the attachment. There were also substantial amounts of free silicon, not bound as oxides, present in the slag phase. The analysis concluded that 8,50% of the total slag mass was these metal droplets of various sizes. The total amount of cast slag was 239 kg, with 20 kg being metal inclusions and 219 kg being slag according to the analysis.

These results show that the slag refining process did not refine well with regard to Al. The combined initial Al concentration in the silicon raw materials was 4,23% and the final concentration was 0,63%, resulting in a removal ratio of 85,09%. In comparison, the removal ratio for Ca was 95,95%. In all of the medium-scale experiments, more Ca was found in the produced metal than Al. The large-scale experiment produced a slag similar to that of experiment 3.2 on the medium scale, with similar silicon purities. Still, the metal produced in experiment 3.2 had 0,35% Al and 1,05% Ca, following the trend of more Ca than Al, and the removal ratios were 92,9% for Al and 93,4% for Ca.

Reasons for this clear exception from the trend could be poor kinetics so that the slag and metal did not have time to achieve even close to equilibrium. This could be caused by the high viscosity of the slag, making stirring and mass transfer more difficult. According to the diagrams presented in Figure 4.21, the viscosity of the slag is somewhere between slightly less than 4 and 6, depending on the source, which are fairly high viscosities compared to molten silicon with a viscosity of less than 1.



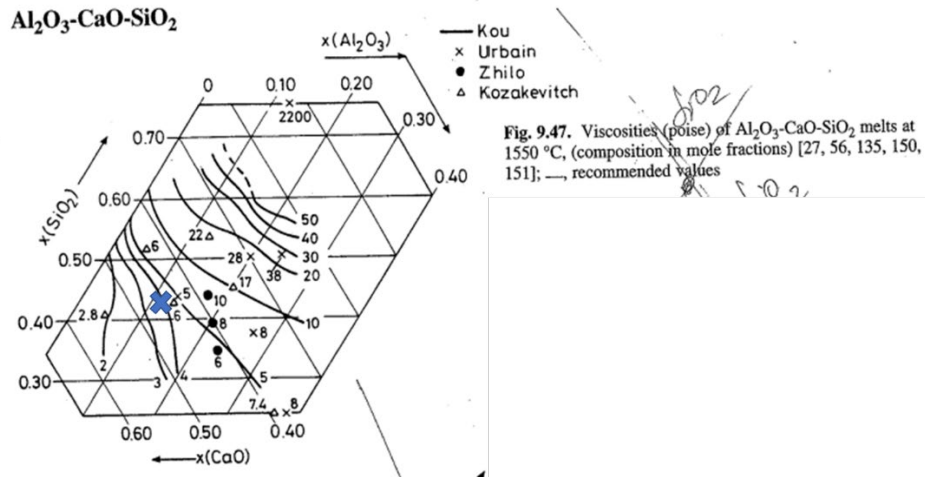


Figure 4.22: The figure shows the viscosity of the CaO-SiO<sub>2</sub>-Al<sub>2</sub>O<sub>3</sub>-slag at 1550°C at different compositions and from various sources. The different sources referred to in the figure refer to the sources in the Slag Atlas [25]. The blue X marks the slag composition.

A larger furnace also opts for more local variations throughout the furnace and the unreacted lumps of highly viscous quartz are believed to have influenced the composition locally. This means both the slag and the metal samples may not have been representative of the entire melt. An important argument to support this idea is that the total amount of Al in the slag, according to the given slag composition, was larger than the amount of Al added through the raw materials. Given the amount of Al added to the system and the analyzed Al concentration in the metal, there was only enough Al available to produce a slag with about 6 % Al<sub>2</sub>O<sub>3</sub>. This is only about half of the measured alumina content and supports the idea that the slag composition was not even throughout the melt.

This does not prove why the Al content in the metal was high, rather indicates that it should have been lower, as lower Al<sub>2</sub>O<sub>3</sub> content in the slag is expected to cause lower Al concentration in the melt. The elevated Al content in the metal may be caused by uneven metal composition as a product of the uneven slag composition. If the stirring was poor, and the slag had high alumina content in an area, it is reasonable that the metal had a high Al content in the same area. Other reasons include that there might have been more Al in the raw materials than expected. Although it is unlikely that this played such a significant role, the composition of the SiAl metal may have varied slightly from the analyzed result.

Figure 4.22 shows the theoretical mass of the compounds after the large-scale slag refining experiments. The theoretical slag composition predicted by FACTSage was 51,78% SiO<sub>2</sub>, 6,59% Al<sub>2</sub>O<sub>3</sub>, and 41,64% CaO, and the combined mass of the slag was 224,32 kg. The calculation found that the experiment should have produced 169,0 kg of silicon, and as in the calculations for the medium-scale trials, the silicon is expected to have no impurities.

### FactSage Calculation for the Large-Scale Trial

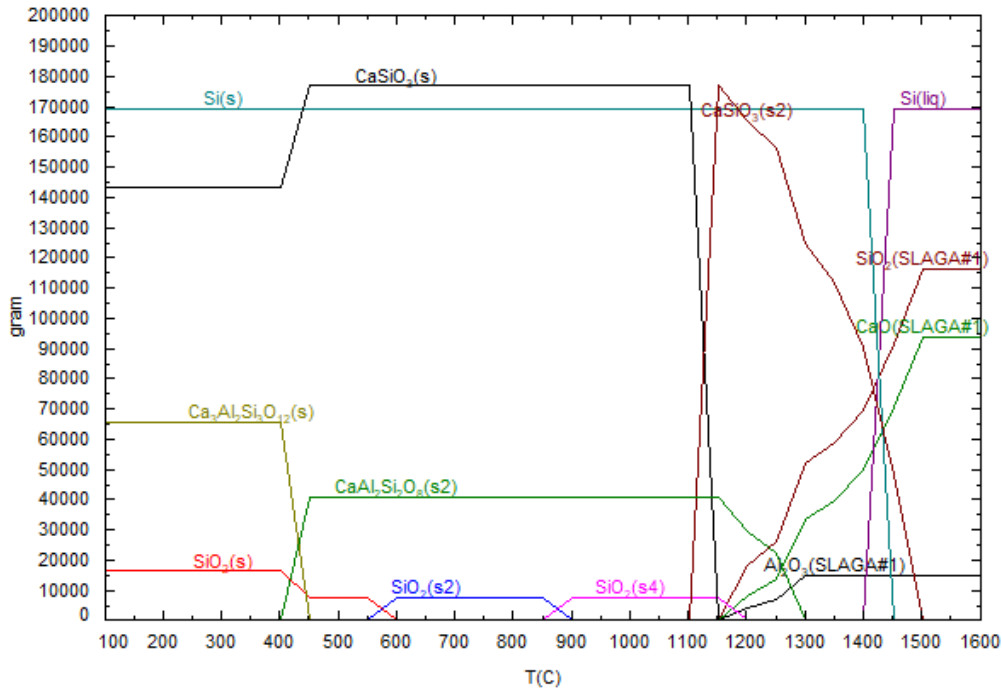


Figure 4.23: FACTSage Calculation based on the raw materials in large-scale slag refining experiment.

Since the metal produced was not 169,0 kg 100% Si but rather 109 kg 97,79% Si, a mass balance was conducted to calculate the slag composition based on the raw materials entering the system, and the materials that end up in the metal. Assuming all Ca and Al that did not go to the metal ended up in the slag as oxides, and that the rest of the O in the system ended up as SiO<sub>2</sub>, the slag composition should have been 52,55% SiO<sub>2</sub>, 41,54% CaO, and 5,91% Al<sub>2</sub>O<sub>3</sub>, illustrated in Figure 4.23. This calculation left 67,6 kg Si unaccounted for, and this is assumed to be found as inclusions in the slag, and as losses through kerf losses.

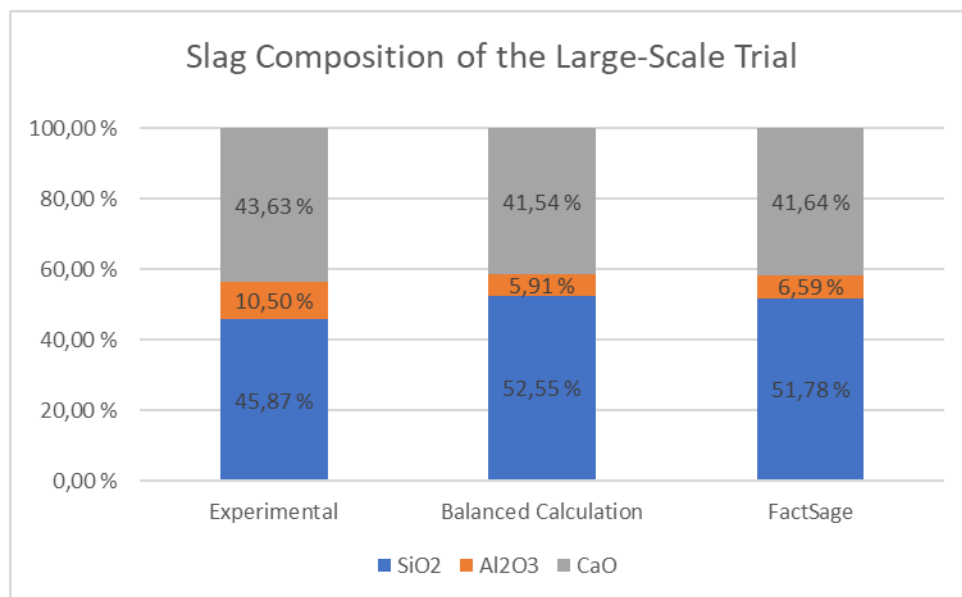


Figure 4.24: The figure shows a graph giving the experimental slag composition from the large-scale trial, the corresponding calculated composition based on mass balance, and the FactSage calculation.

Figure 4.23 compare the experimental slag composition with the slag composition found through mass balance calculations and the FactSage calculation. The balanced calculation and the FactSage calculation are quite similar to the experimental result, but there are still interesting differences. The SiO<sub>2</sub> concentration is substantially higher for the balanced and FactSage calculations than for the experimental result. When looking at this in combination with the fact that the FactSage calculations produced more silicon show that the mass balance of the experimental results for the large-scale trials does not add up. This further supports the idea that the slag composition varied throughout the melt.

#### 4.1.3.3 Mass Balance and Silicon Yield

There are several issues with the mass balance of this experiment. The Sankey diagram in Figure 4.24 shows the raw materials and the results according to the analysis, and the diagram in Figure 4.25 shows the same, but for a calculated mass balance.

As shown in the FactSage calculation, the expected silicon production was 169,0 kg, which is much higher than the 109 kg metal that was produced from the experiment. During casting, metal droplets of various sizes were observed in the slag. The larger droplets were removed from the slag and added to the cast metal as part of the produced metal, but the smaller metal droplets were left in the slag. According to an analysis done at Elkem, 8,5% of the total mass of the slag was free Si, not bound as oxides, which is 20 kg silicon. That gives only 129 kg of silicon in total, leaving 45,5 kg of silicon unaccounted for.

The expected slag production in the FactSage calculation was 224,32 kg, which is close to the actual amount of slag cast, which was 219 kg when leaving the analyzed amount of metal inclusions out.

About 40 kg of material was left in the crucible after casting, consisting of unreacted quartz covered with viscous slag. Even if these losses were 100% silicon, there would still be too little Si in the products for the mass balance to add up. The large amount missing from the mass balance indicates that there may have been even more silicon in the slag than the 8,5%. Kerf fines lost to the off-gas may also have had a substantial impact on the silicon losses. The mass balance of the process according to the measured compositions and masses is given in Figure 4.24.

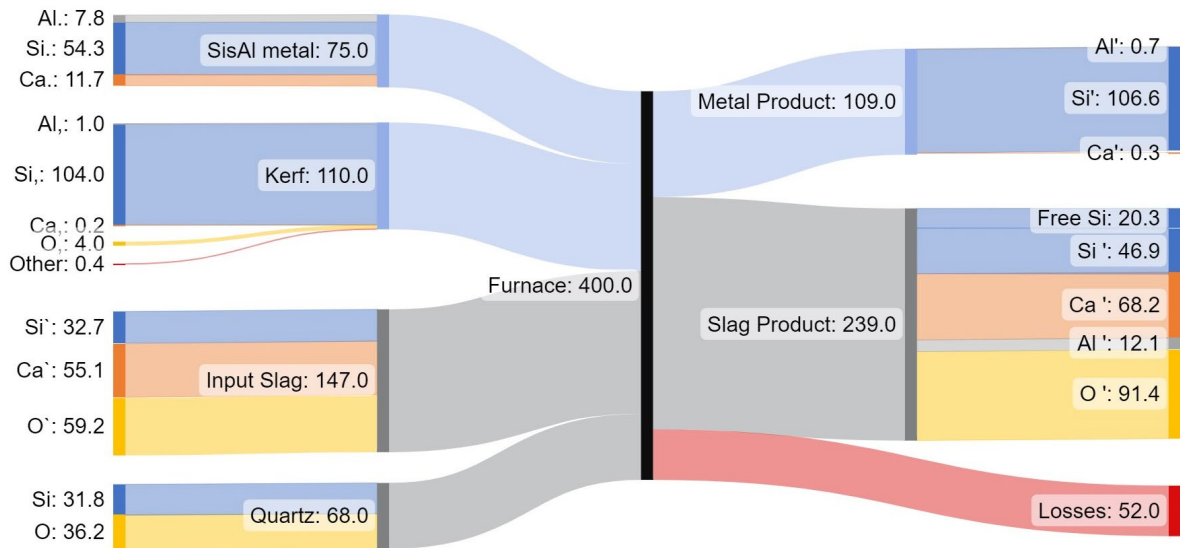


Figure 4.25: The Sankey diagram shows the raw materials and analyzed results.

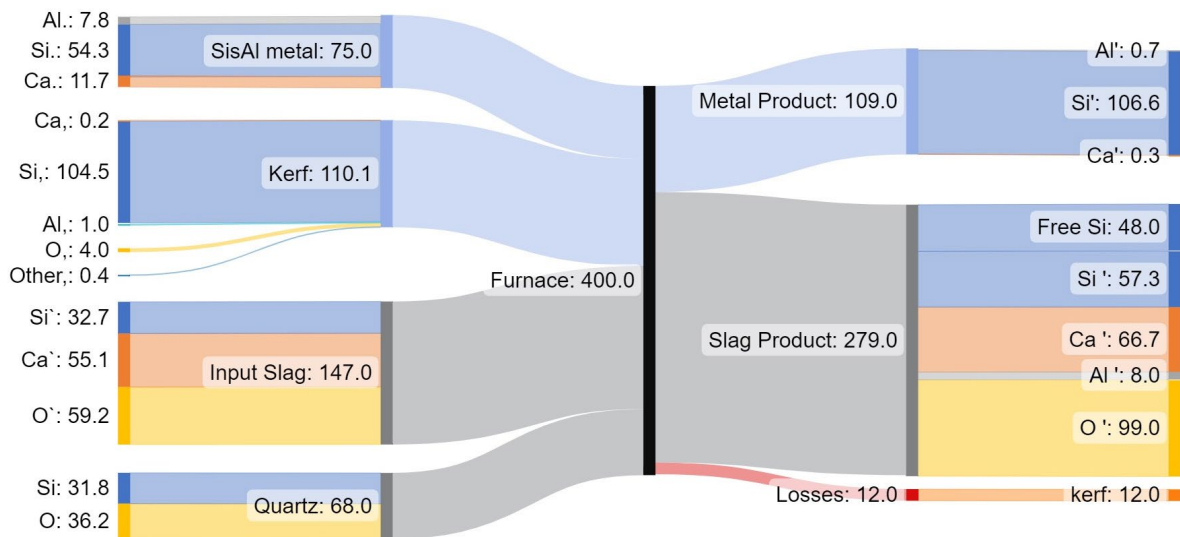


Figure 4.26: The theoretical mass balance calculations based on the analyzed metal composition and the experimental amount of cast metal given as a Sankey diagram. The losses remaining in the crucible are calculated as part of the slag product.

A calculation was conducted to find the theoretical slag composition based on the raw materials added to the system, the analyzed metal composition, and the assumption that 12 kg kerf was lost. The calculation is given in the appendix and a Sankey diagram illustrating the mass balance is given by Figure 4.25. The slag composition is given in Figure 4.23 and can be viewed as an average slag composition based on the available elements in the system. The actual bulk slag composition would have been shifted towards lower quartz content to compensate for the quartz lumps observed in the slag and the remaining materials in the furnace. The calculations found that the slag must have contained as much as 17,2% free silicon for the mass balance to add up, resulting in a total silicon production of about 155 kg, which is much closer to the FactSage calculation at 169 kg. Most of the difference left can be



found in the assumed kerf losses. The silicon inclusions in the slag were most likely unevenly distributed and therefore difficult to analyze. The silicon inclusions in the slag were not pure silicon, but more likely had a composition similar to the composition of the produced metal, or less pure.

Previous unpublished work in the SisAl project has shown that the silicon inclusions in slags similar to the slag produced in this experiment had high Ca contents, which may also be the case here. This could partially explain the high  $\text{Al}_2\text{O}_3$  content found in the analysis of the produced slag. With substantial amounts of inclusions made up of Si and Ca, the relative Al concentration in the slag would increase.

With such substantial amounts of metal in the slag, it will be important to recycle the slag through a process that can benefit from the silicon. One option is to use the slag in the aluminothermic step of the SisAl process, where the silicon is produced. This process is being investigated in ongoing work in the SisAl Project.

The silicon yield of this experiment can be calculated in two manners, one that only takes the produced metal into account and one that assumes that the free Si in the slag can be utilized. When only considering the Si in the produced metal, the yield is 67,1%. This is significantly worse than the medium-scale trials where the yield was above 80% for all but one experiment. The slag-to-metal ratio of the products in this experiment was 2,2, even though is used the 1,5:1:2 mass ratio, which gave slag-to-metal ratios of about 1,5 in the medium scale trials. This verifies that the amount of metal produced was much lower than expected and is the main source of the low yield. Still, the compares well to other slag refining routes for kerf where yields of about 60% are quite common [52], [55].

When including the metal inclusions in the slag in the yield calculation the number compares better to the medium-scale trials. When assuming 8,5% free Si in the slag, as found in the analysis, the yield is 79,9%. If the free Si content in the slag corresponded to the theoretical calculations and was 17,2%, the yield was 97,4 %. In this calculation, the only source for silicon losses is assumed to be the kerf losses that occurred during charging. Although it cannot be assumed that all the silicon inclusions in the slag can be recycled, the hope is that a substantial amount is reintroduced to the silicon feedstock. The actual silicon yield of the experiment can therefore only be found when the slag recycling step has been further investigated.

The large amount of free Si in the slag was most likely caused by similar densities. Molten Si has a density of 2,49  $\text{g}/\text{cm}^3$  [5] and the slag produced in the large-scale trial had a density of about 2,59 according to Figure 2.10 [25]. In the medium-scale trials, the slag composition was shifted towards less alumina and more quartz, which gave a density of 2,54  $\text{g}/\text{cm}^3$ , which is even closer to the silicon density. This show that density was not the reason behind the substantial increase in free Si in the slag from the medium-scale to the large-scale experiments. Still, the small density difference is cause for poor separation. The high viscosity of the slag is also believed to be an important reason, as the slag may have trapped silicon below the slag-metal interface. In future experiments, reduced amounts of quartz should be investigated with regard to slag properties and silicon content in the slag.

## **4.1.4 Evaluation of the Suggested Slag Refining Process**

### **4.1.4.1 The Purity of the Product**

Based on the studies presented in this thesis, 99,5% silicon seemed to be an achievable purity for slag refining of kerf [50], [51]. When comparing this to the results of the slag refining of kerf diluted with SisAl metal, it is clear that the impurities in the SisAl alloy are limiting the purity that could be achieved after slag refining.

When refining SisAl metal with slag, the produced metal can reach purities of up to 98,8% silicon (results from work in progress). The product of slag refining of a mix of kerf and SisAl metal would then be expected to lay somewhere between the results for the slag refining of each raw material on its own. However, the slag refining conducted in this thesis produced metal of about the same purity as slag refining of SisAl metal, showing that the kerf did not dilute the impurities in the SisAl metal to any noticeable extent.

### **4.1.4.2 The Ease and Sustainability of the Process**

The raw materials used in the process presented in this thesis mainly originate from secondary sources. The SisAl metal is produced from aluminium scraps or dross together with silica fines not suitable for state-of-the-art silicon production. The kerf is a waste material from solar cell production. The process presented shows a viable route to upcycle these materials into metallurgical-grade silicon, a product of high value.

The process has been shown to give fairly consistent results, even with varying raw materials. Three different kerfs were used, with different compositions and different physical properties. SisAl metals produced through different experiments from different raw materials were also used. Different ratios of the materials have also been investigated and showed promising results. The raw materials were also added to the furnace in different orders for some of the experiments, and different amounts of quartz were used. Although the amount of quartz used influenced the composition of the metal and slag, and the properties of the melt, it appears that a range of amounts would be suitable to the process.

By diluting the kerf with a silicon alloy, the process was able to use kerf that had gone through little pretreatment. The kerf was dried, but neither pressing nor sintering was needed to melt the kerf, avoiding a process step. Although dilution with silicon is not necessary to recycle kerf through slag refining, it made the overall process easier. For industrial-scale applications there are large benefits to skipping a process step and diluting the kerf with an alloy allows for that.

The process also had a high silicon yield. By operating at a fairly low temperature, close to no material was lost to fuming. The silicon yield was above 80 % in most experiments, with the large-scale trial being an exception. This is high compared to the yield for other kerf recycling routes, such as the slag refining done by Wei et al. which achieved 60% silicon yield [55], and Huang et al. with a silicon yield of 63,2% [52]. Some other routes reached similar results, such as Yang et al with up to 79,25% silicon recovery rate [50]. This shows that the presented route measures well up to other suggested slag refining routes for kerf with regard to silicon yield.

The process does not require any advanced equipment. The process needs heating to reach the right temperature and stirring with inert gas, but other than that there are no requirements. The refining reactions are exothermic, so the need for additional heat when all raw materials are melted is limited. In these experiments, a graphite crucible was used, but other refractory materials may also be suitable.

Overall, the process is simple and insensitive, and it can be used for a variety of secondary raw materials and mixing ratios. The process can be adapted to upcycle the materials available. The product is metallurgical-grade silicon, which has a wide range of applications and options for further refining.

## 4.2 Vacuum Refining

### 4.2.1 Experiment V1

The first vacuum refining experiment showed promising results, with the product being 99,5% pure silicon. The vacuum was held between 0,1 and 0,5 mbar, which equals to 10-50 Pa, and the holding temperature was 1550 °C. Samples were taken throughout the experiment, and the results show that the metal was likely exposed to some oxygen sometime before the 20-minute sample was taken. This exposure reduced the purity of the metal, but after some time almost all oxygen was removed from the metal. The impurity concentrations throughout the initial small-scale vacuum refining experiment are shown in Figure 4.26.

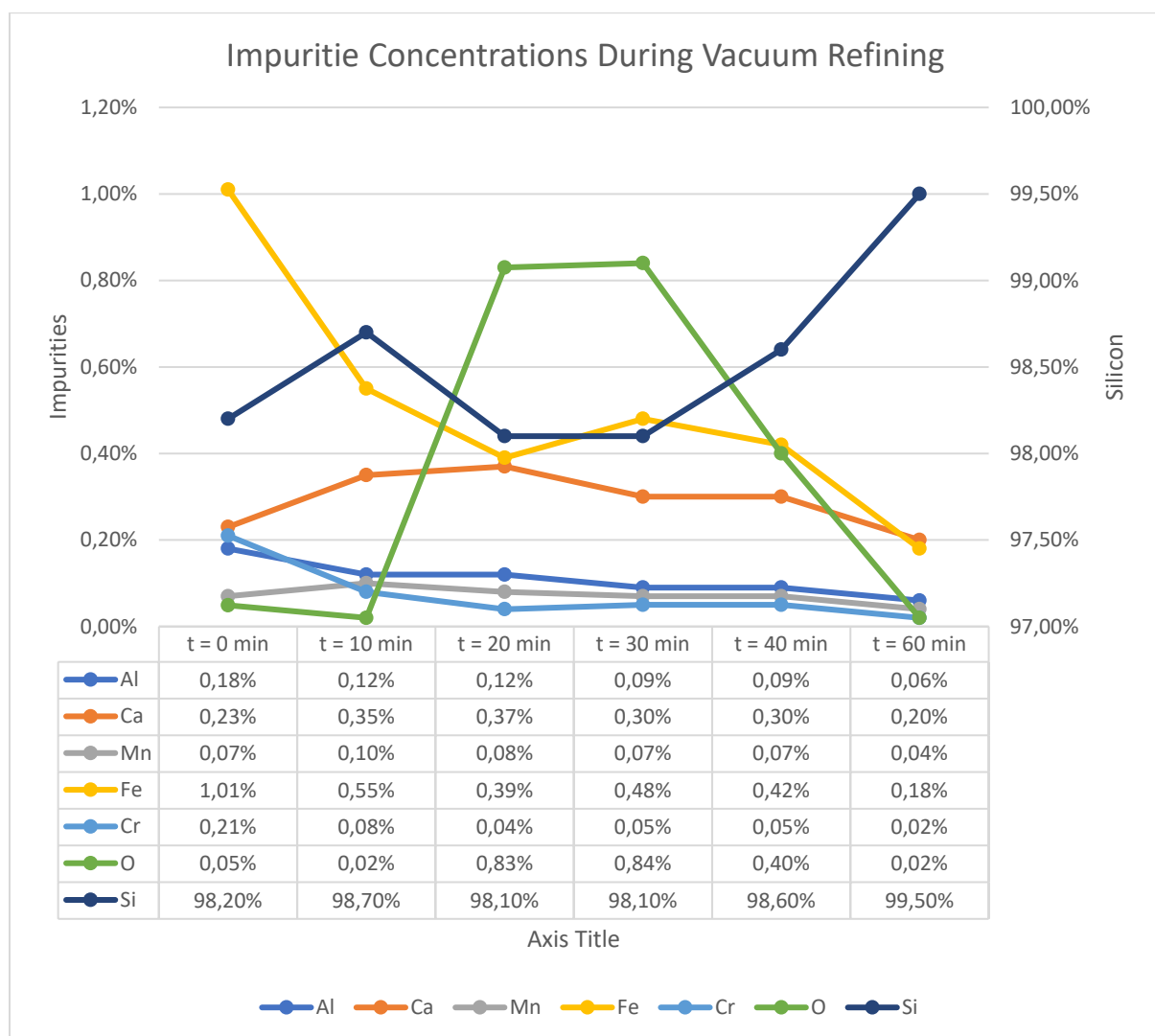


Figure 4.27 The graph shows the impurity concentrations in the melt throughout the vacuum refining experiment.

The green line shows the oxygen content in the sample, and it shows that the oxygen content had a rapid increase between the 10- and 20-minute samples. The vacuum in the furnace was most likely broken to some extent during the extraction of the 20-minute sample, exposing the molten metal to air. The contamination reduced the silicon content in the sample taken

to the same as the silicon content before the vacuum refining was started. The high oxygen content was also observed in the sample taken after 30 minutes. After this, a strong decline was seen in the oxygen content, and most of the other impurity contents were also reduced. Even with this contamination, the final product reached a purity of 99,5% silicon, with significantly lower impurity concentrations in the final product than in the initial metal.

As explained in section 2.3.2, all elements above silicon in Figure 2.13 can be removed through vacuum refining. The Ca content was expected to be reduced more efficiently than Al and Fe due to the high standard vapor pressure of Ca. Figure 4.26 show that the opposite is the case and that both Al and Fe were removed quite efficiently, with removal ratios of 66,7 % and 82,2%, respectively, while Ca had a removal ratio of only 13 %. During the vacuum treatment, the Ca concentration increased, which was unexpected and inconsistent with the presented literature.

One reason for this behavior could be the O that enters the system. Ca forms strong bonds with O, which could reduce the evaporation rate of Ca. An argument against this suggestion is that the increase of Ca started before the introduction of O to the system. Another explanation could be interactions between Fe and Ca, although these interactions would not typically enhance the evaporation of Fe. A third option is the strong interaction between P and Ca. The samples were not analyzed for P, and it can hence not be shown to which degree this is a viable option. Although all three reasons presented are possible, they are not expected to influence evaporation enough to explain the major difference in behavior. This behavior was not found in the literature reviewed for this work, and further experiments should be conducted to determine if it is a trend or just a special occurrence.

Due to the contamination, this experiment cannot be used to say exactly how much time in vacuum refining the metal needs to reach a certain composition. Still, some conclusions can be drawn from the results of the experiment. The experiment was successful in increasing the purity of the metal from 98,2% to 99,5%. Already after 10 minutes of vacuum refining, substantial improvements could be seen, with purity going from 98,1% to 98,7%. Longer time gave higher purity, but further experiments are needed to find the optimal holding time.

## **4.2.2 Experiments V2 and V3**

In the second and third vacuum refining experiments samples were only taken from the cast material after the total holding times of 90 and 100 minutes for experiments V2 and V3 respectively.

### **4.2.2.1 Composition of Product**

The results from the second and third vacuum refining experiments were more in line with the theory, and the results are presented in Figure 4.27.

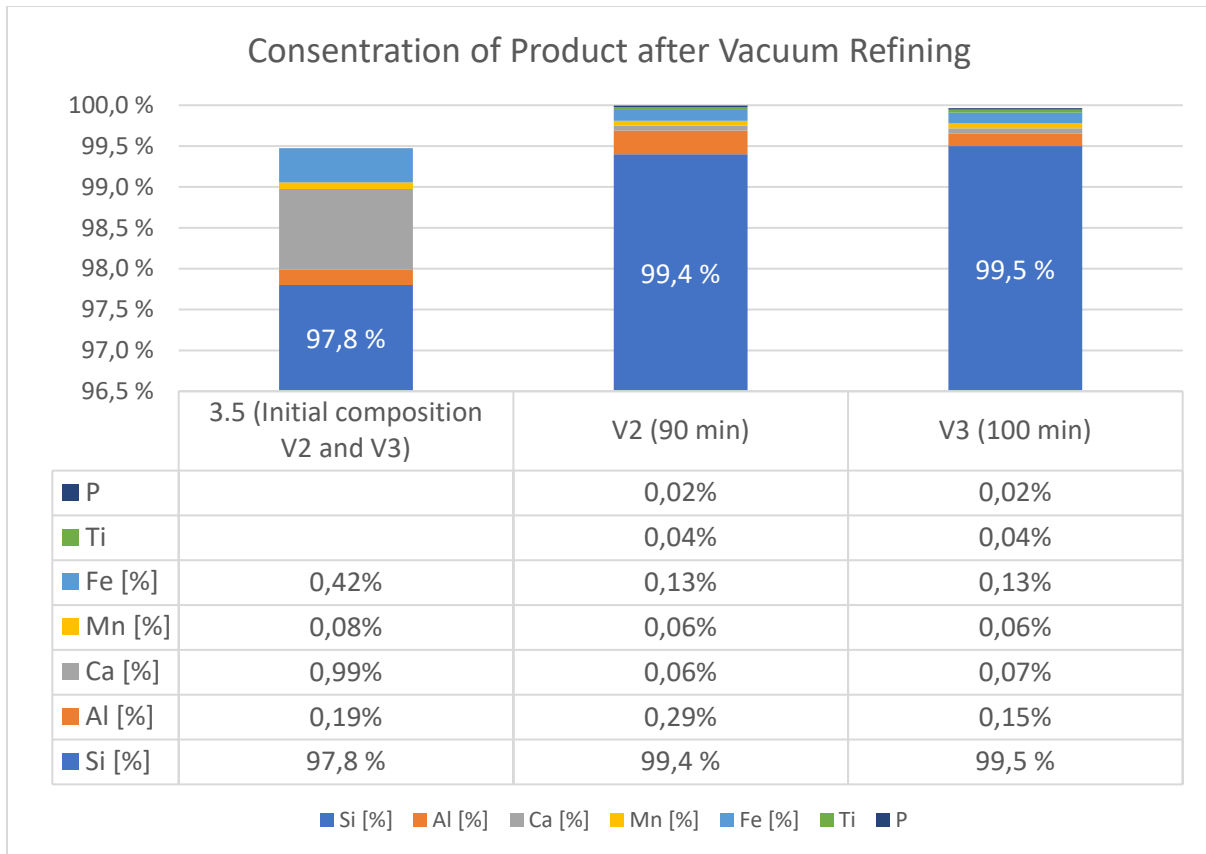


Figure 4.28: The graph shows the impurity concentration in the metal for the raw material produced in experiment 3.5, the product from V2 (vacuum refined for 90 minutes) and V3 (vacuum refined for 100 minutes).

There was a small, but noticeable improvement from experiment V2 to experiment V3, indicating that the extended holding time, though short, might have had a positive effect on the purity of the product.

The Al concentration was significantly higher in the metal produced after V2 than after experiment 3.5. This indicates that there might have been local variations in the metal composition after experiment 3.5, as it is unlikely that the Al content increased to the extent observed here. Some increases in the concentrations of the metals least prone to evaporation can be expected, as the evaporation of other elements and silicon reduces the total mass, and the concentration of said element is elevated as a result. However, this will only cause smaller variations. In V3, the Al content was reduced by 21% from the original content, which corresponds better to the theory, as Al is expected to evaporate, but to a smaller degree than for example Ca. The Ca concentration was successfully reduced in both experiments to about the same amount. The removal ratio of Ca was 93,0% and 93,9% for V2 and V3, respectively. This does not correlate to the finds from experiment V1, and the results presented here are more in line with theory and other published research. This supports the idea that the high Ca content from experiment V1 was a special occurrence rather than a trend.

The removal ratio of Fe was 68,6% for both experiments V2 and V3, which is fairly well considering Fe is one of the more difficult elements to evaporate from silicon, according to the literature presented around the evaporation coefficients of different metals. Mn had a removal ratio of 25% for both experiments. As the metal produced in experiment 3.5 was not

analyzed for Ti or P, their removal ratio cannot be calculated. However, it can be seen that both experiments produced metal with the same, low contents of both elements.

Compared to V1, the final products have many similarities. The main difference is that the product from V1 had about three times the Ca content and one-third of the Al content of experiment V3. As the results from V2 and V3 correspond better to theory, these are believed to be the most representative.

The results compare well to the final silicon purity found by Kong et al. [47] of 99,65%, where the kerf was pelletized and then melted and vacuum refined. All three refining times tested produced metal of approximately the same purity. This shows that 60 minutes may be sufficient refining time, but due to the inconsistencies in the analyses during the holding time, more experiments should be conducted to verify. The product is not suitable for solar applications but can be used in aluminium alloys, silicon steel, and silicones.

#### 4.2.2.2 Material Losses and Silicon Yield

During vacuum refining experiments material is lost to evaporation, but for the experiments conducted here, the main source of material losses is the larger droplets of metal that erupted out of the crucible during refining. Due to the small surface area of the crucible, the metal that erupted out of the crucible was very unlikely to land in the melt again and was scattered around the furnace chamber. There was observed more metal scattered in the furnace after experiment V3 (100 minutes holding time). The material losses are presented in Figure 4.28. Based on these losses, and assuming most of the losses were silicon, an approximate silicon yield for the vacuum refining process can be assumed to be about 95%.

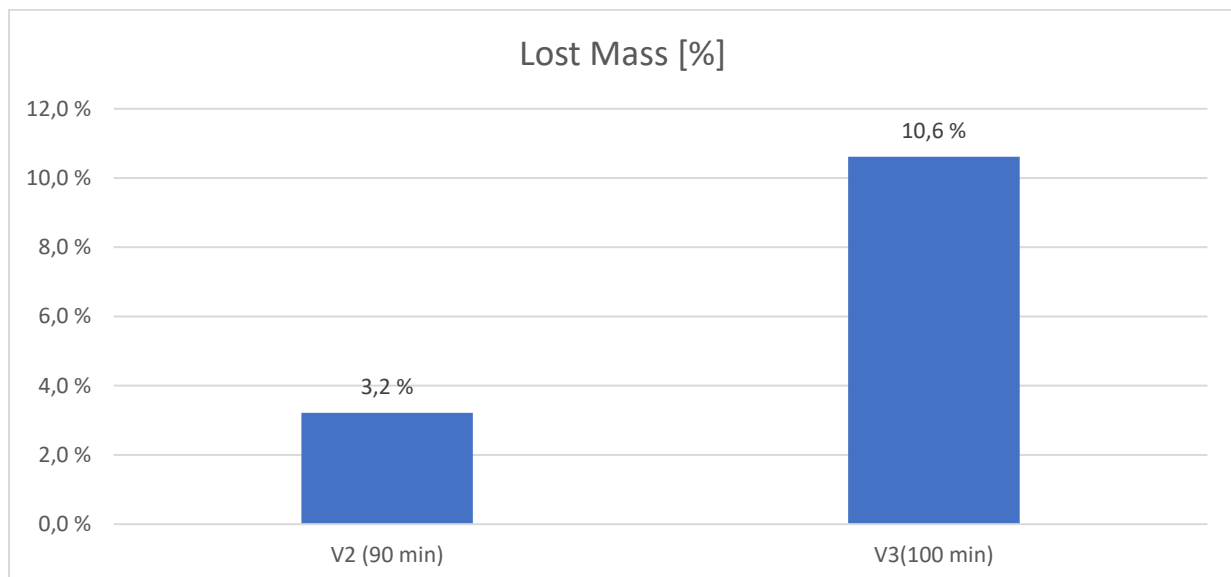


Figure 4.29: The graph shows the mass lost during the experiments for the second and third vacuum experiments of 90 and 100 minutes respectively.

### 4.3 Directional Solidification

The possibility for impurity removal through directional solidification was calculated using the Gulliver-Scheil equation. The composition of the metal produced in experiment 3.5 was used as the initial composition of the impurities, which is given in Table 4.11 along with the segregation coefficients of the same elements. The results of the calculations are illustrated in Figure 4.29.

Table 4.11: Initial concentrations and segregation coefficient for the three main impurities in the produced metal.

Element	Initial Concentration	Segregation Coefficient
Al	0,10%	$2 \cdot 10^{-3}$
Fe	0,25%	$8 \cdot 10^{-3}$
Ca	0,37%	$8 \cdot 10^{-6}$

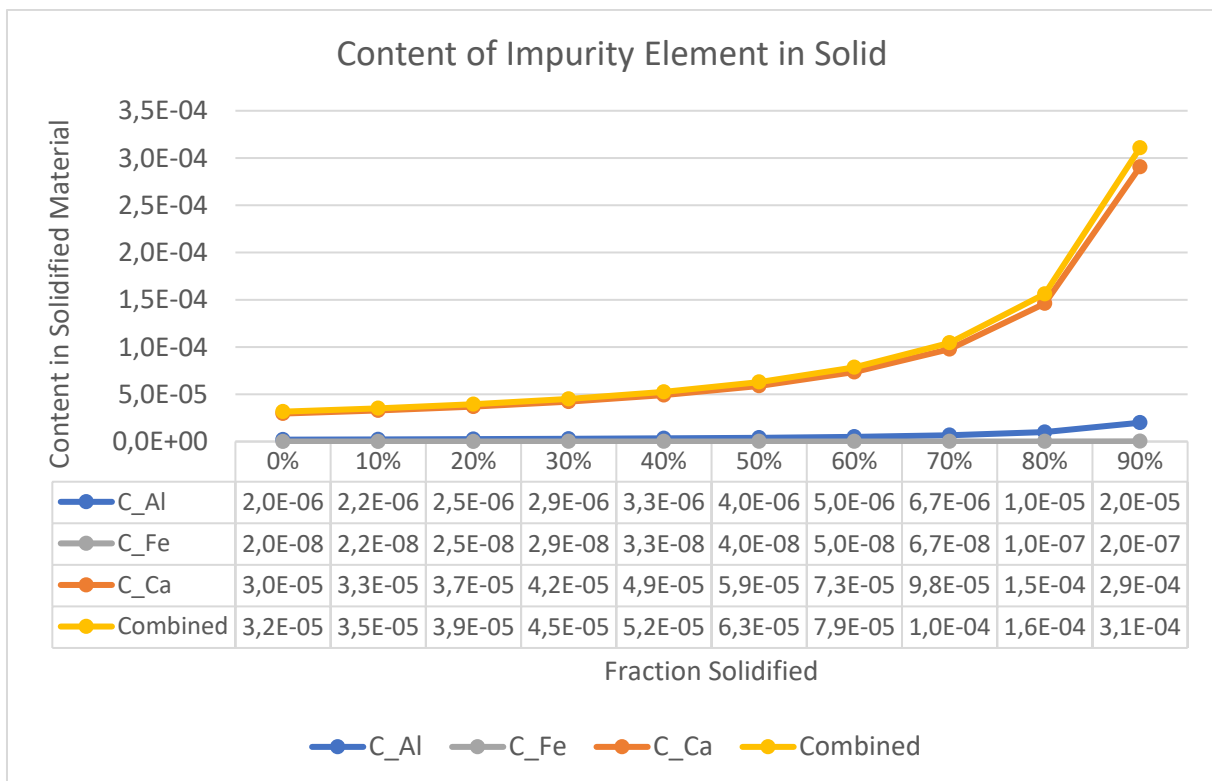


Figure 4.30: The graph shows the contents of the impurities in the solidified metal by fraction solidified.

The impurity concentration increases slowly for the first part of the diagram. As more metal is solidified, the impurity concentration increases more drastically. Ca was the largest contributor as it had the largest initial concentration and segregation coefficient that was a thousand times larger than that of Fe, as shown in Table 4.11. The segregation coefficients used for these calculations are valid at equilibrium, and the real behavior of the impurities will have to be investigated through experimental work.

As the figure shows, directional solidification is efficient for impurity removal. By removing the last 30% of the metal to solidify, the combined concentration of Al, Ca, and Fe is reduced from 0,72% to 0,01%, a reduction of 98,55%. The silicon yield is then about 70% as silicon



makes up most of the metal removed. Keeping in mind that this is a theoretical calculation done for equilibrium values, the actual impurity removal is expected to be smaller, but these results are promising. Still, even the first material to solidify does not meet the requirements of solar-grade silicon, as the combined impurity content is more than the allowed  $1,0 \cdot 10^{-6}$ . Studies have shown that it is possible to reach almost 5,5N through directional solidification of kerf [58], but reaching solar grade seems challenging. By conducting several rounds of directional solidification, removing the material with high impurity content each time, could the final composition potentially reach high purities. A disadvantage to this strategy is that the silicon yield would decrease drastically for each round.

The initial purity of the metal is important for the result of directional solidification. When the impurity concentrations are too high, the solidification front may not be level, and impurities can solidify low in the ingot. Interactions between the impurities may also influence the process and reduce the purity of the product. The initial impurity content in the material investigated here was higher than what is common for directional solidification. The calculation presented may therefore be far from the results of an experiment. Directional solidification may, therefore, be more suitable for material that has already gone through vacuum refining. When the experiments are conducted, trials should be done for both metal directly from slag refining and metal that has gone through vacuum refining.

## 4.4 Evaluation of the Combined Refining Route

### 4.4.1 The Purity of the Product

Solar-grade silicon has a purity of 99,9999%. The process presented in this thesis has shown insufficient produce metal of said purity. The metal can still be relevant for the solar industry with further refining and for blending with material from other sources. In the Resilex project, the goal was to reach the impurity concentrations presented in Table 4.12. After vacuum refining the silicon only reached around 99,5% purity. It is not expected that directional solidification will reach the limits of solar-grade silicon, or the impurity limits presented in the table, based on the theoretical calculations.

Table 4.12: The table shows the requirements for the material to be suitable for Czochralski pulling when blending at 10%

Element	Concentration limit
<b>B</b>	<0,1 ppmw
<b>P</b>	<0,1 ppmw
<b>Ga</b>	<0,5 ppmw
<b>Al</b>	<0,3 ppmw
<b>Ti</b>	<0,6 ppmw
<b>Fe</b>	<0,01 ppmw
<b>O</b>	<1,5*10 <sup>18</sup> at/cm <sup>3</sup>
<b>C</b>	<8,2*10 <sup>16</sup> at/cm <sup>3</sup>

### 4.4.2 The Sustainability of the Process

The main purpose of the process investigated in this thesis is to contribute to a circular silicon value chain where waste materials and secondary raw materials are upcycled rather than downcycled. Already after the slag refining step the materials have increased in value and become a versatile product. Vacuum refining showed efficiency for impurity removal and further purifying the material, increasing the options for applications of the product. Directional solidification could further refine the material, and the product could reach a higher purity.

In every refining step, some material is lost, and power is consumed. Assuming that the silicon yields along the process were 80% for slag refining, 95% for vacuum refining, and 70% for directional solidification, the combined refining route had a silicon yield of 53,2%. Although the metal lost as inclusions in the slag and the cut-off from directional solidification can be recycled, the combined yield shows how each refining step reduces the yield substantially. Even higher losses must be anticipated if the aim is to produce solar-grade silicon.

Since the vacuum refining and directional solidification did not make the product reach solar grade, and the literature review shows that kerf recycling hardly reaches solar grade, it should be contemplated whether this should be the goal.

As discussed in the literature study conducted by Li et. al., kerf recycling to lower-purity products can house advantages concerning silicon yield, environment, and economy [22]. Although the demand for solar-grade silicon is large and rising, the demand for silicon for alloying is still much larger, and the kerf feedstock seems to be more suited to meet the purity requirements for the latter application.

Closed-loop recycling is often preferred as it reduces the need for virgin material in a value chain and avoids downcycling of materials. However, these advantages must be weighed against the energy and materials that are used in the recycling steps, and the economic feasibility of the process. In the case presented, recycling to meet other needs in the market may be even more sustainable, as it requires less processing of the materials. When viewing the silicon value chain as a whole, the circularity is preserved as the secondary silicon materials are still put to use. If more of the applications that require less pure silicon could utilize secondary materials, the purer silicon sources could be redirected to the production of solar-grade silicon. This would increase the sustainability of the silicon value chain.

In the future, the goal should be to recycle kerf to solar-grade silicon. Changes could be made to the cutting process to reduce the impurity concentration of the kerf, and new refining schemes could be investigated. The kerf is made from silicon that has already gone through the refining process to reach solar-grade and it is therefore preferable to keep its high purity and loop it back into the solar-grade feedstock. Although the present solutions may not be suited for industrial-scale recycling of kerf to solar-grade silicon, it should remain a long-term goal.

## 5 Conclusions

This thesis investigated a process to increase the circularity of the silicon value chain through upcycling of waste products and secondary raw materials. During the production of solar cells, about half of the silicon becomes waste products. The silicon powder waste (kerf) created during wafer sawing is a major waste product. This kerf consists of almost pure silicon powder but holds some impurities from the cutting process and an inert oxide layer on the surface particles, which causes challenges in the recycling processes. [2], [3] Silicon production through aluminothermic reduction of quartz in slag enables a carbon-free process, that can utilize materials unsuited for state-of-the-art silicon production. The metal produced through this process contains about 10% Al and 16% Ca and will be referred to as SisAl metal. [1]

This thesis has studied a combined refining route for these two materials starting with slag refining, followed by vacuum treatment and directional solidification. Slag refining is widely agreed to be a fitting first step of kerf refining, as it removed the inert oxide layer on the surface of the kerf particles [22], [53]. It is also suitable for refining the SisAl metal, as both main impurities Ca and Al can be removed through slag refining [15]. Thereafter, vacuum refining can remove several of the remaining impurities from both kerf and SisAl metal [18]. To reach higher purity results, the literature shows that directional solidification is a suitable process step [57], [58],[59].

The following conclusions can be drawn from the thesis:

- Lab-scale experiments showed that slag refining at 1550°C for 40 minutes with 1,5:1:2 and 2:1:2 ratios of kerf : SisAl metal : slag, and 0,32 to 0,9 parts quartz were all suitable parameters, that produced silicon with about 98% purity, well within the range of metallurgical-grade silicon. This product is hence suited for all the same applications as metallurgical-grade silicon.
- The process was upscaled to produce 109 kg silicon, which reached a purity of 97,79%.
- The silicon yield in the slag refining process was above 80 % for most experiments. For the large-scale trial, the yield was 67,1%. If metal inclusions in the slag can be recycled, the silicon yield can increase to above 90%.
- The slag refining process proposed in this thesis is robust and suited for a variety of raw materials and mixing ratios.
- Vacuum refining at 1550°C for 60, 90, and 100 minutes with 0,5-0,1 mbar improved the purity of the metal from 98,2%, 97,8%, and 97,8% Si to 99,5%, 99,4%, and 99,5 % Si, respectively.
- Theoretical calculations showed that directional solidification should be considered as a step for further refining the material.
- The recycling process succeeded in upcycling the raw materials, although it did not reach solar grade. The product is nevertheless valuable and is suitable for alloying among other applications.



## 6 Further work

This thesis is part of the first year of the Resilex project, and further research is to be conducted in the following years. The author of this thesis suggests that the following areas are investigated:

### **Directional Solidification**

Due to limitations in time and equipment, no experimental work was done regarding directional solidification. The literature review and the theoretical calculations showed that the process shows promise for removing the relevant impurities. Directional solidification should hence be investigated further as a part of the refining process.

### **Recycling of the Refining Slag**

The slag product from the slag refining contained about 5% free silicon. This slag should therefore be recycled to eliminate the silicon losses, and the possibilities for this should be investigated. One option is to use the refining slag in the metallothermic step, for example in the SisAl process. It would then be important to achieve good metal slag separation in this step, as a metal-free slag is a valuable byproduct that can be used for cement production, retrieving alumina, and other applications.

### **Different Applications of the Produced Silicon**

As the silicon produced in the process presented in this thesis is not of solar grade, different applications should be investigated. The impurity content should be kept in mind while evaluating different applications and their requirements.

### **Further Refining Steps**

Although the metal produced in the process proposed did not reach solar grade, it is suitable for further refining. The product after vacuum refining had higher purity than the limit for metallurgical-grade silicon, for which there already exists refining schemes to reach solar-grade purity. When finding the most appropriate refining steps, sustainability should be a factor.

### **Hydrometallurgical Steps**

Several of the impurities present in the kerf and the SisAl metal are suited for removal through hydrometallurgical processes. This should be investigated as a step in the process of reducing the impurity content of the metal.



## 7 Bibliography

- [1] G. Tranell, J. Safarian, and M. Wallin, "SisAl – A New Process for Production of Silicon," in *Silicon for the Chemical and Solar Industry XV*, Trondheim: Norges teknisk-naturvitenskapelige universitet, 2020, pp. 129–139.
- [2] X. Yijiang, S. Gaute, S. Anne-Karin, R. Birgit, B. Irene, and B. Martin, "INVENTORY OF WASTE MATERIALS FROM SILICON INGOT AND WAFER MANUFACTURING FOR A CIRCULAR PV VALUE CHAIN," Zenodo, Milan, Italy, Sep. 30, 2022. doi: 10.5281/zenodo.7540826.
- [3] G. Stokkan, Y. Xu, and M. Bellmann, "Waste inventory for a circular solar cell production value chain." ICARUS, Jun. 07, 2022. Accessed: Dec. 11, 2022. [Online]. Available: [https://www.icarus.eu.com/wp-content/uploads/2022/06/ICARUS\\_D1.2\\_website.pdf](https://www.icarus.eu.com/wp-content/uploads/2022/06/ICARUS_D1.2_website.pdf)
- [4] "European Critical Raw Materials Act," *European Commission - European Commission*. [https://ec.europa.eu/commission/presscorner/detail/en/IP\\_23\\_1661](https://ec.europa.eu/commission/presscorner/detail/en/IP_23_1661) (accessed Apr. 20, 2023).
- [5] A. Schei, J. Kr. Tuset, and H. Tveit, *Production of High Silicon Alloys*. Trondheim: Tapir, 1998. Accessed: Oct. 13, 2022. [Online]. Available: [https://urn.nb.no/URN:NBN:no-nb\\_digibok\\_2010021004001](https://urn.nb.no/URN:NBN:no-nb_digibok_2010021004001)
- [6] H. L. Yang, I. T. Liu, C. E. Liu, H. P. Hsu, and C. W. Lan, "Recycling and reuse of kerf-loss silicon from diamond wire sawing for photovoltaic industry," *Waste Manag.*, vol. 84, pp. 204–210, Feb. 2019, doi: 10.1016/j.wasman.2018.11.045.
- [7] K. et. al. Hachichi, "Silicon Recovery from Kerf Slurry Waste: a Review of Current Status and Perspective." © Springer Science+Business Media B.V., 2017. [Online]. Available: <https://doi.org/10.1007/s12633-017-9642-x>
- [8] G. A. Blengini, C. E. Latunussa, and U. Eynard, "Study on the EU's list of Critical Raw Materials - Final report (2020)," European Commission, Luxembourg, ISBN 978-92-76-21049-8, doi: 10.2873/11619, ET-01-20-491-EN-N, 2020.
- [9] "Silicon Statistics and Information | U.S. Geological Survey," *USGS.gov*. <https://www.usgs.gov/centers/national-minerals-information-center/silicon-statistics-and-information> (accessed Dec. 14, 2022).
- [10] E. K. Schnebele, "2018 Minerals Yearbook Silicon (Advanced Release)." U.S. Department of the Interior, U.S. Geological Survey, Aug. 2021.
- [11] D. Yang, *Handbook of Photovoltaic Silicon*. Berlin, Heidelberg: Springer, 2019. doi: 10.1007/978-3-662-56472-1\_1.
- [12] "Prosess 21 Hovedrapport," *Prosess21*, Feb. 2021. Accessed: Dec. 14, 2022. [Online]. Available: [prosess21.no](https://prosess21.no)
- [13] R. Secretariat, "Renewables Global Status Report," *REN21*. <https://www.ren21.net/reports/global-status-report/> (accessed Dec. 14, 2022).
- [14] S. Carrara *et al.*, "Supply chain analysis and material demand forecast in strategic technologies and sectors in the EU – A foresight study," *JRC Publications Repository*, Mar. 16, 2023. <https://publications.jrc.ec.europa.eu/repository/handle/JRC132889> (accessed Apr. 20, 2023).
- [15] E. L. Bjørnstad, "Oxidative Ladle Refining of Metallurgical Grade Silicon: Refining of Ca and Al Impurities," Doctoral thesis, NTNU, 2021. Accessed: Feb. 17, 2023. [Online]. Available: <https://ntnuopen.ntnu.no/ntnu-xmlui/handle/11250/2768770>
- [16] G. Sævarsdóttir, H. Kvande, and T. Magnusson, "Greenhouse Gas Emissions from Silicon Production -Development of Carbon Footprint with Changing Energy Systems." Rochester, NY, Sep. 12, 2021. doi: 10.2139/ssrn.3926088.
- [17] H. Philipson *et al.*, "Preliminary Techno-Economic Considerations of the Sisal Process - Closing Materials Loops through Industrial Symbiosis." Rochester, NY, Apr. 06, 2022. doi: 10.2139/ssrn.4116381.
- [18] J. Safarian and M. Tangstad, "Vacuum Refining of Molten Silicon," *Metall. Mater. Trans. B*, vol. 43, no. 6, pp. 1427–1445, Dec. 2012, doi: 10.1007/s11663-012-9728-1.



- [19] M. Tangstad, *Metal production in Norway*. Akademika Publishing, 2013. Accessed: Dec. 12, 2022. [Online]. Available: <https://www.fagbokforlaget.no/Metal-production-in-Norway/19788232102419>
- [20] J. Safarian, G. Tranell, and M. Tangstad, "Processes for Upgrading Metallurgical Grade Silicon to Solar Grade Silicon," *Energy Procedia*, vol. 20, pp. 88–97, Jan. 2012, doi: 10.1016/j.egypro.2012.03.011.
- [21] M. Zhu, "Silicon purification by acid leaching and slag refining techniques," Doctoral thesis, NTNU, 2021. Accessed: Dec. 12, 2022. [Online]. Available: <https://ntnuopen.ntnu.no/ntnu-xmlui/handle/11250/2738488>
- [22] -Yun Lei *et al.*, "Recent progress in upgrading metallurgical-grade silicon to solar-grade silicon via pyrometallurgical routes," - *Int. J. Miner. Metall. Mater.*, vol. 29, no. 4. p. 767, 2022.
- [23] A. Hosseinpour and L. Tafaghodi Khajavi, "Slag refining of silicon and silicon alloys: a review," *Miner. Process. Extr. Metall. Rev.*, vol. 39, no. 5, pp. 308–318, Sep. 2018, doi: 10.1080/08827508.2018.1459616.
- [24] R. Al-khazraji, Y. Li, and L. Zhang, "Application of slag refining technique to metallurgical grade silicon purification process: A review," *Funct. Mater.*, vol. 25, no. 2, pp. 364–370, 2018, doi: 10.15407/fm25.02.364.
- [25] *Slag Atlas*. 1995.
- [26] Y. Sato *et al.*, "Viscosity of molten silicon and the factors affecting measurement," *J. Cryst. Growth*, vol. 249, no. 3, pp. 404–415, Mar. 2003, doi: 10.1016/S0022-0248(02)02153-X.
- [27] L. K. Jakobsson and M. Tangstad, "Thermodynamic Activities and Distributions of Calcium and Magnesium Between Silicon and CaO-MgO-SiO<sub>2</sub> Slags at 1873 K (1600 °C)," *Metall. Mater. Trans. B*, vol. 46, no. 2, pp. 595–605, Apr. 2015, doi: 10.1007/s11663-014-0268-8.
- [28] S. Thomas, M. Barati, and K. Morita, "A Review of Slag Refining of Silicon Alloys," *JOM*, vol. 73, Nov. 2020, doi: 10.1007/s11837-020-04474-0.
- [29] L. Q. Huang *et al.*, "Distribution of Representative Impurities in Metallurgical-Grade Silicon Using CaO-SiO<sub>2</sub>-CaF<sub>2</sub> and CaO-SiO<sub>2</sub>-CaCl<sub>2</sub> Slags," *Adv. Mater. Res.*, vol. 813, pp. 11–15, 2013, doi: 10.4028/www.scientific.net/AMR.813.11.
- [30] G. Taposhe and L. Tafaghodi, "Thermodynamics of Impurities Removal From Si-Fe Alloy by CaO-Al<sub>2</sub>O<sub>3</sub>-SiO<sub>2</sub>-Na<sub>2</sub>O Slag Refining," *Metall. Mater. Trans. B*, vol. 53, Oct. 2022, doi: 10.1007/s11663-022-02662-8.
- [31] Z. Shan *et al.*, "Inclusions Removal in Industrial Silicon by SiO<sub>2</sub>-CaO-Al<sub>2</sub>O<sub>3</sub> Based Slag System," *Silicon*, Mar. 2023, doi: 10.1007/s12633-023-02404-8.
- [32] A. Hoseinpour Kermani, K. Tang, and J. Safarian, "Kinetic study of vacuum evaporation of elements from ternary melts; case of dilute solution of P in Si-Al melts," *15*, 2019, doi: 10.1016/j.seppur.2019.116284.
- [33] G. K. Sigworth, "Thermodynamic of dilute liquid silicon alloys," *Can. Metall. Q.*, vol. VOL. 59, NO. 3, 251–261, no. NO. 3, pp. 251–261, 2020.
- [34] J. F. White and D. Sichen, "Mass Transfer in Slag Refining of Silicon with Mechanical Stirring: Transient Interfacial Phenomena," *Metall. Mater. Trans. B*, vol. 45, no. 1, pp. 96–105, Feb. 2014, doi: 10.1007/s11663-013-0010-y.
- [35] J. Lee, J. F. White, K. Hildal, and D. Sichen, "Study on the Kinetics of Aluminum Removal from Liquid Silicon to Slag with Mechanical Stirring," *Metall. Mater. Trans. B Process Metall. Mater. Process. Sci.*, vol. 47, no. 6, pp. 3511–3518, 2016, doi: 10.1007/s11663-016-0768-9.
- [36] R. Tanaka, M. A. Uddin, and Y. Kato, "Flow characteristics related to liquid/liquid mixing pattern in an impeller-stirred vessel," *ISIJ Int.*, vol. 58, no. 4, pp. 620–626, 2018, doi: 10.2355/isijinternational.ISIJINT-2017-619.
- [37] P. Valentin, C. Bruch, Y. Kyrylenko, H. Köchner, and C. Dannert, "Influence of the stirring gas in a 170-t ladle on mixing phenomena - Formation and on-line control of open-eye at an industrial LD steel plant," *Steel Res. Int.*, vol. 80, no. 8, pp. 552–558, 2009, doi: 10.2374/SRI08SP125;

- [38] P. K. Shivaram, M. Gruber, and T. Spudic, "A comparison of the dynamics, mixing efficiency & ladle wall wear in gas-stirred ladles," presented at the AISTech - Iron and Steel Technology Conference Proceedings, 2021, pp. 454–464. doi: 10.33313/382/044.
- [39] A. Hoseinpur and J. Safarian, "Vacuum refining of silicon at ultra-high temperatures," *Vacuum*, vol. 184, p. 109924, 2021, doi: <https://doi.org/10.1016/j.vacuum.2020.109924>.
- [40] X. Deng, L. Zhou, K. Wei, and W. Ma, "The use of vacuum refining to separate Ca, Al, and P from crude metallurgical grade silicon," *Vacuum*, vol. 207, p. 111581, Jan. 2023, doi: 10.1016/j.vacuum.2022.111581.
- [41] R. H. Hopkins and A. Rohatgi, "Impurity effects in silicon for high efficiency solar cells," *J. Cryst. Growth*, vol. 75, no. 1, pp. 67–79, May 1986, doi: 10.1016/0022-0248(86)90226-5.
- [42] M. A. Martorano, J. B. F. Neto, T. S. Oliveira, and T. O. Tsubaki, "Refining of metallurgical silicon by directional solidification," *Mater. Sci. Eng. B Solid-State Mater. Adv. Technol.*, vol. 176, no. 3, pp. 217–226, 2011, doi: 10.1016/j.mseb.2010.11.010.
- [43] "File:Scheil graphics.gif - Wikipedia," Apr. 27, 2008. [https://commons.wikimedia.org/wiki/File:Scheil\\_graphics.gif](https://commons.wikimedia.org/wiki/File:Scheil_graphics.gif) (accessed Jun. 07, 2023).
- [44] C. Ramírez-Márquez and M. Martín, "Chapter 10 - Photovoltaic solar energy," in *Sustainable Design for Renewable Processes*, M. Martín, Ed., Elsevier, 2022, pp. 397–439. doi: 10.1016/B978-0-12-824324-4.00029-9.
- [45] S. Pizzini, "Towards solar grade silicon: Challenges and benefits for low cost photovoltaics," *Sol. Energy Mater. Sol. Cells*, vol. 94, no. 9, pp. 1528–1533, Sep. 2010, doi: 10.1016/j.solmat.2010.01.016.
- [46] Y. Okamoto, M. Sumiya, Y. Nakamura, and Y. Suzuki, "Effective silicon production from SiCl<sub>4</sub> source using hydrogen radicals generated and transported at atmospheric pressure," *Sci. Technol. Adv. Mater.*, vol. 21, no. 1, pp. 482–491, Jan. 2020, doi: 10.1080/14686996.2020.1789438.
- [47] J. et. al. Kong, "Recycling high-purity silicon from diamond-wire saw kerf slurry waste by vacuum refining process." *Journal of Cleaner Production*, 2020. [Online]. Available: <https://doi.org/10.1016/j.jclepro.2020.124979>
- [48] X. Li *et al.*, "Review of resource and recycling of silicon powder from diamond-wire sawing silicon waste," *J. Hazard. Mater.*, vol. 424, p. 127389, Feb. 2022, doi: 10.1016/j.jhazmat.2021.127389.
- [49] Y. Zhang *et al.*, "Preparation of Low-Boron Silicon from Diamond Wire Sawing Waste by Pressure-Less Sintering and CaO–SiO<sub>2</sub> Slag Treatment," *ACS Sustain. Chem. Eng.*, vol. 8, no. 31, pp. 11755–11763, Aug. 2020, doi: 10.1021/acssuschemeng.0c03875.
- [50] S. Yang, X. Wan, K. Wei, W. Ma, and Z. Wang, "Investigation of Na<sub>2</sub>CO<sub>3</sub>–CaO–NaCl (or Na<sub>3</sub>AlF<sub>6</sub>) additives for the remanufacturing of silicon from diamond wire saw silicon powder waste," *J. Clean. Prod.*, vol. 286, p. 125525, Mar. 2021, doi: 10.1016/j.jclepro.2020.125525.
- [51] X. Li, J. Wu, M. Xu, and W. Ma, "Separation and purification of silicon from cutting kerf-loss slurry waste by electromagnetic and slag treatment technology," *J. Clean. Prod.*, vol. 211, pp. 695–703, 2019, doi: 10.1016/j.jclepro.2018.11.195.
- [52] L. Huang, A. Danaei, M. Fang, S. Thomas, X. Luo, and M. Barati, "A metallurgical route to upgrade silicon kerf derived from diamond-wire slicing process," *Vacuum*, vol. 163, pp. 164–171, 2019, doi: 10.1016/j.vacuum.2019.02.019.
- [53] "Recycling silicon kerf waste: Use cryolite to digest the surface oxide layer and intensify the removal of impurity boron | Elsevier Enhanced Reader." <https://reader.elsevier.com/reader/sd/pii/S0304389421019476?token=412210F287D86A45430EE4D736DD1D89F5ECF8730D6BDB39781659D0FB95DCF413911267BDA0AF876C70A136347AE31F&originRegion=eu-west-1&originCreation=20230315104523> (accessed Mar. 15, 2023).
- [54] Y. Li, Z. Li, L. Zhang, X. Wen, C. Ren, and Y. Yu, "Silicon recovery from Si sawing waste through slag refining," *Sep. Purif. Technol.*, vol. 274, p. 119065, Nov. 2021, doi: 10.1016/j.seppur.2021.119065.
- [55] D. Wei, J. Kong, Z. Zhang, P. Xing, and Y. Zhuang, "Study on recycling Si from silicon diamond-wire saw cutting waste by a slag refining process in industrial scale," *J. Clean. Prod.*, vol. 398, p. 136557, Apr. 2023, doi: 10.1016/j.jclepro.2023.136557.

- [56] T. Lu, Y. Tan, J. Li, and D. Deng, "Recycling of silicon powder waste cut by a diamond-wire saw through laser-assisted vacuum smelting," *J. Clean. Prod.*, vol. 203, pp. 574–584, 2018, doi: 10.1016/j.jclepro.2018.08.226.
- [57] Y. Zhu, J. Wu, K. Wei, and W. Ma, "Recovery and Purification of Silicon From Diamond Wire Saw Wasted Silicon Powder by a Technique of Induction Smelting Followed by Directional Solidification," *Metall. Mater. Trans. B Process Metall. Mater. Process. Sci.*, vol. 53, no. 4, pp. 2704–2711, 2022, doi: 10.1007/s11663-022-02561-y.
- [58] Z. Hu, G. Wang, J. Li, Y. Tan, Y. Liu, and P. Li, "Recycling of diamond-wire sawing silicon powder by direct current assisted directional solidification," *Waste Manag.*, vol. 157, pp. 190–198, Feb. 2023, doi: 10.1016/j.wasman.2022.12.023.
- [59] M. Imose, D. Araki, M. A. Uddin, Y. Kato, and K. Kinoshita, "Purification of Waste Silicon Powder Derived from Kerf Loss Slurry by Radial Directional Solidification and Comparison with Other Directional Solidification Practices," *J. Sustain. Metall.*, vol. 8, no. 1, pp. 288–296, 2022, doi: 10.1007/s40831-021-00489-2.
- [60] K. Tomono *et al.*, "Recycling of kerf loss silicon derived from diamond-wire saw cutting process by chemical approach," *Sep. Purif. Technol.*, vol. 120, pp. 304–309, Dec. 2013, doi: 10.1016/j.seppur.2013.10.014.
- [61] D. Wei *et al.*, "Recycling silicon from silicon cutting waste by Al–Si alloying," *J. Clean. Prod.*, vol. 251, p. 119647, Apr. 2020, doi: 10.1016/j.jclepro.2019.119647.
- [62] M. Meling, "A Parametric Study on the Recycling of Kerf through Remelting with a Silicon Alloy," *Unpubl. Work.*
- [63] "FactSage Summary of Databases." <https://www.crct.polymtl.ca/fact/documentation/FSDData.htm> (accessed May 22, 2023).

## 8 Appendix

### 8.1 First set of Experiments

#### 8.1.1 Method

The experiment used the same experimental setup as described for the small-scale experiments in this thesis, except for the casting, as the material was cooled down inside the crucible instead. None of the experiments used gas stirring. The experiments were conducted by Nishan Simkhada.

*Table 3 Inputs of different experiments during experimental trails*

Ratio (Kerf: Si: Slag)	Trial	Kerf [g]	Si metal [g]	Slag [g]	Atmosphere	Target Temperature [C]
1:1:2	1o	250	250	500	Open	1650
	1c	250	250	500	closed	1650
	2	125	125	250	closed	1550
	3	125	125	250	closed	1550
1.5:1:2	1	187.5	125	250	closed	1650
	2	187.5	125	250	closed	1550
	3	375	250	500	closed	1550
2:1:2	1	250	125	250	closed	1650
	2	250	125	250	closed	1550

#### 8.1.2 Results

Silicon and slag samples from all trials have been analyzed using the X-Ray Fluorescence (XRF) technique at Degerfors Laboratories AB in Bruksparken, Sweden. Thermo Fischer Scientific's ARL 9900 Series XRF device was used to analyze slag and alloy samples, recognizing the composition of Si, Al, and Ca was the primary goal, but other impurities in significant amounts such as Fe, B, C, and P were also studied focused. The composition of Si, Al, and Ca in alloys and SiO<sub>2</sub>, CaO, and Al<sub>2</sub>O<sub>3</sub> in slags from the first trials have been mentioned in Table 5 and Table 6, respectively.

*Table 5 Si, Al, and Ca composition in alloy from different trails*

Ratio (Kerf: Si: Slag)	Trial	Si wt. %	Average Si wt. %	Al wt. %	Average Al wt. %	Ca wt. %	Average Ca wt. %
(1:1:2)	1c	92.66	89.72	0.83	2.34	5.64	6.39
	2	85.20		3.90		8.35	
	3	91.30		2.30		5.18	
(1.5:1:2)	1	91.85	91.95	1.75	1.55	5.92	5.97
	2	91.60		1.17		6.78	
	3	92.40		1.72		5.20	
(2:1:2)	1	82.56	86.63	1.49	2.02	7.63	6.74
	2	90.70		2.55		5.84	

Table 6 SiO<sub>2</sub>, Al<sub>2</sub>O<sub>3</sub>, and CaO composition in alloy from different trails

Ratio (Kerf: Si: Slag)	Trial	SiO <sub>2</sub> wt. %	Average SiO <sub>2</sub> wt. %	Average Al <sub>2</sub> O <sub>3</sub> wt. %	Al <sub>2</sub> O <sub>3</sub> wt. %	Average CaO wt. %	CaO wt. %
(1:1:2)	1c	52.30	54.10	8.94	5.27	38.50	40.23
	2	58.30		4.04		37.20	
	3	51.70		2.83		45.00	
(1.5:1:2)	1	63.50	58.77	2.63	2.96	33.50	37.87
	2	60.30		3.16		36.20	
	3	52.50		3.10		43.90	
(2:1:2)	1	67.30	57.50	2.08	2.50	30.30	39.55
	2	47.70		2.91		48.80	

Table 7 Material losses and silicon production

Ratio (Kerf: Si: Slag)	Trial	Target Temperature [C]	Loss in weight	Si alloy
1:1:2	1o	1650	353	148.7
	1c	1650	230.45	228
	2	1550	24.32	172.14
	3	1550	68.98	131
1.5:1:2	1	1650	110.37	206.67
	2	1550	25.66	239.1
	3	1550	114.18	240.8
2:1:2	1	1650	119.23	226
	2	1550	36.32	230

## 8.2 Small-Scale Trials (Second Set of Experiments)

### 8.2.1 Element Mapping by EPMA

For this set of experiments, the exact composition was not analyzed, due to time limitations in planning the medium-scale trials. Here, element mapping was prioritized, as it gives a visual overview of the composition of the sample. The scale bars to the right of the mappings show the intensity of the given element.

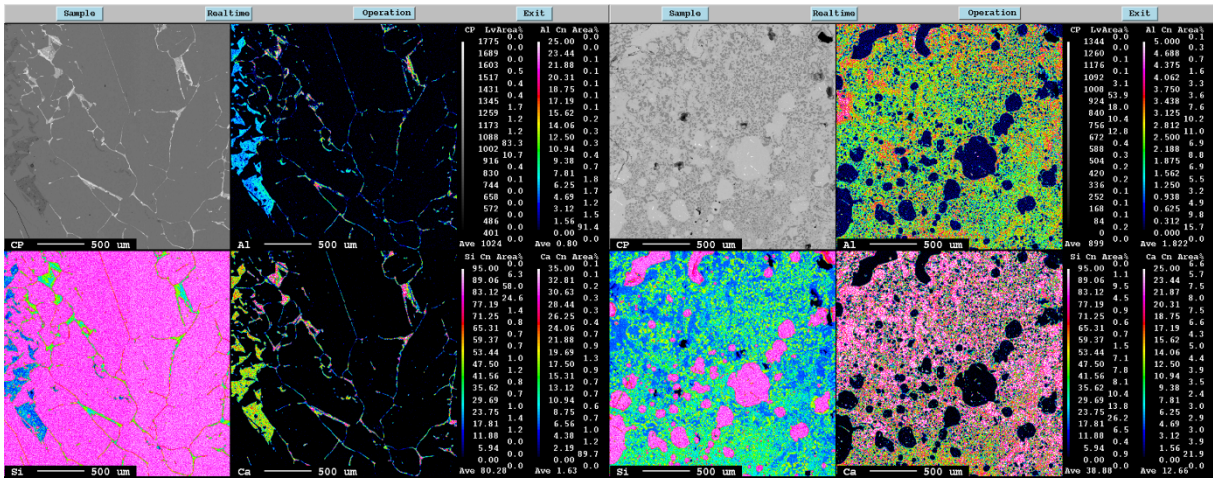


Figure 8.1: Element mapping of samples from experiment 2.2. To the left: metal, to the right: slag. Both samples were taken from the material in the crucible after casting.

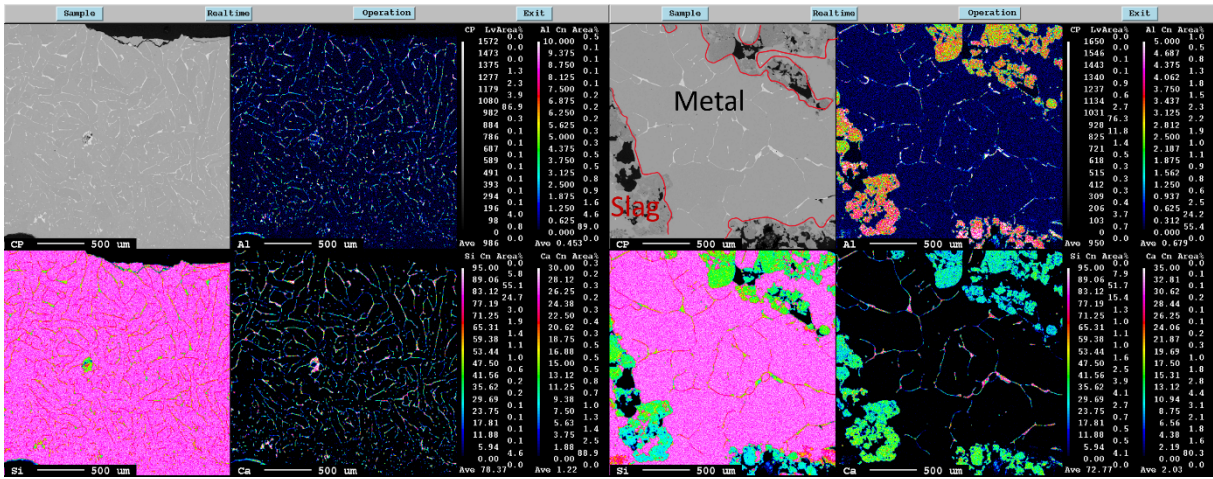


Figure 8.2: Element mapping of samples from experiment 2.3. To the left: metal that was cast. To the right: metal and slag left in the crucible. The slag is enclosed by a red line.

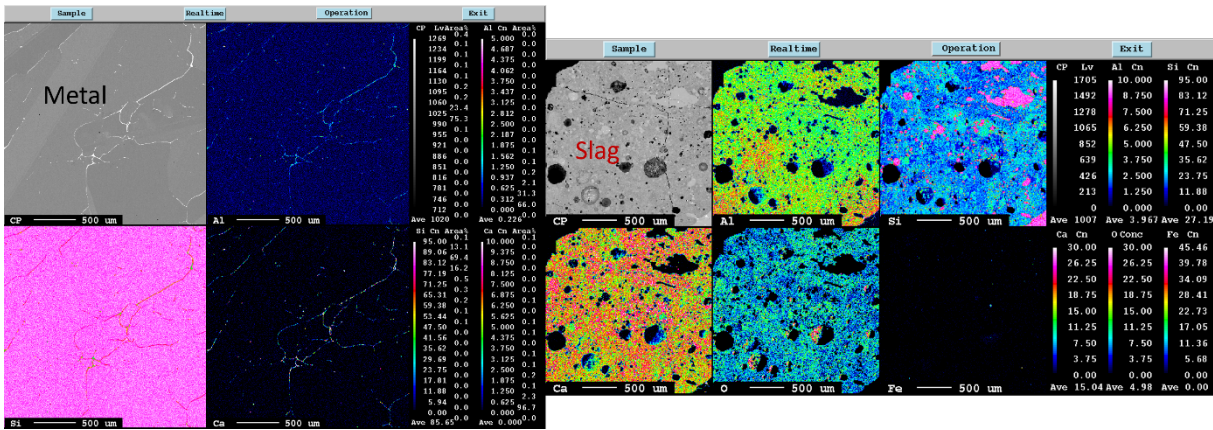


Figure 8.3: Element mapping of samples from experiment 2.4. To the left: metal, to the right: slag. Both samples were taken from the material in the crucible after casting.



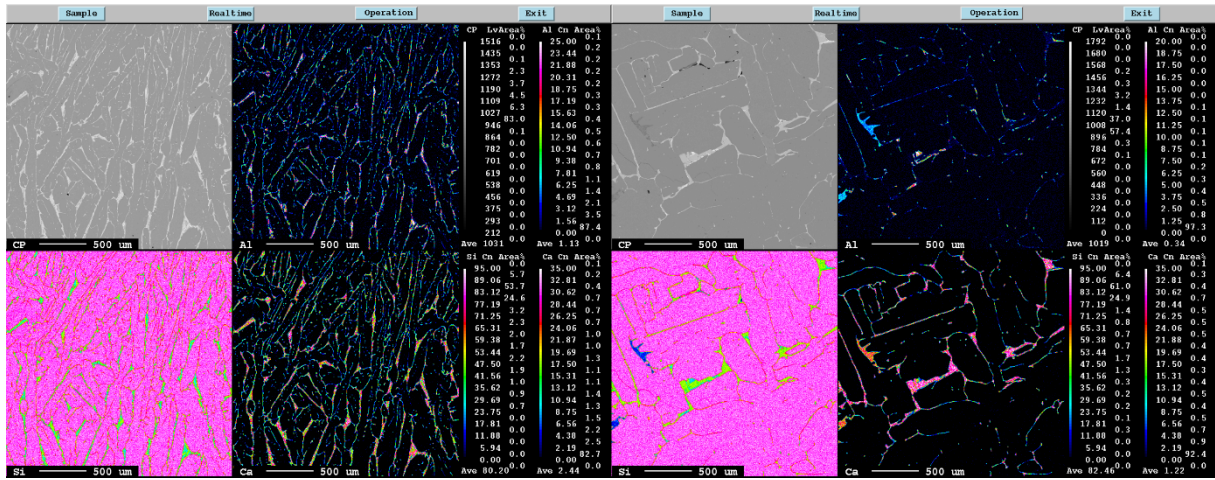


Figure 8.4: Element mapping of samples from experiment 2.5. To the left: a sample of cast metal, to the right: a sample of metal left in the crucible.

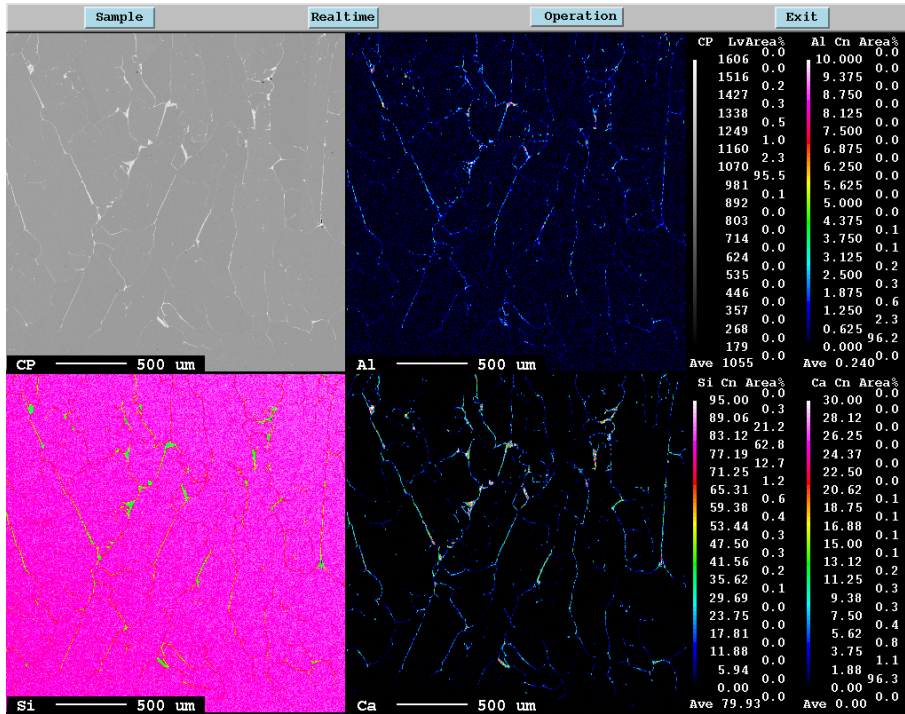


Figure 8.5: Element mapping of a sample from the cast material from experiment 2.6.

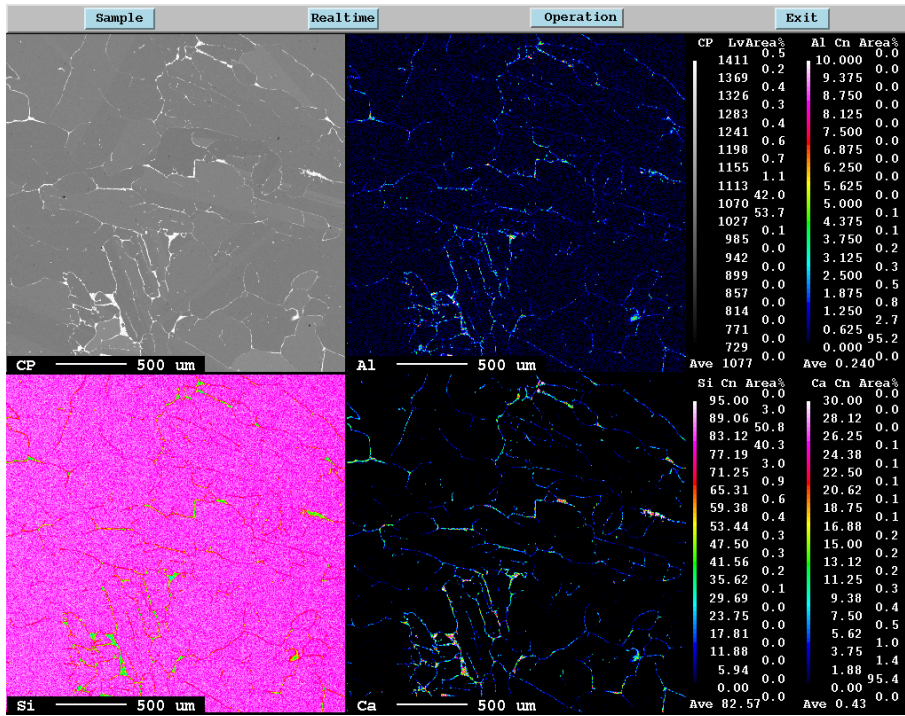


Figure 8.6: Element mapping from a sample from the cast material from experiment 2.7.

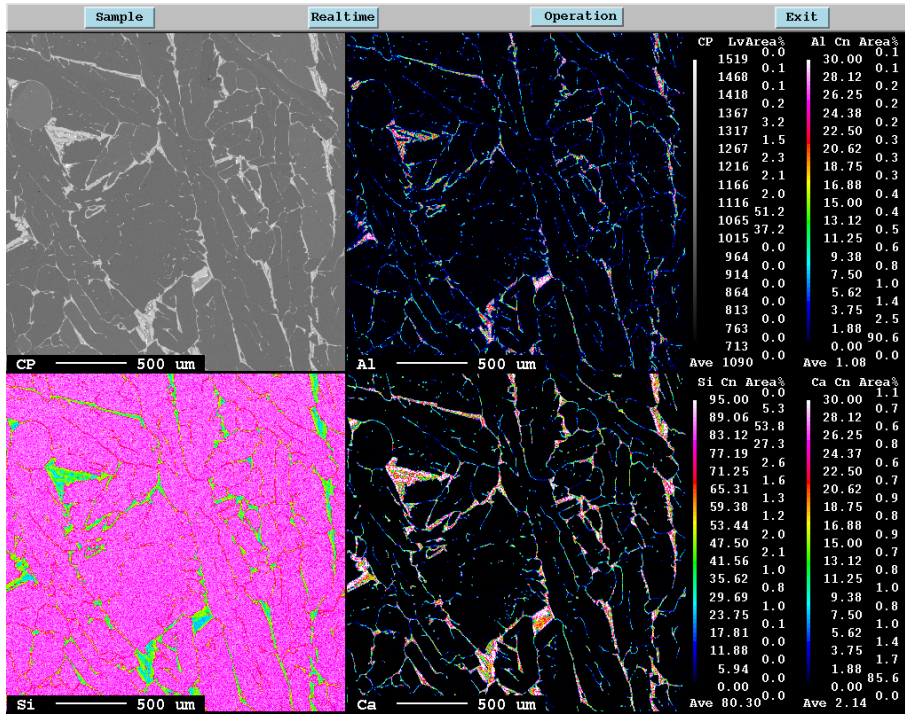


Figure 8.7: Element mapping of the cast metal from experiment 2.8.



## 8.3 Medium-scale trials

### 8.3.1 Mass Balance

The mass of the raw materials and products used in experiment 3.3 are presented in Table 8.1.

Table 8.1: Mass of raw materials and products for experiment 3.3

	11 kg SisAl Metal [kg]	16,5 kg Kerf [kg]	22 kg Slag [kg]	10,2 kg Quartz [kg]	Total in [kg]	18,6 kg Metal Out	38 kg Slag Out	Total Out
Si	7,59	15,56	0,00	0,00	23,15	18,32	1,75	20,06
Ca	2,07	0,02	0,00	0,00	2,08	0,03	0,00	0,03
Al	1,35	0,00	0,00	0,00	1,36	0,06	0,00	0,06
O		0,77			0,77			0,00
CaO	0,00	0,00	11,53	0,00	11,53	0,00	14,45	14,45
Al <sub>2</sub> O <sub>3</sub>	0,00	0,00	0,00	0,00	0,00	0,00	2,88	2,88
SiO <sub>2</sub>	0,00	0,00	10,47	10,20	20,67	0,00	18,93	18,93
Total	11,01	16,35	22,00	10,20	59,56	18,41	38,00	56,41

### 8.3.2 Material Losses and Silicon Yield

Table 8.2: Materials used in the medium-scale trials (third set of experiments), outputs, and losses.

Experiment	SisAl metal [kg]	Kerf [kg]	Slag [kg]	Quartz [kg]	In(total) [kg]	Out (slag) [kg]	Out (metal) [kg]	Out (total) [kg]	Loss [kg]
3.1	11	16,5	22	3,52	53,02	29,8	20	49,8	3,22
3.2	11	16,5	22	3,52	53,02	30	20,4	50,4	2,62
3.3	11	16,5	22	10,2	59,7	38	18,6	56,6	3,1
3.4	11	22	22	10,2	65,2	38,7	22,5	61,2	4
3.5	11	16,5	22	9	58,5	34,3	19,9	54,2	4,3
3.6	11	22	22	9	64	40,3	20,35	60,65	3,35

Table 8.3: Silicon yield in the different experiments based on Si in through the SisAl metal and the kerf, and Si out in the produced metal.

Exp.	Si in					Si out			Yield [%]
	SisAl Metal [kg]	Si content [%]	Kerf [kg]	Si content [%]	Total [kg]	Produced metal [kg]	Si content [%]	Total [kg]	
3.1	11,00	69,00	16,50	84,70	2157	20,00	96,23	1925	89,24
3.2	11,00	69,00	16,50	84,70	2157	20,40	97,52	1989	92,25
3.3	11,00	69,00	16,50	84,70	2157	18,60	98,48	1832	84,94
3.4	11,00	71,80	22,00	84,70	2653	22,50	98,91	2225	83,88
3.5	11,00	71,80	16,50	84,70	2187	19,90	98,79	1966	89,88
3.6	11,00	71,80	22,00	84,70	2653	20,35	97,80	1990	75,01

### 8.3.3 EPMA

EPMA was used to make element mappings of samples from the cast metal produced in the medium-scale experiments, and the mappings are shown in Figure 8.8 through Figure 8.13.

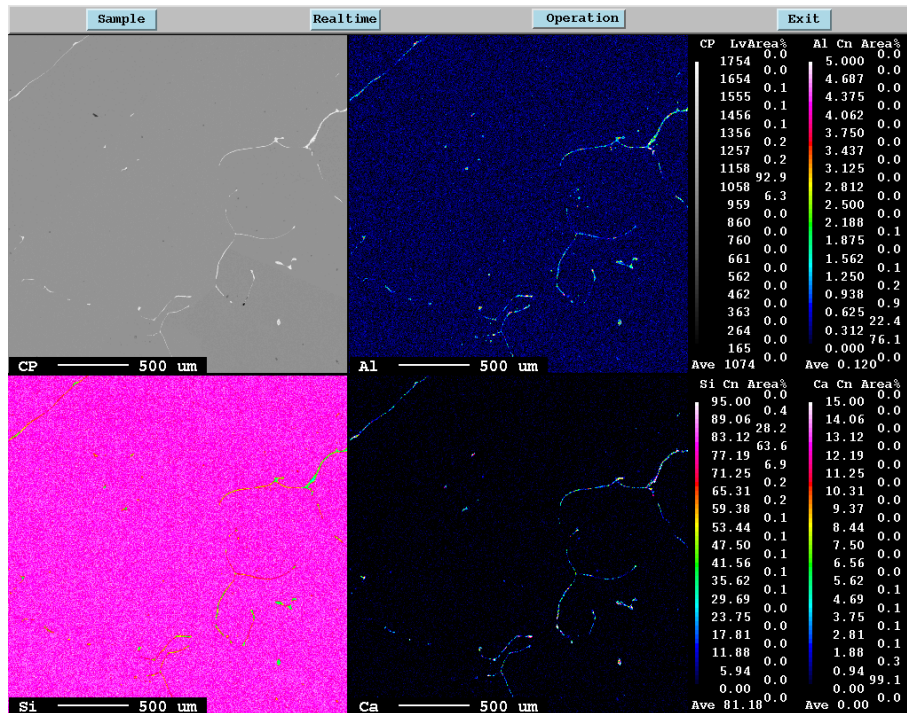


Figure 8.8: Element mapping of metal produced in experiment 3.1.

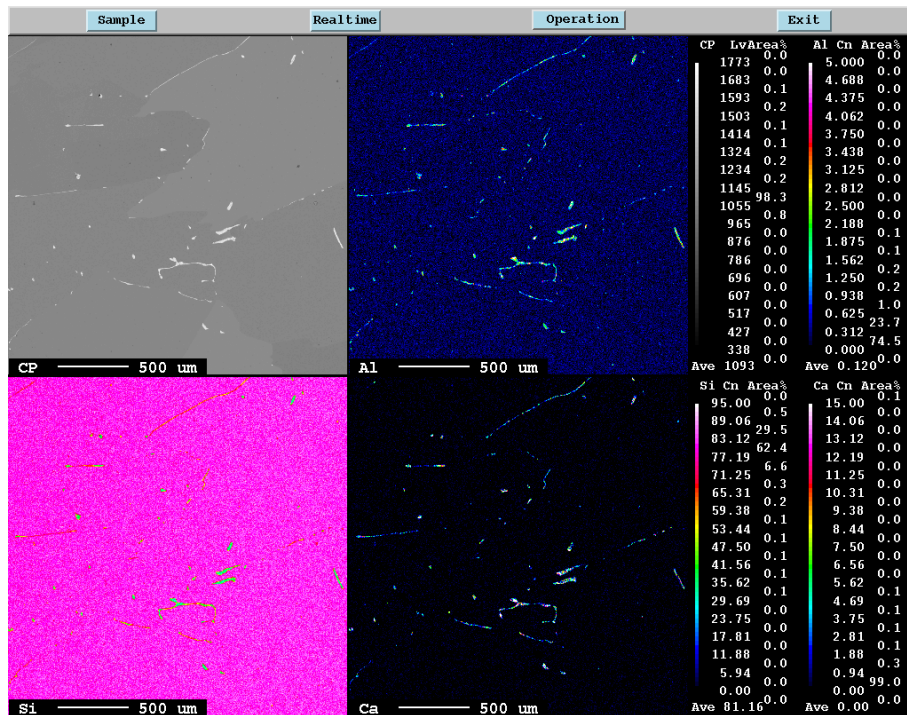


Figure 8.9: Element mapping of metal produced in experiment 3.2.

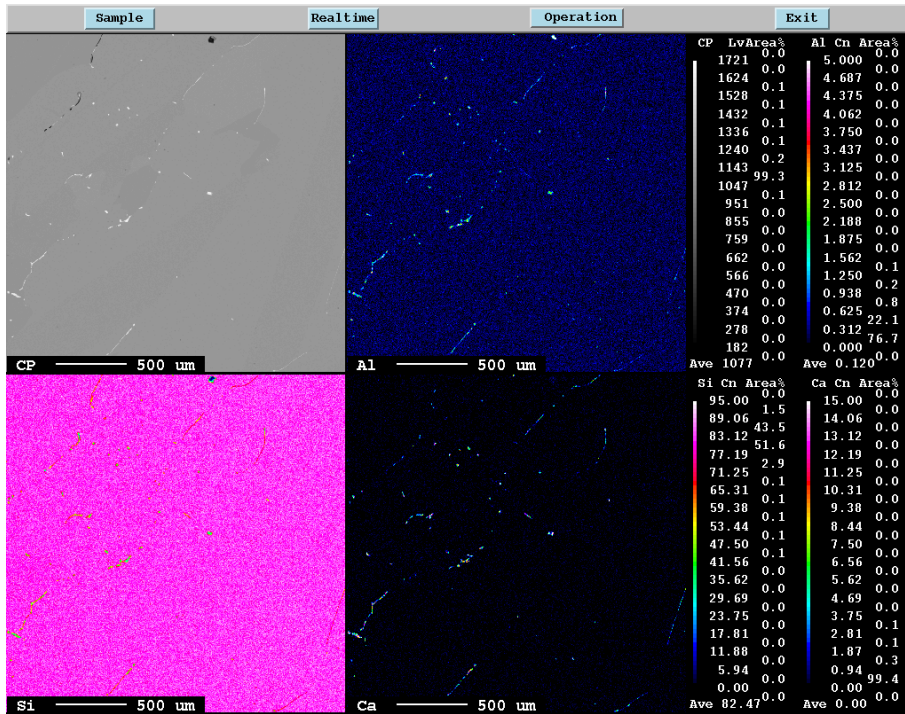


Figure 8.10: Element mapping of metal produced in experiment 3.3.

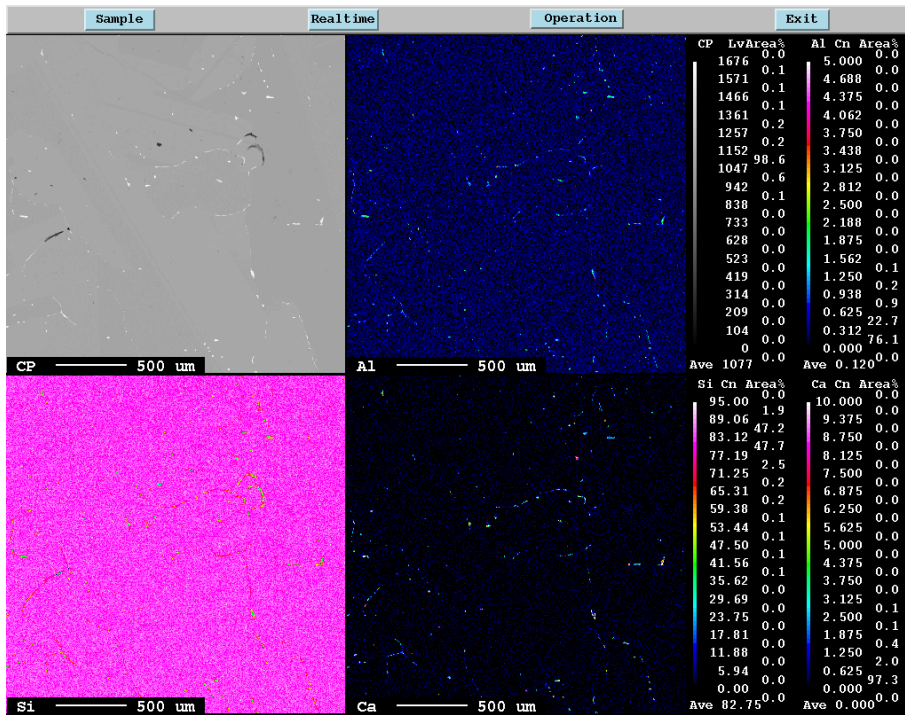


Figure 8.11: Element mapping of metal produced in experiment 3.4.



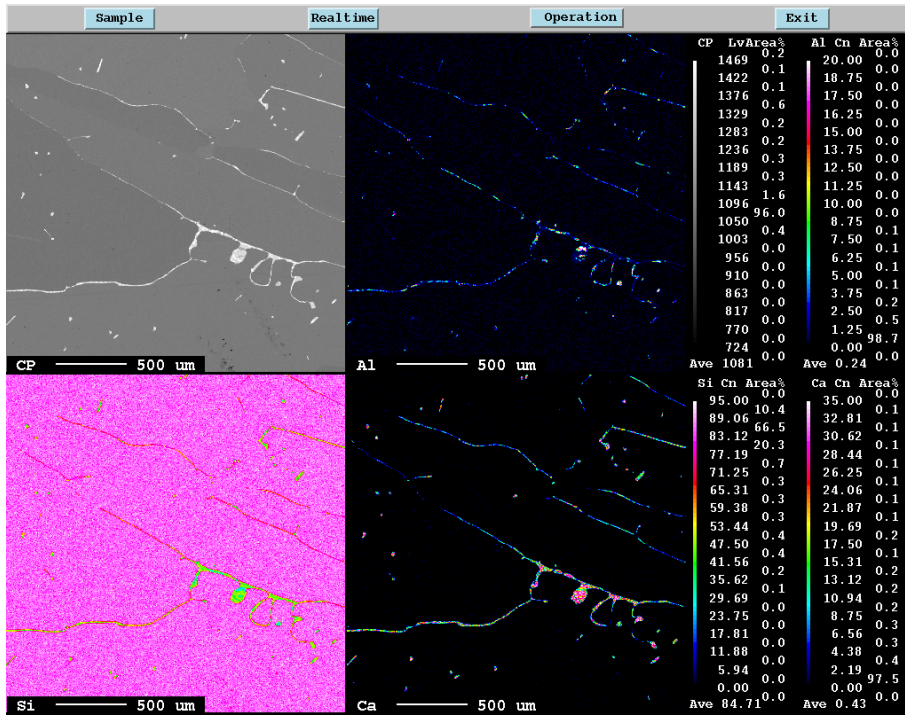


Figure 8.12: Element mapping of metal produced in experiment 3.5.

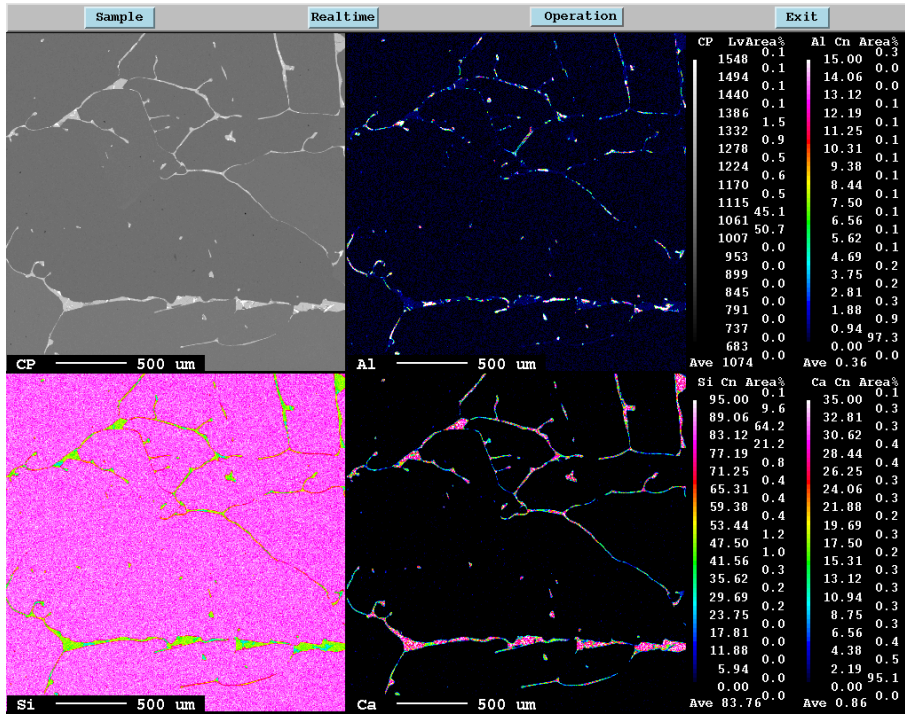


Figure 8.13: Element mapping of metal produced in experiment 3.6.

### 8.3.4 Metal and Slag Analysis

Conversion between experiment names:

In the table	In this thesis
1a	3.1
1b	3.2
2a	3.3
2b	3.4
3a	3.5
3b	3.6

Extra information about the slag:

Element	Method	3.1	3.2	3.3	3.4	3.5	3.6
Ca	XRF	35,12	32,85	27,77	27,99	26,18	26,65
Free Si	Titration		6,5	4,7	6,4		

# Metal



Elkem Technology Lab - Chemical Analysis

## Certificate of Analysis

Page 1 of 2  
Report No.: 004873  
20.03.23

Recipient:  
Elkem Technology  
MUC120NO

Request information:  
Request ID: 2-23-00229  
Request Description: Resilex - casted metal  
Project:

### SisAl metal

Analysis	Method	Unit	2-23-00229-001	2-23-00229-002	2-23-00229-003	2-23-00229-004
			Resilex 1a utstøpt metall	Resilex 1b utstøpt metall	Resilex 2a utstøpt metall	Resilex 2b utstøpt metall
Mg	XRF	%	<0,2	<0,2	<0,2	<0,2
Al	XRF	%	0,510	0,350	0,100	<0,10
P	XRF- Informative	%	<0,1	<0,1	<0,1	<0,1
Ca	XRF	%	1,94	1,05	0,227	<0,2
Ti	XRF	%	<0,5	<0,5	<0,5	<0,5
Cr	XRF	%	<0,1	<0,1	<0,1	<0,1
Mn	XRF	%	0,109	0,132	0,118	0,101
Fe	XRF	%	0,390	0,310	0,340	0,270
Sr	XRF	%	<0,02	<0,02	<0,02	<0,02
Ba	XRF	%	<0,50	<0,50	<0,50	<0,50
La	XRF	%	<0,1	<0,1	<0,1	<0,1
Ce	XRF	%	<0,05	<0,05	<0,05	<0,05
Cu	XRF	%	<0,05	<0,05	<0,05	<0,05
Ni	XRF	%	<0,05	<0,05	<0,05	<0,05
Si	XRF	%	36,23	37,52	38,48	38,91
Zr	XRF	%	<0,05	<0,05	<0,05	<0,05

Analysis	Method	Unit	2-23-00229-005	2-23-00229-006
			Resilex 3a utstøpt metall	Resilex 3b utstøpt metall
Mg	XRF	%	<0,2	<0,2
Al	XRF	%	<0,10	0,190
P	XRF- Informative	%	<0,1	<0,1
Ca	XRF	%	0,374	0,985
Ti	XRF	%	<0,5	<0,5
Cr	XRF	%	<0,1	<0,1
Mn	XRF	%	0,100	0,0800
Fe	XRF	%	0,250	0,420
Sr	XRF	%	<0,02	<0,02
Ba	XRF	%	<0,50	<0,50
La	XRF	%	<0,1	<0,1
Ce	XRF	%	<0,05	<0,05
Cu	XRF	%	<0,05	<0,05
Ni	XRF	%	<0,05	<0,05
Si	XRF	%	38,70	37,80
Zr	XRF	%	<0,05	<0,05

# Slag



Elkem Technology Lab - Chemical Analysis

## Certificate of Analysis

Page 1 of 2  
Report No.: 004946  
23.03.23

Recipient:  
Elkem Technology  
MUC120NO

Request information:  
Request ID: 2-23-00227  
Request Description: Resilex - casted slag  
Project:

### SisAl slag

Analysis	Method	Unit	2-23-00227-001	2-23-00227-002	2-23-00227-003	2-23-00227-004
			Resilex 1a utstøpt slagg	Resilex 1b utstøpt slagg	Resilex 2a utstøpt slagg	Resilex 2b utstøpt slagg
Mg	XRF	%	0,790	0,316	0,730	0,743
Al	XRF	%	4,05	4,39	4,10	4,00
P	XRF- Informative	%	<0,10	<0,10	<0,10	<0,10
Ca	XRF	%	>5,1	>5,1	>5,1	>5,1
Ti	XRF- Informative	%	<0,5	<0,5	<0,5	<0,5
Cr	XRF	%	<0,1	<0,1	<0,1	<0,1
Mn	XRF	%	<0,05	<0,05	<0,05	<0,05
Fe	XRF	%	0,173	<0,10	0,103	0,103
Sr	XRF	%	0,0210	<0,02	<0,02	<0,02
Ba	XRF	%	<0,50	<0,50	<0,50	<0,50
La	XRF	%	<0,10	<0,10	<0,10	<0,10
Ce	XRF	%	<0,05	<0,05	<0,05	<0,05
Cu	XRF	%	<0,05	<0,05	<0,05	<0,05
Ni	XRF	%	<0,05	<0,05	<0,05	<0,05
Si	XRF	%	25,8	27,5	28,5	33,3
Zr	XRF	%	<0,05	<0,05	<0,05	<0,05
Free Si	Titration	%				

Analysis	Method	Unit	2-23-00227-005	2-23-00227-006
			Resilex 3a utstøpt slagg	Resilex 3b utstøpt slagg
Mg	XRF	%	0,703	0,703
Al	XRF	%	4,00	4,04
P	XRF- Informative	%	<0,10	<0,10
Ca	XRF	%	>5,1	>5,1
Ti	XRF- Informative	%	<0,5	<0,5
Cr	XRF	%	<0,1	<0,1
Mn	XRF	%	<0,05	<0,05
Fe	XRF	%	<0,10	<0,10
Sr	XRF	%	<0,02	<0,02
Ba	XRF	%	<0,50	<0,50
La	XRF	%	<0,10	<0,10
Ce	XRF	%	<0,05	<0,05
Cu	XRF	%	<0,05	<0,05
Ni	XRF	%	<0,05	<0,05
Si	XRF	%	30,4	31,2
Zr	XRF	%	<0,05	<0,05
Free Si	Titration	%		

## 8.4 Large-Scale Trials

### 8.4.1 Analysis of Metal and Slag

SisAl Unknown = metal, Unknown = slag



Elkem Technology Lab - Chemical Analysis

Certificate of Analysis

Page 1 of 2  
Report No.: 005483  
25.05.23

Recipient:  
Elkem Technology  
MUC120NO

Request information:  
Request ID: 2-23-00505  
Request Description: Resilex - 600kW  
Project: B2777EXT - RESILEX

#### Silicon - Unknown

Analysis	Method	Unit	2-23-00505-001 Resilex metall
Mg	XRF	%	<0,2
Al	XRF	%	0,630
P	XRF- Informative	%	<0,1
Ca	XRF	%	0,257
Ti	XRF	%	<0,5
Cr	XRF	%	<0,1
Mn	XRF	%	0,0730
Fe	XRF	%	0,370
Sr	XRF	%	<0,02
Ba	XRF	%	<0,50
La	XRF	%	<0,1
Ce	XRF	%	<0,05
Cu	XRF	%	<0,05
Ni	XRF	%	<0,05
Si	XRF	%	97,79
Zr	XRF	%	<0,05

#### Unknown

Analysis	Method	Unit	2-23-00505-002 Resilex slagg
Mg	XRF	%	0,220
Al	XRF	%	5,88
P	XRF- Informative	%	<0,10
Ca	XRF	%	>5,1
Ti	XRF- Informative	%	<0,5
Cr	XRF	%	<0,1
Mn	XRF	%	<0,05
Fe	XRF	%	<0,10
Sr	XRF	%	<0,02
Ba	XRF	%	<0,50
La	XRF	%	<0,10
Ce	XRF	%	<0,05
Cu	XRF	%	<0,05
Ni	XRF	%	<0,05
Si	XRF	%	31,2
Zr	XRF	%	<0,05



## 8.4.2 Theoretical Mass Balance

The theoretical mass balance was calculated in these steps:

1. Calculating the total mass of each of the main elements Si, Al, Ca, and O in the raw materials.
2. Assuming the analyzed metal composition is correct, calculating how much material is used in the produced metal.
3. Calculating how much material is lost in the assumed kerf losses.
4. Subtract the calculation obtained in steps 2 and 3 from step 1 to find the materials available for slag.

	Input [kg]	Metal Product [kg]	Assumed kerf-losses [kg]	Left for slag [kg]
Si	223,3	106,6	11,4	105,3
Al	8,8	0,7	0,1	8,0
Ca	67,0	0,3	0,0	66,7
O	99,4		0,4	99,0

5. Assume all Ca and Al in the slag are oxidized.
6. Assume the rest of the oxygen is used to oxidize Si.
7. The remaining Si is assumed to be Free Si in the slag.

	%
SiO <sub>2</sub>	53,1 %
Al <sub>2</sub> O <sub>3</sub>	6,6 %
CaO	40,4 %

Mass balance based on the calculated slag composition:

	SisAl Metal [kg]	Kerf [kg]	Slag [kg]	Quartz [kg]	Total in [kg]	Metal Out [kg]	Slag Out [kg]	Kerf losses	Total Out [kg]
Si	54,3	104,5	0,0	0,0	158,8	106,6	48,0	11,4	166,0
Al	7,8	1,0	0,0	0,0	8,8	0,7	0,0	0,1	0,7
Ca	11,7	0,2	0,0	0,0	11,9	0,3	0,0	0,0	0,3
O		4,0			4,0			0,4	0,0
CaO	0,0	0,0	77,0	0,0	77,0	0,0	0,0		0,0
Al <sub>2</sub> O <sub>3</sub>	0,0	0,0	0,0	0,0	0,0	0,0	0,0		0,0
SiO <sub>2</sub>	0,0	0,0	70,0	68,0	138,0	0,0	57,3		57,3

Elemental mass balance	SisAl Metal [kg]	Kerf [kg]	Slag [kg]	Quartz [kg]	Total in [kg]	Metal Out [kg]	Slag Out [kg]	Kerf losses	Total Out [kg]
Si	54,3	104,5	32,7	31,8	223,3	106,6	105,3	11,4	223,3
Al	7,8	1,0	0,0	0,0	8,8	0,7	8,0		8,7
Ca	11,7	0,2	55,1	0,0	67,0	0,3	67,0		67,2
O			59,2	36,2	95,4		99,4		99,4
Total	73,9	105,6	147,0	68,0	394,5	107,6	279,7	11,4	398,7

